UNIVERSITÀ DEGLI STUDI DI TRENTO
Dipartimento di Matematica

DOTTORATO DI RICERCA IN MATEMATICA
XXII CICLO

Laura Fumanelli

Mathematical modeling of amoeba-bacteria population dynamics

A thesis submitted for obtaining the degree of Doctor of Philosophy

Advisor:
Prof. Mimmo Iannelli

December 2009

Contents

List of Figures

Acknowledgements

I am grateful to my advisor Mimmo Iannelli, for offering me the possibility to work with him on this topic, for his expertise, patience and valuable guidance during these three years. I would like to thank also Olivier Jousson and Hussnain Ahmed Janjua for providing the results of their experiments and for interesting discussions on the biological aspects of this thesis; Andrea Pugliese for many useful suggestions on the model; Daniela Visetti for her great contribution to the proof of the well-posedness of the problem.

It is with pleasure that I thank Michel Langlais and Fabio Augusto Milner for being members of the Examination Committee.

My deepest gratitude goes to Fabio Bagagiolo and Anneliese Defranceschi for giving me the opportunity of being their teaching assistant: it has been a great experience from both the professional and the personal point of view.

Thanks to my relatives, to the friends of a lifetime and to those I have had the chance to meet more recently, for all the support that I have received during the writing of this thesis. In particular, I would like to thank my aunt Lucia for her unconditional support and pride.

A special mention goes to my friends in doctoral school: Valentina, Ilaria, Antonella, Ester, Davide, Andrea, Philipp, Anna. Thanks for coffee, lunches, chocolate and gossip; for sharing joys and difficulties of PhD; for all the laughter and for being by my side every time I was sad or discouraged. I am particularly indebted to Valentina, my dearest friend and companion in this experience.
Thanks also to the other people with whom I shared the open space and to Denise who has given a lovely touch of Brazil to the last months of my stay!

My parents and my brother Paolo, with their love and their silent yet continuous support, have been determinant during these years as well as through my entire life. I cannot find the words to express what they mean to me.

Finally, thanks to Marco, for his loving support, for always giving me the motivation to face difficulties in my work, for his fundamental help in many situations. And, though we are going through hard times, thanks for every single moment we have lived together.

In nature's infinite book of secrecy
A little I can read
William Shakespeare, *Antony and Cleopatra*

Introduction

In this thesis we present a mathematical model describing the population dynamics occurring between two interacting populations, one of amoebae and one of virulent bacteria; it is meant to describe laboratory experiments with these two species in a mathematical framework and help understanding the role of different mechanisms involved. In particular we aim to focus on how bacterial virulence may affect the dynamics of the system.
Our model is a modified reaction-diffusion-chemotaxis predator-prey one, with two key features that make it interesting to analyze. The first is that bacteria behave both as prey and as pathogens, while amoebae are considered both as predators and as hosts. In fact amoebae feed on bacteria, but these are also able to infect amoeboid cells, so there is an interplay between predation and toxicity which may result either in coexistence or in the prevalence of one population on the other.
The second feature is that the amount of biomass due to the consumption of bacteria by amoebae is redistributed over the total population, which therefore takes advantage of the food ingested by single cells. This mechanism is included because it is known that, upon starvation, amoeboid cells, stimulated by the secretion of a chemical substance, aggregate and behave as a sole organism, so that the uptake of resources by one cell contributes to the growth of the others. These non-local effects are taken into account by considering an integral predation term (see [36], [10], [31] for some examples of reaction-diffusion equation with non-local terms).

This thesis has been developed as the mathematical counterpart of the work by Olivier Jousson and his group at the Laboratory of Microbial Genomics of CIBio (Centre for Integrative Biology), University of Trento. The focus of this research team is to study bacterial pathogenicity from a comparative and functional genomics point of view, in order to understand how genes contribute to virulence, pathogenicity and drug resistance of bacteria. In particular they have been performing *in vivo* experiments aimed at identifying the genes involved in the virulence of many different *Pseudomonas aeruginosa* clinical isolates, from weakly to highly virulent strains ([21], [19]). For these experiments, social amoeba *Dictyostelium discoideum* was firstly used as a host model organism (as done by

other authors, see for instance [4], [9]).

The choices adopted in the mathematical model seem to be adequate to describe these mechanisms: numerical simulations performed are in good agreement with *in vivo* experiments.

The structure of the thesis is the following: Chapter 1 gives an overview of the biological motivations of our study and presents the mathematical model; in Chapter 2 we prove, with fixed point techniques, that the model without chemotaxis admits a unique continuous solution. The case where chemotaxis is included poses some difficulties that are currently being investigated.
Chapters 3 and 4 are devoted to the analysis of the spatially homogeneous model: we first study the existence and acceptability of homogeneous steady states, and then we analyze their stability, giving some conditions on parameters. In detail, existence and stability of positive steady states are investigated with the quantity accounting for bacterial virulence as a bifurcation parameter. In this way, given a set of parameters for the model, we are able to derive how many homogeneous steady states there are and whether they are stable or not. When no positive equilibrium is stable, periodic orbits may also appear: some examples are given.

In Chapter 5 we study the occurrence of pattern formation resulting from our model: following Turing's theory of diffusion-driven instability, we give conditions on diffusion and chemotaxis to be satisfied for obtaining patterns. In particular, we obtain that patterns always appear from the system with the integral term, while in the case without integral some conditions must be satisfied.

The two chapters that follow concern the numerical aspects of this work: Chapter 6 presents the discretization choices and numerical methods implemented for simulations. Chapter 7 collects some of the simulations performed to validate the model: in the first part we show results regarding pattern formation on one-dimensional and circular domains, highlighting the differences between the two models (with and without integral) and when varying the chemotactic sensitivity; in the second part we present some simulations for the model with non-local term related to the experiments performed at CIBio, from which we can conclude that it gives a good description of the dynamics observed in real populations.

Finally, in Chapter 8 we collect some considerations on this thesis and on future work to be carried on.

This doctoral thesis has been developed under PRIN-MIUR project *Mathematical Population Theory: methods, models, comparison with data.*

Chapter 1

The model

1.1 Biological motivations

Pseudomonas aeruginosa is a common opportunistic bacterium, living in soil, water but also artificial environments; this pathogen rarely affects healthy people, but, due to its great resistance to antibiotics, it is quite dangerous for immunocompromised people (cancer or HIV patients) and people affected by severe diseases (such as cystic fibrosis); moreover, it is responsible of pneumonia, septicaemia and many other nosocomial infections. Therefore, due to this public health concern, it is important to study and understand virulence factors, mechanisms of pathogenesis and drug resistance of different strains of *Pseudomonas aeruginosa* [19], [21].
To this end, non-mammalian host models are used to reproduce infection by human pathogens; one of the simple organisms normally used is *Dictyostelium discoideum* [17]. It is an amoeba (also known as *slime mold*) living in the soil, feeding on bacteria; as long as nutrient is available cells grow and multiply, but upon starvation they produce cyclic adenosine monophosphate (cAMP), a chemical substance used for signal transduction, and they start aggregating, thus becoming a multicellular slug. Upon suitable environmental conditions cells differentiate into a fruiting body with a stalk and spores; when the fruiting body is mature the latter are released and new unicellular organisms appear. Its simple life cycle makes *Dictyostelium discoideum* a suitable model organism, so it is widely used in microbiology (see [38], [41] and many others), and also for studying virulence of *Pseudomonas aeruginosa* [35], [4], [9].

The research team leaded by Olivier Jousson at CIBio, University of Trento, works on the application of comparative and functional genomics to bacterial pathogenicity; to this end, *Pseudomonas aeruginosa* is used as pathogen model to identify genetic factors

involved in virulence of this bacterium. Two host models are used for these experiments: the aforementioned amoeba *Dictyostelium discoideum* and the nematode *Caenorhabditis elegans*.

Mathematical models are a useful tool to describe biological phenomena and help understanding the underlying mechanisms. This is the object of the thesis: to give a mathematical interpretation to the population dynamics emerging from experiments.
In particular, we are interested in the experiments with *Dictyostelium discoideum* because of the specific features of this organism which are mathematically challenging.

1.2 Derivation of the model

Our aim is to give and analyze a model describing the *in vivo* interaction between two populations (namely, social amoebae *Dictyostelium discoideum* and bacteria *Pseudomonas aeruginosa* - even though the model may be adapted to other species behaving similarly). Partial differential equations, and in particular parabolic equations, are a widely used tool when there is the need to describe the change over time of species whose distribution in the environment is not uniform (a review can be found in [14]).
Our mathematical model therefore consists of a system of partial differential equations describing the spatio-temporal evolution of two populations, namely the one of bacteria $u = u(t, x)$ and that of amoebae $v = v(t, x)$. The model is given on a spatial domain Ω with smooth boundary $\partial\Omega$; for simplicity we start by considering a one–dimensional domain, that is, $\Omega = [0, L]$, but then also the two-dimensional case (which is more adherent to the biological experimental setting) will be taken into account.
In particular we are going to develop a reaction-diffusion system, falling into the category of semilinear parabolic systems, in which a chemotaxis mechanism is included (so actually we will speak of a *reaction-diffusion-chemotaxis system*, see [27] for reference).

Our system has a diffusion-chemotaxis part accounting for the spatial variation of the two species' concentrations. We assume that both bacterial and amoeboid populations diffuse across Ω; in fact, modeling dispersal of populations across the environment by means of diffusion is a classic assumption (see [28], [29], [14], [2], [37], [33], [34]). The diffusion coefficients for bacteria and amoebae, measuring the rate at which the two species disperse, are called d_1 and d_2 respectively.
Moreover, we assume that amoebae feed on bacteria, and so they are also attracted by larger bacterial concentrations, so that we include a chemotactic term $-(v\chi(u, v)u_x)_x$ to model this phenomenon; due to the lack of specific indications from biology, for greater mathematical tractability the chemotactic sensitivity $\chi(u, v)$ is assumed to be equal to a

linear function of the amoeboid concentration, with coefficient c.
For a deeper insight on chemotaxis and the possible form of chemotactic sensitivity in reaction-diffusion problems, see Chapter 11 in [26].
We are not taking into account any aggregation process by chemotaxis between amoeboid cells, which is a well-known mechanism in biology (see for instance [17]); this would result in a third equation for cAMP, which is the chemical signal produced by amoebae for initiating aggregation when food abundance is low. This topic has been addressed by many authors with mathematical models involving the amoeboid population, the nutrient and cAMP concentration; see for example [22], [6], [44] among others.
Some models also deal with the formation of patterns by amoebae when aggregating ([30], [18]). These issues will not be addressed in this thesis.

Now we are going to focus on the reaction part of the system.
We suppose that, in the absence of amoebae, the bacterial population follows a self-limiting growth, which is described by a logistic term $ru(1-u/K)$, where r is the intrinsic growth rate and K is the carrying capacity of bacteria; this term, firstly suggested by [8], [45], [46], is classic in literature.

When both populations are present, instead, bacteria undergo predation at a rate proportional to the amount of amoebae, with constant of proportionality a. This is the simplest modeling choice; other possibilities may be considered too.
Predation of bacteria results in the growth of the amoeboid population; this term is quite different from classical predator-prey models: in fact, usually the predation term in the equation for the prey and the growth term in the equation for the predator have the same form, except for the sign and possibly the constant rates. Here instead we want to take into account the fact that amoebae upon starvation behave like a sole organism ([47], [22], [30]), so that food supply is redistributed between all the cells. This kind of non-local behavior is modeled with an integral term (see for instance [36], [10], [31]); we will come back to the motivation for this in Section 1.3 below. As we have already said, we are not considering aggregation processes for amoebae explicitly, but only their effect on the growth of the population (that is, nutrient redistribution).

Another feature of our model that makes it different from classical predator-prey models is the following: since the bacterial population under investigation belongs to a virulent strain, we have to include the fact that amoebae are infected by bacteria and die. This is taken into account by assuming that amoebae are attacked by bacteria following a Holling type II functional response $\dfrac{buv}{1+bTv}$ [13], [20], with handling time T and attack rate b. We choose this term because we assume that it takes some time to bacteria to search and kill amoebae; notice, however, that a simpler version can be used by imposing

$T = 0$.

Finally, when bacteria are absent, there is no other food source for the amoeboid population, which consequently undergoes an exponential decay mv with death rate m.

Therefore our model can be written as follows:

$$\begin{cases} u_t = d_1 u_{xx} + ru\left(1 - \dfrac{u}{K}\right) - auv \\ v_t = d_2 v_{xx} - c(vu_x)_x - mv + fv\dfrac{\int_0^L uvdx}{\int_0^L vdx} - \dfrac{buv}{1+bTv} \end{cases} . \tag{1.1}$$

By introducing the following non–dimensional variables

$$t' = rt \ , \ x' = \frac{x}{L} \ , \ u' = \frac{u}{K} \ , \ v' = \frac{a}{r}v$$

and dropping primes, system (1.1) becomes

$$\begin{cases} u_t = D_1 u_{xx} + u(1-u) - uv \\ v_t = D_2 v_{xx} - \chi(vu_x)_x - \mu v + \delta v\dfrac{\int_0^1 uvdx}{\int_0^1 vdx} - \dfrac{\gamma uv}{1+\tau v} \end{cases} \tag{1.2}$$

where

$$D_1 = \frac{d_1}{rL^2} \ , \ D_2 = \frac{d_2}{rL^2} \ , \ \chi = \frac{cK}{rL^2} \ ,$$
$$\mu = \frac{m}{r} \ , \ \delta = \frac{fK}{r} \ , \ \gamma = \frac{bK}{r} \ , \ \tau = \frac{bTr}{a}$$

with initial conditions

$$u(0,x) = u_0(x) \ \ \forall\, x \in \Omega$$
$$v(0,x) = v_0(x) \ \ \forall\, x \in \Omega$$

and zero–flux Neumann boundary conditions

$$\frac{\partial u}{\partial \nu}(t,x) = \frac{\partial v}{\partial \nu}(t,x) = 0 \ \ \forall x \in \partial\Omega, \ \ \forall t \geq 0$$

where ν is the outer normal versor to the boundary of the domain, $\partial\Omega$. These no-flux boundary conditions have been chosen because they are reasonable for the experimental setting of the problem.

When considering a two-dimensional spatial domain, the system in normalized form (where L has been replaced by $\mathrm{mis}(\Omega)$) reads

$$\begin{cases} u_t = D_1 \Delta u + u(1-u) - uv \\ v_t = D_2 \Delta v - \chi \nabla \cdot (v \nabla u) - \mu v + \delta v\dfrac{\iint_\Omega uvd\mathbf{x}}{\iint_\Omega vd\mathbf{x}} - \dfrac{\gamma uv}{1+\tau v} \\ u(0,\mathbf{x}) = u_0(\mathbf{x}) \ \ \forall\, \mathbf{x} \in \Omega \\ v(0,\mathbf{x}) = v_0(\mathbf{x}) \ \ \forall\, \mathbf{x} \in \Omega \\ \dfrac{\partial u}{\partial \nu}(t,\mathbf{x}) = \dfrac{\partial v}{\partial \nu}(t,\mathbf{x}) = 0 \ \ \forall \mathbf{x} \in \partial\Omega, \ \ \forall t \geq 0 \end{cases} \tag{1.3}$$

In Table 1.1 the terms appearing in the model are summarized.

Quantity	Meaning
x	position
t	time
$u(t,x)$	concentration of bacteria
$v(t,x)$	concentration of amoebae
D_1	diffusion rate of bacteria
D_2	diffusion rate of amoebae
χ	chemotactic coefficient
μ	natural mortality rate of amoebae
δ	growth rate of amoebae
γ	killing rate of bacteria
τ	handling time of amoeba by bacteria
$u_0(x)$	initial concentration of bacteria
$v_0(x)$	initial concentration of amoebae

Table 1.1: Terms appearing in models (1.2) and (1.3).

1.3 Motivations for the integral term

We come back to the predation term, to explain the choice in models (1.2) and (1.3), that is,

$$\delta v \frac{\int_0^1 uvdx}{\int_0^1 vdx} \tag{1.4}$$

(for a one-dimensional spatial domain, keeping in mind that u stands for bacteria and v for amoebae).

Every amoeboid cell predates a quantity u of bacteria, so the total amount of bacteria predated over all the domain is proportional to $\displaystyle\int_0^1 uvdx$; since we are assuming that ingested bacteria are redistributed to the whole population, we divide by $\displaystyle\int_0^1 vdx$, and so the quantity received by a single cell after redistribution is proportional to $\dfrac{\int_0^1 uvdx}{\int_0^1 vdx}$. Therefore the contribution of predation to the variation in time of the amoeboid population is given by (1.4), where δ is a conversion parameter.

We decided this form for the predation term because it is the simplest possible. Other choices can be made to model this mechanism of food redistribution; or we may assume different hypotheses: for instance we may assume that, if a cell predates bacteria, only the nearest cells receive nutrient, so we would have to use a specific kernel in the integral.

Chapter 2

Well-posedness of the problem without chemotaxis

Now that we have built our model for this amoeba-bacteria system, we need to show that it is well-posed. Actually, we are going to prove existence and uniqueness of a solution to a generalized version of system (1.2), where the spatial domain is a subset of $\mathbb{R}^n$ (instead of $\mathbb{R}$ or $\mathbb{R}^2$), but without chemotaxis (namely, $\chi = 0$). The proof for the complete model (1.2) in $\mathbb{R}^n$ with chemotaxis requires other tools and at the moment of writing (November 2009) is under investigation. To this end, we wish to follow the approach used in [12]. This part of the work has been elaborated in collaboration with Mimmo Iannelli and Daniela Visetti from the University of Trento.

Given a bounded domain Ω in $\mathbb{R}^n$ with smooth boundary $\partial\Omega$ and $t \in [0, +\infty)$, we consider the following Cauchy problem with Neumann boundary conditions

$$\begin{cases} \dfrac{\partial u}{\partial t} = D_1 \Delta u + u(1-u) - uv \\ \dfrac{\partial v}{\partial t} = D_2 \Delta v - \gamma \dfrac{uv}{1+\tau v} + \delta \dfrac{\int_\Omega uv\,dx}{\int_\Omega v\,dx} v - \mu v \\ u(0,x) = u_0(x) \quad \forall x \in \Omega \\ v(0,x) = v_0(x) \quad \forall x \in \Omega \\ \dfrac{\partial u}{\partial \nu}(t,x) = \dfrac{\partial v}{\partial \nu}(t,x) = 0 \quad \forall t \in [0,+\infty],\ x \in \partial\Omega \end{cases} \tag{2.1}$$

where $u = u(t,x)$, $v = v(t,x)$, ν is the outer normal vector to $\partial\Omega$ and $D_1, D_2, \delta, \gamma, \mu, \tau$ are nonnegative constants.

Problem (2.1) falls in the class of reaction-diffusion systems with special non local terms.

We want to prove the existence and uniqueness of solutions to problem (2.1), following the approach presented in [15] and [16].
For technical reasons it is better to consider the following transformed variables:

$$\overline{u}(t,x) = u(t,x) \quad \overline{v}(t,x) = e^{-(\omega-\mu)t}v(t,x) \quad \forall (t,x) \in [0,+\infty) \times \Omega\,,$$

where ω is a suitable constant, that will be chosen in the sequel. The Cauchy problem then becomes

$$\begin{cases} \dfrac{\partial \overline{u}}{\partial t} = D_1 \Delta \overline{u} + \overline{u}(1-\overline{u}) - e^{(\omega-\mu)t}\overline{u}\,\overline{v} \\ \dfrac{\partial \overline{v}}{\partial t} = D_2 \Delta \overline{v} - \gamma \dfrac{\overline{u}\,\overline{v}}{1+\tau e^{(\omega-\mu)t}\overline{v}} + \delta \dfrac{\int_\Omega \overline{u}\,\overline{v}\,dx}{\int_\Omega \overline{v}\,dx}\overline{v} - \omega \overline{v} \\ \overline{u}(0,x) = u_0(x) \\ \overline{v}(0,x) = v_0(x) \\ \dfrac{\partial \overline{u}}{\partial \nu}(t,x) = \dfrac{\partial \overline{v}}{\partial \nu}(t,x) = 0 \end{cases} \tag{2.2}$$

From now on we will write simply u, v, instead of $\overline{u}, \overline{v}$.

This problem can be embedded in an abstract framework in the following way. Let X be the Banach space $L^1(\Omega) \times L^1(\Omega)$ with the usual norm

$$\|W\|_X = \|u\|_{L^1} + \|v\|_{L^1}\,, \qquad \forall\ W = (u,v) \in X\,. \tag{2.3}$$

We consider the linear operator $A : D_A \subset X \to X$

$$\begin{aligned} D_A &= \left\{W = (u,v) \in X \mid u, v \in W^{2,1}(\Omega) \cap W_0^{1,1}(\Omega)\right\} \\ A:\ D_A \subset X &\ \to\ X \\ W &\ \mapsto\ (D_1\Delta u, D_2 \Delta v)\ ; \end{aligned} \tag{2.4}$$

then, for $R \geq 1$, we consider the closed convex subset of X

$$K = \{W = (u,v) \in X \mid u, v \in L^\infty(\Omega);\ 0 \leq u(x) \leq R,\ 0 \leq u(x) \leq R \ \text{ a.e.}\}\,. \tag{2.5}$$

For $t \in [0,+\infty)$ we can define the nonlinear operator on K $F(t) : K \subset X \to X$

$$F(t)W = \left(u(1-u) - e^{(\omega-\mu)t}uv, -\frac{\gamma uv}{1+\tau e^{(\omega-\mu)t}v} + \frac{\delta \int_\Omega uv\,dx}{\int_\Omega v\,dx}v - \omega v\right)\,, \tag{2.6}$$

where $W = (u,v)$.

With the previous definitions, problem (2.2) can now be written as an abstract Cauchy problem in X:

$$\begin{cases} \dfrac{dW}{dt} = A(W) + F(t)W \\ W(0) = (u_0, v_0) \end{cases} \tag{2.7}$$

where $(u_0, v_0) \in K$.

The operator A is the infinitesimal generator of an analytic semigroup $S(t)$ on $L^1(\Omega)$ such that $S(t)K \subset K$(see for example [32]).
For any $\alpha > 0$ we consider the mild form of problem (2.7)

$$W(t) = e^{-\frac{1}{\alpha}t}S(t)(u_0, v_0) + \frac{1}{\alpha}\int_0^t e^{-\frac{1}{\alpha}(t-s)}S(t-s)(W(s) + \alpha F(s)W(s))\,ds\,,\ t > 0\,. \tag{2.8}$$

Then we can prove

Theorem 2.1 *Let $u_0, v_0 \in K$. Then problem (2.8) admits one and only one solution $W(t) \in C([0,T], K)$, $W(t) \in K$.*

Proof. In order to prove existence of a mild solution, we fix $T > 0$ and look for fixed points of the operator

$$\Psi(W)(t) = e^{-\frac{1}{\alpha}t}S(t)(u_0, v_0) + \frac{1}{\alpha}\int_0^t e^{-\frac{1}{\alpha}(t-s)}S(t-s)(W(s) + \alpha F(s)W(s))\,ds \tag{2.9}$$

in $C([0,T], X)$. We first check that $\Psi K \subset K$.
Since K is convex and $S(t)(u_0, v_0) \in K$, it is sufficient to prove that

$$W(s) + \alpha F(s)W(s) \in K\,. \tag{2.10}$$

Indeed, for $\alpha > 0$ sufficiently small ($\alpha \leq \min\left\{1/R(1 + e^{(\omega-\mu)T}), 1/R(\gamma+\delta)\right\}$) and $\omega >$

δR, we have

$$\begin{aligned}
(W+\alpha F(t)W)_1 &= u+\alpha u(1-u)-\alpha e^{(\omega-\mu)t}uv \\
&\geq u(1-\alpha u-\alpha e^{(\omega-\mu)t}v) \\
&\geq u(1-\alpha R-\alpha e^{(\omega-\mu)T}R) \\
&\geq 0\,, \\
(W+\alpha F(t)W)_1 &= u(1+\alpha-\alpha u-\alpha e^{(\omega-\mu)t}v) \\
&\leq R(1-\alpha e^{(\omega-\mu)t}v) \\
&\leq R\,, \\
(W+\alpha F(t)W)_2 &= v\left(1-\alpha\gamma\frac{u}{1+\tau e^{\omega t}v}+\alpha\delta\frac{\int_\Omega uv\,dx}{\int_\Omega v\,dx}-\alpha\omega\right) \\
&\geq v\left(1-\alpha\gamma R-\alpha\omega\right) \\
&\geq 0\,, \\
(W+\alpha F(t)W)_2 &\leq R(1+\alpha\delta R-\alpha\omega) \\
&= R\,.
\end{aligned}$$

On the other hand, function $F(t)$ is Lipschitz continuous in K: in fact for any $W=(u,v), \overline{W}=(\overline{u},\overline{v})\in K$ and for any $t\in[0,T]$,

$$\begin{aligned}
\|\left(F(t)W-F(t)\overline{W}\right)_1\|_{L^1} &= \|u(1-u)-e^{(\omega-\mu)t}uv-\overline{u}(1-\overline{u})+e^{(\omega-\mu)t}\overline{u}\,\overline{v}\|_{L^1} \\
&\leq \|u-\overline{u}\|_{L^1}+\|u^2-\overline{u}^2\|_{L^1}+e^{(\omega-\mu)T}\|(u-\overline{u})v\|_{L^1}+\|\overline{u}(v-\overline{v})\|_{L^1} \qquad (2.11)\\
&\leq (1+2R+Re^{(\omega-\mu)T})\|W-\overline{W}\|_X\,,
\end{aligned}$$

and

$$\begin{aligned}
&\left\|\left(F(t)W-F(t)\overline{W}\right)_2\right\|_{L^1} = \\
&= \left\|-\gamma\frac{uv}{1+\tau e^{\omega t}v}+\delta\frac{\int_\Omega uv\,dx}{\int_\Omega v\,dx}v-\omega v+\gamma\frac{\overline{u}\,\overline{v}}{1+\tau e^{\omega t}\overline{v}}\overline{v}-\delta\frac{\int_\Omega \overline{u}\,\overline{v}\,dx}{\int_\Omega \overline{v}\,dx}\overline{v}+\omega\overline{v}\right\|_{L^1} \\
&\leq \gamma\left\|\frac{uv}{1+\tau e^{\omega t}v}-\frac{\overline{u}\,\overline{v}}{1+\tau e^{\omega t}\overline{v}}\overline{v}\right\|_{L^1}+\delta\left\|\frac{\int_\Omega uv\,dx}{\int_\Omega v\,dx}v-\frac{\int_\Omega \overline{u}\,\overline{v}\,dx}{\int_\Omega \overline{v}\,dx}\overline{v}\right\|_{L^1}+\omega\left\|v-\overline{v}\right\|_{L^1} \\
&\leq R\left(\gamma+R\gamma\tau e^{\omega T}+3\delta+\omega\right)\left\|W-\overline{W}\right\|_X\,;
\end{aligned} \qquad (2.12)$$

in fact,

$$\left\|\frac{uv}{1+\tau e^{\omega t}v}-\frac{\overline{u}\,\overline{v}}{1+\tau e^{\omega t}\overline{v}}\overline{v}\right\|_{L^1} \leq R(1+R\tau e^{\omega T})\|(u,v)-(\overline{u},\overline{v})\|_X\,, \qquad (2.13)$$

$$\left\|\frac{\int_\Omega uv\,dx}{\int_\Omega v\,dx}v-\frac{\int_\Omega \overline{u}\,\overline{v}\,dx}{\int_\Omega \overline{v}\,dx}\overline{v}\right\|_{L^1} \leq 3R\|(u,v)-(\overline{u},\overline{v})\|_X\,. \qquad (2.14)$$

Finally, we estimate Ψ:

$$\begin{aligned}
&\|\Psi(W)(t) - \Psi(\overline{W})(t)\|_X \leq \\
&\quad \leq \frac{1}{\alpha}\int_0^t \left\| e^{-\frac{1}{\alpha}(t-s)} S(t-s)\left(W(s) - \overline{W}(s) + \alpha F(s)W(s) - \alpha F(s)\overline{W}(s)\right)\right\|_X ds \\
&\quad \leq \frac{1}{\alpha}\int_0^t e^{-\frac{1}{\alpha}(t-s)}(1+\alpha L)\left\|W(s) - \overline{W}(s)\right\|_X ds \\
&\quad \leq \left(\frac{1}{\alpha} + L\right)\int_0^t \left\|W(s) - \overline{W}(s)\right\|_X ds
\end{aligned} \tag{2.15}$$

where we use the fact that $F(s)$ is Lipschitz continuous in K for any $s \in [0,T]$. From this we can evaluate any iterate:

$$\left\|\Psi^k(W) - \Psi^k(\overline{W})\right\|_{C([0,T],X)} \leq \frac{\left(\frac{1}{\alpha} + L\right)^k}{k!} T^k \left\|W - \overline{W}\right\|_{C([0,T],X)} \tag{2.16}$$

and taking k sufficiently large we can conclude.

□

Chapter 3

Homogeneous steady states of the system

We consider the spatially homogeneous problem related to (1.2):

$$\begin{cases} u' = u(1-u) - uv \\ v' = \delta uv - \dfrac{\gamma uv}{1+\tau v} - \mu v \end{cases} \tag{3.1}$$

We look for the steady states of system (3.1), that is, the intersections of zero-isoclines. We can immediately see that there are always the trivial steady state $(0, 0)$ and the bacteria-only state $(1, 0)$.
The existence of positive, or coexistence, steady states (that is, steady states whose predator and prey components are both strictly positive) is not so straightforward and needs to be investigated accurately.
Due to the biological motivations of this study, the parameter we are most interested in is clearly the one accounting for virulence, that is, γ: in fact, different bacterial strains have different degrees of pathogenicity. Thus γ will be our bifurcation parameter.
The other parameter we take into account in the parameter space is the amoeba death rate μ; this seems to be a reasonable assumption because, in the following calculations, we will see that many quantities can be expressed in terms of it.
Both γ and μ will be related to expressions depending on the aggressiveness of amoeboid cells δ.

3.1 Existence of steady states

First of all, looking at the plots of the isoclines, namely the straight line

$$v = 1 - u \tag{3.2}$$

and the hyperbola

$$v = \frac{(\gamma - \delta)u + \mu}{\tau(\delta u - \mu)}\,, \tag{3.3}$$

one easily sees that no meaningful intersection (that is, such that $0 < u^*, v^* < 1$) occurs when $\mu > \delta$. The case with $\mu < \delta$ and $\gamma > \delta(1 + \tau)$ is easily dealt with too: in fact, in this case the horizontal asymptote of the hyperbola is over $v = 1$, so that there are no intersections between the two isoclines. Figure 3.1 shows two examples of these situations.

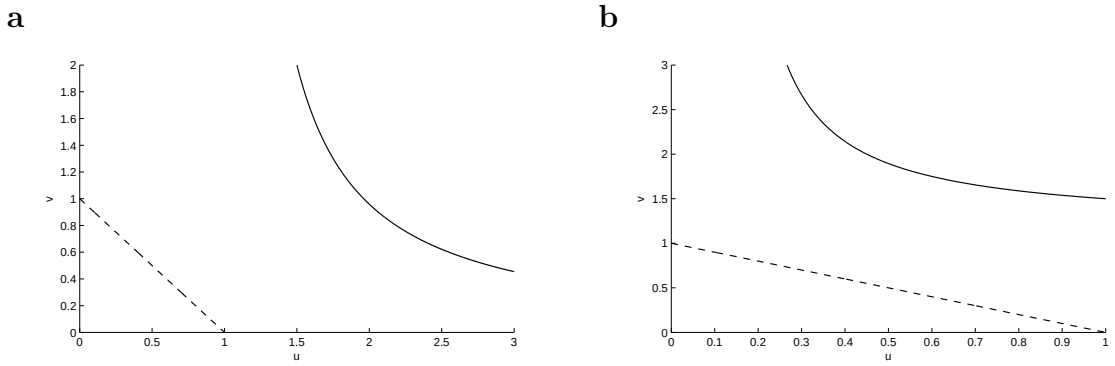

Figure 3.1: Example of isoclines of system (3.1) for the cases $\mu > \delta$ (**a**, values for parameters: $\delta = 5.0$, $\gamma = 4.8$, $\mu = 5.1$, $\tau = 1.0$) and $\gamma > \delta(1 + \tau)$ (**b**, values for parameters: $\delta = 5.0$, $\gamma = 11.0$, $\mu = 0.6$, $\tau = 1.0$).

When $\mu < \delta$ and $\gamma < \delta(1 + \tau)$, instead, we need to look at the prey component of the positive equilibria, which is found by solving, from (3.2) and (3.3),

$$\delta u - \frac{\gamma u}{1 + \tau v} - \mu = 0 \quad \text{with} \quad v = 1 - u :$$

substituting the expression for v into the first equation, we get

$$\delta\tau u^2 + (\gamma - \delta - \tau(\delta + \mu))\, u + \mu\,(1 + \tau) = 0 \tag{3.4}$$

The number of coexistence equilibria depends on the sign of the discriminant of Equation (3.4); in particular, we have two equilibria if and only if it is positive.
This does not mean, of course, that both intersections are acceptable; as a consequence,

when we find a region in the parameter space where $\Delta > 0$, we also have to check which of these equilibria are actually meaningful for the situation considered.
The discriminant turns out to be a quadratic expression in μ, namely

$$\Delta = \tau^2\mu^2 - 2\tau\left(\tau\delta + \gamma + \delta\right)\mu + \left(\gamma - \delta - \delta\tau\right)^2 ; \tag{3.5}$$

its two roots are given by

$$\begin{aligned} \mu_\pm &= \delta + \frac{\gamma+\delta}{\tau} \pm \frac{1}{\tau}\sqrt{\left(\tau\delta+\gamma+\delta\right)^2 - \left(\gamma-\delta-\tau\delta\right)^2} \\ &= \delta + \frac{\gamma+\delta}{\tau} \pm \frac{2\sqrt{\gamma\delta(1+\tau)}}{\tau} : \end{aligned}$$

therefore the discriminant is positive (i.e. the isoclines intersect twice) if and only if either $\mu < \mu_-$ or $\mu > \mu_+$. But, since μ_+ is clearly larger than δ whatever the value of γ (and we have already seen that for $\mu > \delta$ no meaningful equilibrium appears) we are only interested in studying what happens with respect to μ_-, which from now on we are going to call $\mu^* = \mu^*(\gamma)$:

$$\mu^*(\gamma) = \delta + \frac{\gamma+\delta}{\tau} - \frac{2\sqrt{\gamma\delta(1+\tau)}}{\tau} . \tag{3.6}$$

Since we are in the region where $\mu < \delta$, $\gamma < \delta(1+\tau)$, we notice that

$$\begin{aligned} \mu^*(\gamma) &= \delta + \frac{\gamma+\delta}{\tau} - \frac{2\sqrt{\gamma\delta(1+\tau)}}{\tau} < \delta \\ &\Leftrightarrow \quad \gamma^2 - 2\delta(1+2\tau)\gamma + \delta^2 < 0 , \end{aligned}$$

which is true if and only if

$$\delta(1+2\tau) - 2\delta\sqrt{\tau(\tau+1)} < \gamma < \delta(1+\tau) .$$

We also point out that $0 < \delta(1+2\tau) - 2\delta\sqrt{\tau(\tau+1)} < \delta$.
Another property of $\mu^*(\gamma)$ is that

$$\begin{aligned} (\mu^*)'(\gamma) &= \frac{1}{\tau} - \frac{2\sqrt{\delta(1+\tau)}}{\tau}\frac{1}{2\sqrt{\gamma}} = 0 \\ &\Leftrightarrow \quad \sqrt{\gamma} - \sqrt{\delta(1+\tau)} = 0 \\ &\Leftrightarrow \quad \gamma = \delta(1+\tau) . \end{aligned}$$

The point where the slope of $\mu^*(\gamma)$ is zero is therefore

$$\left(\delta(1+\tau), \mu^*(\delta(1+\tau))\right) = \left(\delta(1+\tau), 0\right) ,$$

(that is, $\mu^*(\gamma)$ is tangent to the γ-axis in $\gamma = \delta(1+\tau)$).

Finally, we want to know the reciprocal position between $\mu = \mu^*(\gamma)$ and $\mu = \delta - \gamma$:

$$\delta - \gamma \;=\; \delta + \frac{\gamma+\delta}{\tau} - \frac{2\sqrt{\gamma\delta(1+\tau)}}{\tau}$$

if and only if $\gamma(1+\tau)+\delta = 2\sqrt{\gamma\delta(1+\tau)}$ or, equivalently, if and only if

$$\gamma = \frac{\delta}{1+\tau}\,;$$

this means that the two curves are tangent in $(\gamma,\mu) = (\delta/(1+\tau), \delta\tau/(1+\tau))$.

Thus we can state the following

Proposition 3.1 *The isoclines related to system* (3.1) *intersect twice (i.e., the discriminant* (3.5) *of* (3.4) *is larger than zero) if and only if one of the two possibilities below holds:*

1. *either* $\begin{cases} 0 < \gamma < \delta(1+2\tau) - 2\delta\sqrt{\tau(\tau+1)} \\ 0 < \mu < \delta \end{cases}$ *;*
2. *or* $\begin{cases} \delta(1+2\tau) - 2\delta\sqrt{\tau(\tau+1)} < \gamma < \delta(1+\tau) \\ 0 < \mu < \mu^*(\gamma) \end{cases}$ *.*

This can be represented on the γ–μ plane, as shown in Figure 3.2.

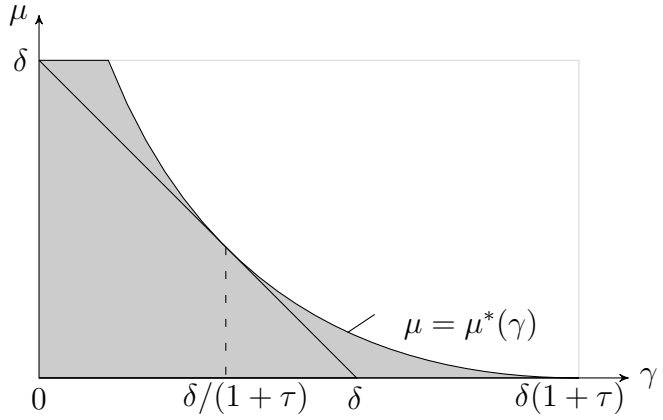

Figure 3.2: In gray, the region of $[0, \delta(1+\tau)] \times [0, \delta]$ on the γ–μ plane where $\Delta > 0$. The remainder is characterized by $\Delta < 0$ instead. The expression for $\mu^*(\gamma)$ is given in Equation (3.6).

To check the results above, if we take the parameters such that the corresponding point on the γ–μ plane lies outside the gray part in Figure 3.2, then no intersection occurs: an example is shown in Figure 3.3.

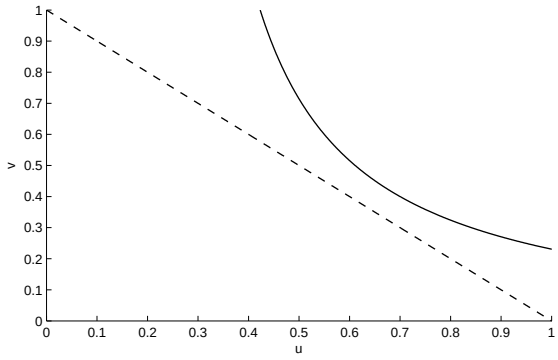

Figure 3.3: Example of isoclines of system (3.1) for the case $\mu^*(\gamma) < \mu < \delta$, $\gamma < \delta(1+\tau)$ (values for parameters: $\delta = 5.0$, $\gamma = 4.8$, $\mu = 1.1$, $\tau = 1.0$).

3.2 Acceptability of isoclines intersections

Now we focus our attention on the region where (3.5) is positive and check the acceptability of the two solutions of (3.4); otherwise stated, we want to find assumptions under which $0 < u_-^* , u_+^* < 1$.

Condition $u_-^* > 0$ is almost straightforward; in fact, it is satisfied if and only if (3.4) evaluated at $u = 0$ is positive and this point lies on the left-hand side of the vertex of the parabola; that is, if and only if

$$\begin{cases} \mu(1+\tau) > 0 \\ \dfrac{\delta - \gamma + \tau(\delta+\mu)}{2\tau\delta} > 0 \end{cases} .$$

The first inequality is obviously true; the second one is verified if and only if $\gamma < \delta(1+\tau) + \tau\mu$, which is also true because here we are taking $\gamma < \delta(1+\tau)$.
This lets us conclude that u_-^* is always larger than zero, which in turn implies that u_+^* is always larger than zero too.

The case of condition $u_-^* < u_+^* < 1$ is more subtle.
Firstly, we want to find regions on the γ-μ plane such that both intersections are not acceptable (so that no coexistence steady state exists). To this end, it is sufficient to impose $u_-^* > 1$; this is verified if and only if (3.4) evaluated at $u = 1$ is positive and this point lies on the left-hand side of the vertex of the parabola:

$$\begin{cases} \gamma - \delta + \mu > 0 \\ \dfrac{\delta - \gamma + \tau(\delta+\mu)}{2\tau\delta} > 1 \end{cases} \quad \Leftrightarrow \quad \begin{cases} \mu > \delta - \gamma \\ \gamma < \delta + \tau(\mu - \delta) \end{cases} .$$

Now, the quantity $\delta + \tau(\mu - \delta)$ is surely smaller than δ, because $\mu < \delta$; but

$$\frac{\delta}{1+\tau} < \delta + \tau(\mu - \delta) \quad \Leftrightarrow \quad \mu > \frac{\tau\delta}{1+\tau} \; .$$

Remember that $\mu = \tau\delta/(1+\tau)$ is the value corresponding to the point where $\mu = \mu^*(\gamma)$ and $\mu = \delta - \gamma$ are tangent; therefore the inequality above is satisfied only when $\gamma < \delta/(1+\tau)$, which also implies that

$$\gamma < \delta + \tau(\mu - \delta)$$

is true. In short, the region in the parameter space γ–μ with $\gamma < \delta/(1+\tau)$ and $\delta - \gamma < \mu < \mu^*(\gamma)$ gives no acceptable coexistence steady state.
An example is shown in Figure 3.4.

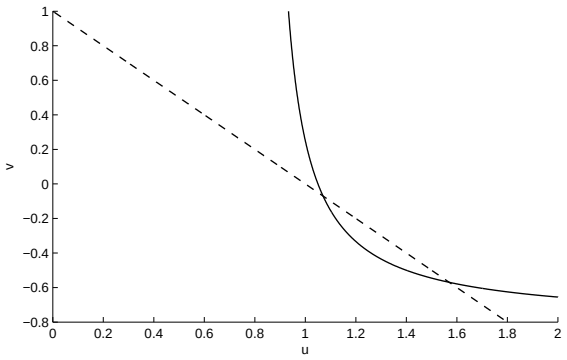

Figure 3.4: Example of isoclines of system (3.1) for the case $\delta - \gamma < \mu < \mu^*(\gamma)$, $\gamma < \delta/(1+\tau)$ (values for parameters: $\delta = 5.0$, $\gamma = 1.0$, $\mu = 4.2$, $\tau = 1.0$).

The second step is to find out when only one of the intersections between the isoclines is acceptable, that is, $u_-^* < 1$ and $u_+^* > 1$; this means that (3.4) evaluated at $u = 1$ has to be negative:

$$\gamma - \delta + \mu < 0 \; \Leftrightarrow \; \mu < \delta - \gamma \, .$$

So the region $\mu < \delta - \gamma$ gives only one acceptable equilibrium (the one with the smallest u^*): see for example Figure 3.5.

Finally, we need to verify if the remaining part of the γ–μ plane where the discriminant (3.5) is positive, i.e.

$$\frac{\delta}{1+\tau} < \gamma < \delta(1+\tau) \; , \; \delta - \gamma < \mu < \mu^*(\gamma) \, ,$$

is characterized by the acceptability of both steady states.
Similarly to what we have previously done, we impose that (3.4) evaluated at $u = 1$ is

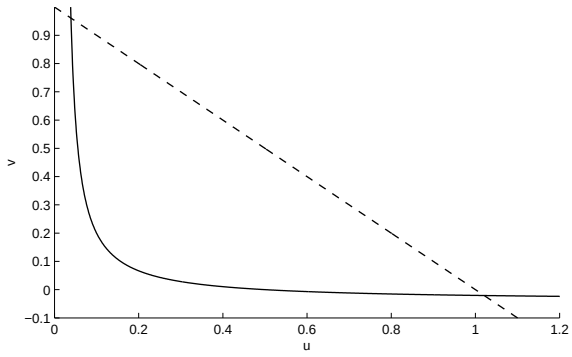

Figure 3.5: Example of isoclines of system (3.1) for the case $\mu < \delta - \gamma$ (values for parameters: $\delta = 5.0$, $\gamma = 4.8$, $\mu = 0.1$, $\tau = 1.0$).

positive and that this point lies on the right-hand side of the vertex of the parabola:

$$\begin{cases} \gamma - \delta + \mu > 0 \\ \dfrac{\delta - \gamma + \tau(\delta + \mu)}{2\tau\delta} < 1 \end{cases} \quad \Leftrightarrow \quad \begin{cases} \mu > \delta - \gamma \\ \gamma > \delta + \tau(\mu - \delta) \end{cases} .$$

In this region

$$\gamma > \delta + \tau(\mu - \delta)$$

holds (because this inequality is satisfied if and only if $\mu < \delta\tau/(1+\tau)$, which is true here); therefore both u^*_- and u^*_+ are smaller than one, and so the corresponding steady states are both acceptable, as can be seen in Figure 3.6.

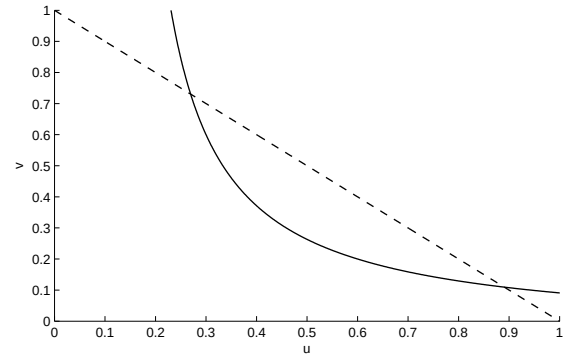

Figure 3.6: Example of isoclines of system (3.1) for the case $\delta/(1+\tau) < \gamma < \delta(1+\tau)$, $\delta - \gamma < \mu < \mu^*(\gamma)$ (values for parameters: $\delta = 5.0$, $\gamma = 4.8$, $\mu = 0.6$, $\tau = 1.0$).

Therefore, we sum up our study on the existence and acceptability of internal equilibria in the following

Proposition 3.2 *Consider the region of the γ-μ plane where the isoclines of system* (3.1) *intersect twice, as given by Proposition 3.1. Then the number of acceptable internal steady states is:*

- zero *for* $\begin{cases} 0 < \gamma < \dfrac{\delta}{1+\tau} \\ \\ \delta - \gamma < \mu < \mu^*(\gamma) \end{cases}$;
- one *for* $\begin{cases} 0 < \gamma < \delta \\ 0 < \mu < \delta - \gamma \end{cases}$;
- two *for* $\begin{cases} \dfrac{\delta}{1+\tau} < \gamma < \delta(1+\tau) \\ \\ \delta - \gamma < \mu < \mu^*(\gamma) \end{cases}$.

Figure 3.7 is a representation on the γ–μ plane of this result.
In this way, given a certain combination of parameters for the problem, we are able to determine how many steady states, other than the trivial ones, the spatially homogeneous system has.

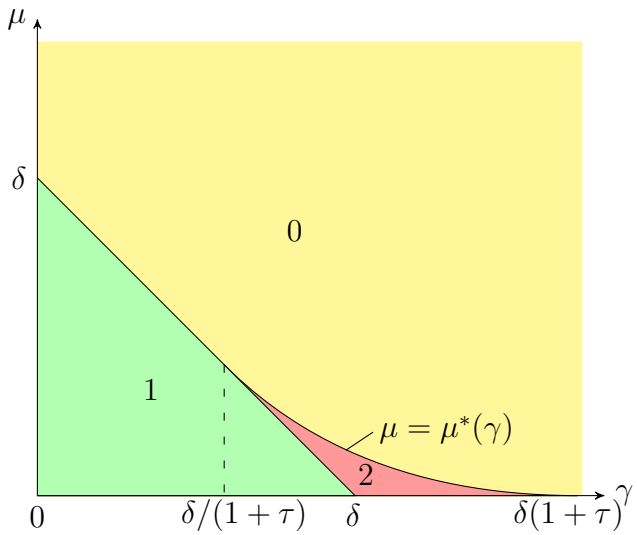

Figure 3.7: Number of coexistence steady states on the γ–μ plane: zero (yellow), one (green) or two (red).

Chapter 4

Analysis of the behavior of the homogeneous model

In the previous chapter we have analyzed the existence of steady states. We are now concerned with their stability and with the behaviors of the solutions in large.

4.1 Stability of $(0,0)$ and $(1,0)$

First of all we consider the zero–steady state $(0,0)$ and the bacteria–only state $(1,0)$. The respective Jacobian matrices for these states are

$$J(0,0) = \begin{pmatrix} 1 & 0 \\ 0 & -\mu \end{pmatrix}, \; J(1,0) = \begin{pmatrix} -1 & -1 \\ 0 & \delta - \gamma - \mu \end{pmatrix}.$$

Consequently, $(0,0)$ is unstable for all values of the parameters, since the eigenvalues at this steady state are 1 and $-\mu < 0$.
When considering $J(1,0)$, instead, the eigenvalues are -1 and $\delta - \gamma - \mu$: therefore when this second quantity is negative, $(1,0)$ is stable, while it is unstable otherwise.

We can conclude

Lemma 4.1 $(0,0)$ *is always unstable;* $(1,0)$ *is stable if* $\delta - \gamma < \mu$ *and unstable otherwise.*

We notice that $(0,0)$ and $(1,0)$ (when unstable) are saddle points.

The analysis of stability for the internal steady states (u^*, v^*) is performed in the following sections.

4.2 Stability of coexistence steady states

Showing the stability of the coexistence steady states is not so straightforward: this is largely due to the fact that the algebraic expressions for u^* and v^* are quite complex, and substitution into the Jacobian matrix

$$J(E^*) = \begin{pmatrix} -u^* & -u^* \\ \left(\delta - \dfrac{\gamma}{1+\tau v^*}\right) v^* & \dfrac{\gamma\tau u^* v^*}{(1+\tau v^*)^2} \end{pmatrix}, \tag{4.1}$$

does not help.
However, we will provide some conditions to determine the sign of trace and determinant of $J(E^*)$.
In fact, we have

$$\mathrm{tr}J(E^*) = u^* \left(-1 + \frac{\gamma\tau v^*}{(1+\tau v^*)^2}\right) \tag{4.2}$$

$$\det J(E^*) = \frac{u^* v^*}{(1+\tau v^*)^2} \left(-\gamma\tau u^* + \delta(1+\tau v^*)^2 - \gamma(1+\tau v^*)\right) . \tag{4.3}$$

Noticing that $\mathrm{tr}J(E^*)$ is negative if and only if

$$\tau^2 v^{*2} + \tau(2-\gamma)v^* + 1 > 0\,, \tag{4.4}$$

and since the discriminant of the quadratic polynomial above is $\Delta = \tau^2\gamma(\gamma-4)$, we have two possibilities:

(T1) if $\gamma < 4$, then $\mathrm{tr}J(E^*) < 0$;

(T2) if $\gamma > 4$, then $\mathrm{tr}J(E^*) < 0$ if and only if either $v^* < v_1$ or $v^* > v_2$ where $v_{1/2}$ are the roots of the quadratic polynomial in (4.4), i.e.

$$v_{1/2} = \frac{\gamma - 2 \pm \sqrt{\gamma(\gamma-4)}}{2\tau} \tag{4.5}$$

Concerning $\det J(E^*)$, we have that it is positive if and only if

$$\delta\tau^2 v^{*2} + 2\delta\tau v^* + \delta - \gamma - \gamma\tau > 0\,. \tag{4.6}$$

Since in this case the discriminant $\Delta = \delta\gamma\tau^2(\tau+1)$ is positive, we have two situations depending on the sign of the y-intercept:

(D1) if $\gamma < \delta/(1+\tau)$, then $\det J(E^*) > 0$;

(D2) if $\gamma > \delta/(1+\tau)$, then $\det J(E^*) > 0$ if and only if

$$v^* > v_3 = \frac{\gamma - 2 \pm \sqrt{\gamma(\gamma-4)}}{2\tau} \tag{4.7}$$

Note that v_3 is the only positive root of the quadratic polynomial (4.6).

Therefore, depending on the value assumed by γ, possibly with some additional conditions E^* changes its stability. In particular, the value $\gamma = \dfrac{\delta}{1+\tau}$ is involved in conditions **(D)** and corresponds to the point of the γ-μ plane where the curves $\mu = \delta - \gamma$ and $\mu = \mu^*(\gamma)$ are tangent (see Figure 3.7).
Thus we have different situations depending on whether $\delta/(1+\tau)$ is larger or less than 4. Therefore, keeping in mind Figure 3.7, we need to consider three situations:

$$\frac{\delta}{1+\tau} < 4 < \delta\,, \qquad \frac{\delta}{1+\tau} < \delta < 4\,, \qquad 4 < \frac{\delta}{1+\tau} < \delta.$$

corresponding to a), b) and c) in Figure 4.1 respectively.

We can immediately notice that, due to **(T1)** and **(D1)**, the following statement holds:

Proposition 4.1 *The unique steady state corresponding to regions (a,I), (b,I) and (c,I) in Figure 4.1 is stable.*

For all the other regions we need to analyze in detail conditions **(T2)** and **(D2)**.

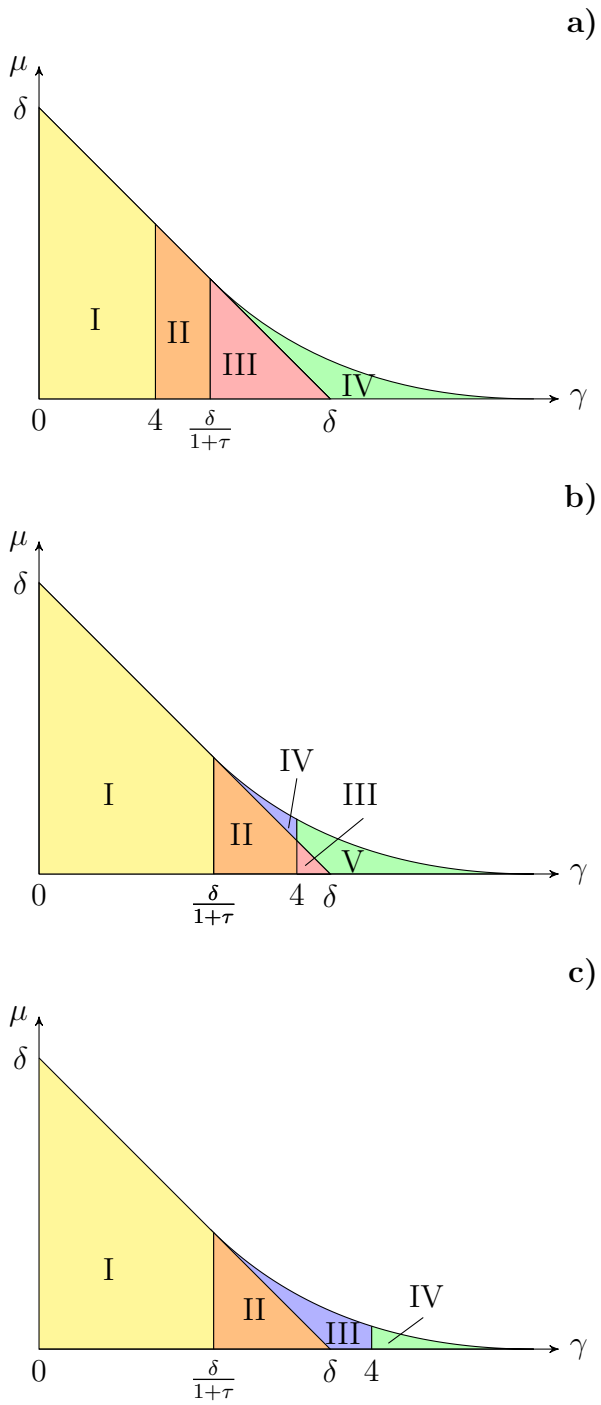

Figure 4.1: Subdivision of the region of the γ–μ plane where internal steady states exist, according to conditions **(T)** and **(D)**. The three graphs differ for the mutual position of $\delta/(1+\tau)$, 4 and δ on the γ-axis. Regions marked with (I) correspond to conditions **(T1)**-**(D1)**; regions (b,II) and (c,II): conditions **(T1)**-**(D2)** region (a,II): conditions **(T2)**-**(D1)**; regions (a,III) and (b,III): conditions **(T2)**-**(D2)**; regions (b,IV) and (c,III): conditions **(D2)**; (a,IV), (b,V) and (c,IV): conditions **(T2)**-**(D2)**.

4.3 Regions (b,II) and (c,II)

Here we consider regions (b,II) and (c,II), where only one internal steady state exists, **(T1)** is satisfied and $\gamma > \delta/(1+\tau)$.
We remind that, in condition (4.7), v^* is the (unique) positive root of

$$p(v) = \delta\tau v^2 + [\tau(\mu-\delta) + \delta - \gamma]\, v + \gamma - \delta + \mu\,. \tag{4.8}$$

Since the algebraic expression of v^* is quite complex, instead of comparing v^* and v_3 directly, we evaluate the polynomial $p(v)$ at $v = v_3$ (see Equation (4.7)): clearly, $v^* > v_3$ whenever the resulting value is negative, otherwise the reverse inequality holds.

By substituting (4.7) into (4.8) we get

$$\begin{aligned} p(v_3) &= \delta\tau\left(\frac{1}{\tau^2} + \frac{\delta\gamma(1+\tau)}{\delta^2\tau^2} - \frac{2}{\delta\tau^2}\sqrt{\delta\gamma(1+\tau)}\right) \\ &\quad + (\tau(\mu-\delta) + \delta - \gamma)\left(-\frac{1}{\tau} + \frac{\sqrt{\delta\gamma(1+\tau)}}{\delta\tau}\right) + \gamma - \delta + \mu\,, \end{aligned}$$

and after some algebra we have

$$p(v_3) = 2\gamma\frac{1+\tau}{\tau} - \frac{\gamma - \mu\tau + \delta\tau + \delta}{\delta\tau}\sqrt{\gamma\delta(1+\tau)}\;.$$

This quantity is negative if and only if

$$\frac{\tau}{\delta}\sqrt{\gamma\delta(1+\tau)}\mu \;<\; \sqrt{\gamma\delta(1+\tau)}\left(\tau + 1 + \frac{\gamma}{\delta}\right) - 2\gamma(1+\tau)\;,$$

that is, if and only if

$$\begin{aligned} \mu &< \delta\frac{\tau+1}{\tau} + \frac{\gamma}{\tau} - 2\gamma\delta\frac{1+\tau}{\tau}\frac{1}{\sqrt{\gamma\delta(1+\tau)}} \\ &= \delta + \frac{\gamma+\delta}{\tau} - \frac{2\sqrt{\gamma\delta(1+\tau)}}{\tau} \\ &= \mu^*(\gamma)\,, \end{aligned} \tag{4.9}$$

where $\mu^*(\gamma)$ has been defined in (3.6).
(4.9) is certainly true, because the existence of positive steady states is guaranteed only for $\mu < \mu^*(\gamma)$, and here in particular $\mu < \delta - \gamma < \mu^*(\gamma)$ (see Section 3.1). Therefore, polynomial in (4.8) evaluated at $v = v_3$ is negative and we can conclude that $v^* > v_3$ in regions (a,II) and (b,II), so that E^* is stable.
Such results are summarized in the following proposition:

Proposition 4.2 *The unique positive steady state E^* corresponding to regions (b,II) and (c,II) is always stable.*

4.4 Regions (a,II), (a,III) and (b,III)

In region (a,II) we have the existence of only one steady state and $4 < \gamma < \dfrac{\delta}{1+\tau}$; so we have to consider condition **(T2)**.
We use the same method seen in Section 4.3: v^* is less than v_1 if and only if $p(v_1)$ is positive; v^* is larger than v_2 if and only if $p(v_2)$ is negative.

Looking at (4.4), we have that v_1 satisfies

$$\tau^2 v_1^2 = \tau(\gamma-2)v_1 - 1 \ ,$$

so we can use this property[1] when evaluating $p(v_1)$:

$$p(v_1) = \delta\tau(\gamma-2)v_1 - \delta + \left(\tau^2(\mu-\delta) + \tau(\delta-\gamma)\right) v_1 + \tau(\gamma-\delta+\mu)\,;$$

substituting the expression for v_1 and rearranging terms, the quantity above can be written as

$$p(v_1) = \frac{1}{2}\left[\delta\gamma^2 - \gamma^2 - 3\delta\gamma + 2\gamma + \tau(\mu\gamma - \delta\gamma + 2\gamma) - (\delta\gamma - \delta - \gamma + \tau(\mu-\delta))\sqrt{\gamma(\gamma-4)}\right] \ ,$$

which is positive if and only if

$$\left(\tau\gamma - \tau\sqrt{\gamma(\gamma-4)}\right)\mu > (\delta\gamma - \delta - \gamma - \tau\delta)\sqrt{\gamma(\gamma-4)} + \gamma^2 - \delta\gamma^2 + 3\delta\gamma - 2\gamma + \tau\delta\gamma - 2\tau\gamma\,,$$

that is, if and only if

$$\begin{aligned} \mu &> \frac{1}{2\tau}\left((\delta-(1+\tau))\sqrt{\gamma(\gamma-4)} - \delta\gamma + \gamma - \tau\gamma + 2\delta + 2\tau\delta\right) && (4.10)\\ &= \delta - \gamma + \frac{1}{2\tau}\left((\delta-(1+\tau))\sqrt{\gamma(\gamma-4)} - \delta\gamma + \gamma + \tau\gamma + 2\delta\right) \ . && (4.11)\end{aligned}$$

For conciseness we call $\eta_1(\gamma)$ the previous expression:

$$\begin{aligned} \eta_1(\gamma) &= \delta - \gamma + \frac{1}{2\tau}\left((\delta-(1+\tau))\sqrt{\gamma(\gamma-4)} + \gamma(1+\tau-\delta) + 2\delta\right)\\ &= \delta - \gamma + \varepsilon_1(\gamma) && (4.12)\end{aligned}$$

where

$$\varepsilon_1(\gamma) = \frac{1}{2\tau}\left((\delta-(1+\tau))\sqrt{\gamma(\gamma-4)} + \gamma(1+\tau-\delta) + 2\delta\right) \ . \qquad (4.13)$$

Figure 4.2 shows the graph of $\varepsilon_1(\gamma) = 0$ as a function of γ and δ.
From (4.12) we notice that (4.10) is never satisfied whenever $\varepsilon_1(\gamma) > 0$, because from this

[1] this of course is not necessary: it is just for convenience during calculations.

condition $\eta_1(\gamma) > \delta - \gamma$ follows, while in the case of one acceptable steady state $\mu < \delta - \gamma$ must necessarily hold.
On the contrary, if $\varepsilon_1(\gamma) < 0$, then $\eta_1(\gamma) < \delta - \gamma$, therefore condition (4.10) becomes $\eta_1(\gamma) < \mu < \delta - \gamma$.

Summarizing:

$$v^* < v_1 \;\Leftrightarrow\; \begin{cases} \varepsilon_1(\gamma) < 0 \\ \eta_1(\gamma) < \mu < \delta - \gamma \end{cases} . \tag{4.14}$$

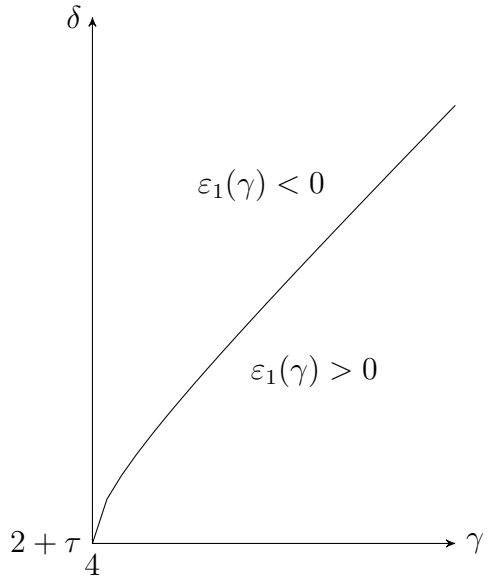

Figure 4.2: Subdivision of the parameter space γ-δ into zones where $\varepsilon_1(\gamma)$ is positive or negative. In the former case $v^* > v_1$ and so stability is ensured if $v^* > v_2$; in the latter case, from (4.14) we need also check that $\eta_1(\gamma) < \mu < \delta - \gamma$.

If we are in a situation where v^* can not be less than v_1 (i.e., if either $\varepsilon_1(\gamma) > 0$ or $\mu < \eta_1(\gamma)$), then we need to check if $v^* > v_2$ holds (at least for some choices of parameters). The procedure is the same used for v_1: we evaluate $p(v_2)$ and impose it to be negative; knowing that

$$\tau^2 v_2^2 = \tau(\gamma - 2)v_2 - 1\,,$$

we have

$$p(v_2) = \delta\tau(\gamma - 2)v_2 - \delta + \left(\tau^2(\mu - \delta) + \tau(\delta - \gamma)\right) v_2 + \tau(\gamma - \delta + \mu)$$

which (substituting the expression for v_2) is equivalent to

$$p(v_2) = \frac{1}{2}\left[\delta\gamma^2 - \gamma^2 - 3\delta\gamma + 2\gamma + \tau(\mu\gamma - \delta\gamma + 2\gamma) + (\delta\gamma - \delta - \gamma + \tau(\mu - \delta))\sqrt{\gamma(\gamma - 4)}\right] .$$

Thus, $p(v_2) < 0$ if and only if

$$\left(\tau\gamma + \tau\sqrt{\gamma(\gamma-4)}\right)\mu < (\delta+\gamma+\tau\delta-\delta\gamma)\sqrt{\gamma(\gamma-4)} + \gamma^2 - \delta\gamma^2 + 3\delta\gamma - 2\gamma + \tau\delta\gamma - 2\tau\gamma\,,$$

i.e., if and only if

$$\begin{aligned}\mu &< \frac{1}{2\tau}\left((1+\tau-\delta)\sqrt{\gamma(\gamma-4)} - \delta\gamma + \gamma - \tau\gamma + 2\delta + 2\tau\delta\right) \\ &= \delta - \gamma + \frac{1}{2\tau}\left((1+\tau-\delta)\sqrt{\gamma(\gamma-4)} + \gamma(1+\tau-\delta) + 2\delta\right)\,. \end{aligned} \tag{4.15}$$

Similarly to what we have already done for v_1, we call

$$\begin{aligned}\eta_2(\gamma) &= \delta - \gamma + \frac{1}{2\tau}\left((1+\tau-\delta)\sqrt{\gamma(\gamma-4)} + \gamma(1+\tau-\delta) + 2\delta\right) \\ &= \delta - \gamma + \varepsilon_2(\gamma) \end{aligned} \tag{4.16}$$

where

$$\varepsilon_2(\gamma) = \frac{1}{2\tau}\left((1+\tau-\delta)\sqrt{\gamma(\gamma-4)} - \delta\gamma + \gamma + \tau\gamma + 2\delta\right)\,. \tag{4.17}$$

$\varepsilon_2(\gamma) = 0$ as a function of γ and δ is represented in Figure 4.3.
Obviously, if $\varepsilon_2(\gamma) > 0$, $\eta_2(\gamma)$ is larger than $\delta - \gamma$; this implies that (4.15) is satisfied, because, again, $\mu < \delta - \gamma$ here. Otherwise, $\eta_2(\gamma) < \delta - \gamma$.
In short,

$$v^* > v_2 \;\Leftrightarrow\; \text{either}\;\; \varepsilon_2(\gamma) > 0 \;\;\text{or}\;\; \begin{cases} \varepsilon_2(\gamma) < 0 \\ \mu < \eta_2(\gamma) \end{cases}\,. \tag{4.18}$$

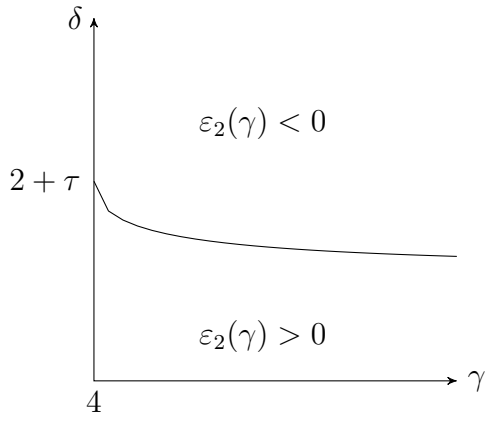

Figure 4.3: Subdivision of the parameter space γ-δ into zones where $\varepsilon_2(\gamma)$ is positive or negative. In the former case $v^* > v_2$ and so E^* is stable; in the latter case, from (4.18) we have that we need also check if $\mu < \eta_2(\gamma)$.

Now let us look at the other two regions. namely (a,III) and (b,III). They are characterized by a unique internal steady state and

$$\max\left\{4, \frac{\delta}{1+\tau}\right\} < \gamma < \delta\,.$$

The calculations necessary to prove that the Jacobian matrix has positive determinant are the same as in Sections 4.3, whereas for showing when the trace is negative we follow the procedure that we have just seen in the first part of this Section for region (a,II); consequently, in this zone of the γ–μ plane the determinant is always positive, and therefore E^* is stable if at least one between (4.14) and (4.18) holds.

Summarizing, we have the following

Proposition 4.3 *The unique steady state corresponding to regions (a,II), (a,III) and (b,III) is stable if and only if one of the following alternatives holds:*

1. $\begin{cases} \varepsilon_1(\gamma) < 0 \\ \eta_1(\gamma) < \mu < \delta - \gamma \end{cases}$;
2. $\varepsilon_2(\gamma) > 0$;
3. $\begin{cases} \varepsilon_2(\gamma) < 0 \\ \mu < \eta_2(\gamma) \end{cases}$.

This result is represented in Figure 4.4.

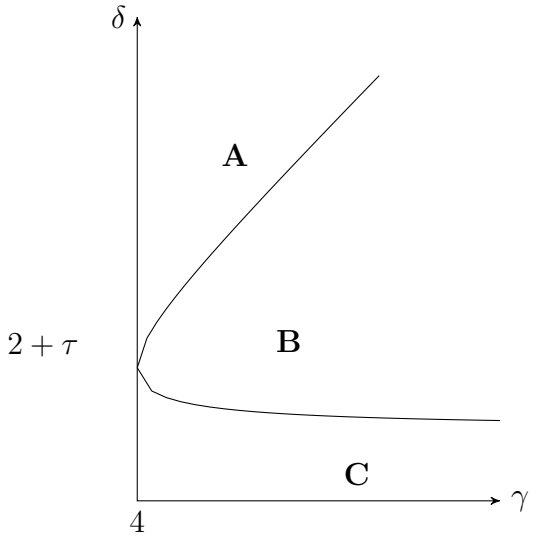

Figure 4.4: Stability regions on the parameter space γ-δ for cases (a,II), (a,III) and (b,III). Region **A**: E^* stable if $\eta_1(\gamma) < \mu < \delta - \gamma$. Region **B**: E^* stable if $\mu < \eta_2(\gamma)$. Region **C**: E^* stable.

4.5 Regions (b,IV) and (c,III)

In regions (b,IV) and (c,III) there are two internal steady states, **(T1)** is satisfied (because $\gamma < 4$) and **(D2)** is the condition to be verified for stability to be guaranteed.

Here we have to take into account the fact that there are two coexistence states E^*_- and E^*_+, whose second components will be from now on called v^*_- and v^*_+; we remind that $v^*_\pm$ are the two (positive) roots of $p(v)$ (see Equation (4.8)), and that $v^*_- < v^*_+$.
In Section 4.3 we proved that $p(v_3) < 0$ if and only if $\mu < \mu^*(\gamma)$, which is the case for the regions of the γ-μ plane under consideration. This means that v_3 lies between v^*_- and v^*_+; consequently, we have that $v^*_+ > v_3$ and $v^*_- < v_3$, i.e., E^*_+ is stable and E^*_- is unstable (in particular, it is a saddle point).

Proposition 4.4 *In regions (b,IV) and (c,III), the steady state E^*_- is unstable, while E^*_+ is always stable.*

Notice that here both $(1, 0)$ and E^*_+ are stable; this means that there are two basins of attraction, separated by the stable manifold of the unstable equilibrium E^*_-, and the behavior of a trajectory depends on where it originates. Figure 4.5 shows such examples: in both **a** and **b** there are two internal steady states; E^*_- is unstable while E^*_+ (which is about $(0.468826, 0.531173)$ in the first plot and $(0.187004, 0.812995)$ in the second) is stable. Notice that solid trajectories tend to E^*_+ and dashed ones tend to the bacteria-only state $(1, 0)$.

4.6 Regions (a,IV), (b,V) and (c,IV)

Here we have two internal steady states and we have to consider **(T2)** and **(D2)**.
As regards the condition on the determinant, what we said in the previous section is still valid; thus we can immediately deduce that E^*_- is unstable (again, a saddle point), because at least one of the two properties required (namely, the one on the determinant) is never satisfied when evaluating $J(E^*_-)$.
We can now focus our attention on the other steady state, E^*_+. From Section 4.5 we already have that **(D2)** is satisfied by E^*_+, so we need only check **(T2)**. We will follow the approach seen in Section 4.4.

First of all we investigate the possibility of having $v^*_+ < v_1$. Here imposing $p(v_1) > 0$ is necessary but not sufficient, because also the points on the left of v^*_- satisfy this condition but of course are smaller than v^*_+. Therefore, there is another property to be verified: v_1

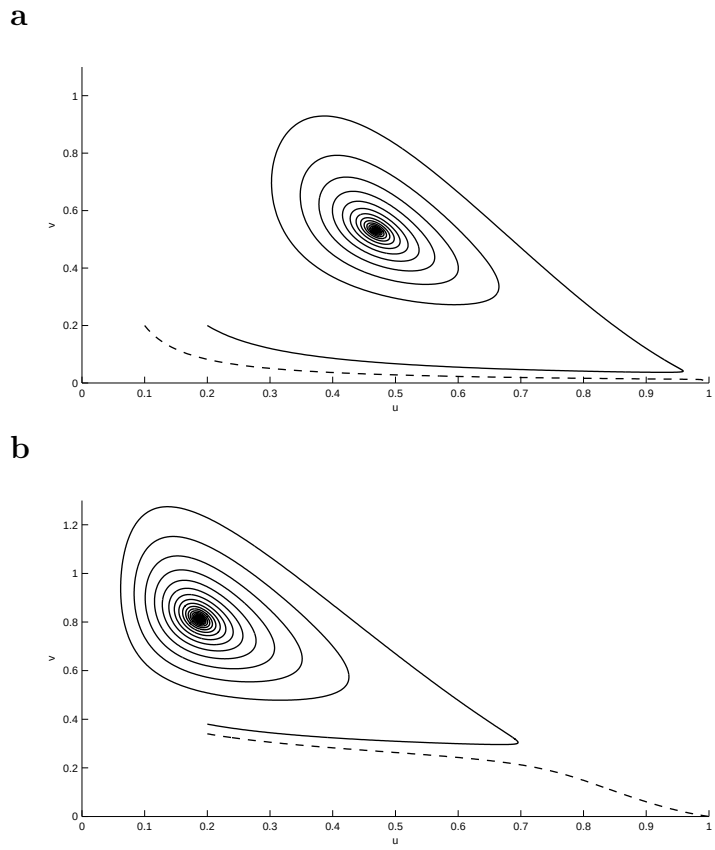

Figure 4.5: Two examples showing that, when E_+^* is stable, the behavior of trajectories depends on their starting points. **a** (case (b,IV)): $\delta = 5.0$, $\gamma = 3.9$, $\mu = 1.5$, $\tau = 1.0$; starting points: $(0.2, 0.2)$ (solid line) and $(0.1, 0.2)$ (dashed line). **b** (case (c,III)): $\delta = 3.0$, $\gamma = 3.5$, $\mu = 0.2$, $\tau = 1.0$; starting points: $(0.2, 0.38)$ (solid line) and $(0.2, 0.34)$ (dashed line).

must lie on the right of the abscissa of the vertex of $p(v)$; that is,

$$v_+^* < v_1 \;\Leftrightarrow\; \begin{cases} p(v_1) > 0 \\ v_1 > \dfrac{\gamma - \delta + \tau(\delta - \mu)}{2\tau\delta} \end{cases} .$$

From the previous cases we know that $p(v_1) > 0$ is satisfied for $\eta_1(\gamma) < \mu < \mu^*(\gamma)$ when $\varepsilon_1(\gamma) > 0$, and for $\delta - \gamma < \mu < \mu^*(\gamma)$ (i.e., for all μ in these regions) when $\varepsilon_1(\gamma) < 0$ (remind that $\eta_1(\gamma)$ and $\varepsilon_1(\gamma)$ have been defined in (4.12) and (4.13) respectively).
In such cases we also have to impose v_1 to be larger than the abscissa of the vertex of $p(v)$:

$$v_1 = \frac{\gamma - 2 - \sqrt{\gamma(\gamma - 4)}}{2\tau} > \frac{\gamma - \delta + \tau(\delta - \mu)}{2\tau\delta} ,$$

which is true if and only if

$$\begin{aligned}\mu &> \frac{\delta}{\tau}\left[\gamma\left(\frac{1}{\delta}-1\right)+\tau+1+\sqrt{\gamma(\gamma-4)}\right] \\ &= \delta+\frac{\gamma+\delta}{\tau}+\frac{\delta}{\tau}\left(-\gamma+\sqrt{\gamma(\gamma-4)}\right).\end{aligned}$$

For conciseness let us set

$$\nu_1(\gamma)=\delta+\frac{\delta+\gamma}{\tau}+\frac{\delta}{\tau}\left(-\gamma+\sqrt{\gamma(\gamma-4)}\right), \tag{4.19}$$

so that

$$v_+^*<v_1 \;\Leftrightarrow\; \text{either } \begin{cases}\varepsilon_1(\gamma)<0\\ \nu_1(\gamma)<\mu<\mu^*(\gamma)\end{cases} \text{ or } \begin{cases}\varepsilon_1(\gamma)>0\\ \max\{\nu_1(\gamma),\eta_1(\gamma)\}<\mu<\mu^*(\gamma)\end{cases}. \tag{4.20}$$

We remind that determining whether $\varepsilon_1(\gamma)$ is positive or negative for a specific pair of parameters (γ,δ) is possible by looking at Figure 4.2.

When none of the possibilities in (4.20) is satisfied, we need to investigate the possibility of having $v_+^*>v_2$. Here two circumstances appear: if v_2 is on the left of the abscissa of the vertex, then surely $v_+^*>v_2$; otherwise, we have to impose a further condition, namely, $p(v_2)<0$.
Now, we find that

$$v_2=\frac{\gamma-2+\sqrt{\gamma(\gamma-4)}}{2\tau}<\frac{\gamma-\delta+\tau(\delta-\mu)}{2\tau\delta}$$

if and only if

$$\mu < \delta+\frac{\delta+\gamma}{\tau}-\frac{\delta}{\tau}\left(\gamma+\sqrt{\gamma(\gamma-4)}\right). \tag{4.21}$$

Therefore, calling

$$\nu_2(\gamma)=\delta+\frac{\delta+\gamma}{\tau}-\frac{\delta}{\tau}\left(\gamma+\sqrt{\gamma(\gamma-4)}\right), \tag{4.22}$$

we can state that, if we have a combination of parameters such that $\mu<\nu_2(\gamma)$, then E_+^* is stable; otherwise, for assuring stability of E_+^* we also have to check that $p(v_2)<0$.
This has already been done in Section 4.4: it must be $\mu<\eta_2(\gamma)$ where $\eta_2(\gamma)$ is the same as in Equation (4.16).
If $\varepsilon_2(\gamma)<0$ then $\eta_2(\gamma)<\delta-\gamma$, so in regions (a,IV), (b,V) and (c,IV) of the γ–μ plane $p(v_2)$ is always positive (and thus the steady state is unstable); on the other hand, if $\varepsilon_2(\gamma)>0$ then condition $\mu<\eta_2(\gamma)$ can be restated as $\delta-\gamma<\mu<\eta_2(\gamma)$. Remember that $\eta_2(\gamma)$ and $\varepsilon_2(\gamma)$ are as in Equations (4.16) and (4.17) respectively.

To summarize, when $v_+^* > v_1$, $\mathrm{tr}J(E_+^*)$ can still be negative if the following holds:

$$v_+^* > v_2 \;\Leftrightarrow\; \begin{array}{l} \text{either} \;\; \delta - \gamma < \mu < \min\{\mu^*(\gamma), \nu_2(\gamma)\} \\ \text{or} \;\; \left\{ \begin{array}{l} \varepsilon_2(\gamma) > 0 \\ \max\{\delta - \gamma, \nu_2(\gamma)\} < \mu < \eta_2(\gamma) \end{array} \right. \end{array} . \tag{4.23}$$

Proposition 4.5 *In regions (a,IV), (b,V) and (c,IV), E_-^* is unstable and E_+^* is stable if and only if one of the following holds:*

1. $\left\{ \begin{array}{l} \varepsilon_1(\gamma) < 0 \\ \nu_1(\gamma) < \mu < \mu^*(\gamma) \end{array} \right.$;
2. $\left\{ \begin{array}{l} \varepsilon_1(\gamma) > 0 \\ \max\{\nu_1(\gamma), \eta_1(\gamma)\} < \mu < \mu^*(\gamma) \end{array} \right.$;
3. $\delta - \gamma < \mu < \min\{\mu^*(\gamma), \nu_2(\gamma)\}$;
4. $\left\{ \begin{array}{l} \varepsilon_2(\gamma) > 0 \\ \max\{\delta - \gamma, \nu_2(\gamma)\} < \mu < \eta_2(\gamma) \end{array} \right.$.

Again, whenever conditions for E_+^* to be stable are satisfied, there are two attractors, so there are two basins of attraction divided by the stable manifold of the saddle point E_-^*.

4.7 Unstable coexistence steady states

In the previous section we found conditions under which a coexistence steady state is stable [2]. Now we focus on the case when all internal states are unstable.

First of all, for the general case we rule out the possibility of unbounded trajectories. In order to do so, we look at the direction of the vector field of the problem: for the first component

$$u' = u(1 - u - v) > 0 \;\Leftrightarrow\; v < 1 - u\,,$$

and for the second component

$$v' = v\left(\delta u - \mu - \frac{\gamma u}{1 + \tau v}\right) > 0 \;\Leftrightarrow\; v > \frac{(\gamma - \delta)u + \mu}{\tau(\delta u - \mu)}\,.$$

So the vector field points down and to the right below both isoclines; up and to the right in the region over the hyperbola and below the line; up and to the left above both isoclines; down and to the left in the region over the line and below the hyperbola.

[2] remember that, when there are two internal states, one is always unstable.

In particular, when a trajectory crosses the line $v = 1$ from below, then

$$u' < -u^2 < 0$$

that is, it always points to the left of the u-v space; so eventually it is forced to cross the hyperbola and then re-enter the region with $v < 1$.
Moreover, a trajectory can never cross the line $u = 1$, and it is also bounded by the coordinate axes (the vector field points down on the v-axis, left on the u-axis for $0 < u < 1$).
This means that every trajectory can be confined in some (possibly large) finite subset of the plane (also known as *trapping region*; see for example [39]), which might be described as $R = [\varepsilon, 1] \times [0, \rho]$, for proper values of $0 < \varepsilon \ll 1$ and $\rho > 0$ depending on the starting point of the trajectory.

This conclusion lets us apply a well-known tool in the study of dynamical systems: the Poincaré–Bendixson theorem (for a reference, see for instance Appendix A in [40]).

Theorem 4.1 (Poincaré–Bendixson theorem) *Let R be a closed, bounded subset of $\mathbb{R}^2$, $\dot{\mathbf{x}} = \mathbf{f}(\mathbf{x})$ a system of differential equations defined on an open set containing R.*
Suppose that R contains finitely many equilibria, and that a forward orbit $\phi(t, \mathbf{x_0})_{t \geq 0}$ starting at $\mathbf{x}(0) = \mathbf{x_0} \in R$ remains in R for all t.
Then the ω–limit set of $\mathbf{x_0}$ is either a fixed point or a periodic orbit.

Here we have finitely many equilibria (the bacteria-only state and one or two coexistence steady states, depending on the choice of parameters) belonging to R, which is properly chosen in order to contain $\phi(t, \mathbf{x_0})_{t \geq 0}$ for a given $\mathbf{x_0} \in R$.
Therefore, according to the Poincaré–Bendixson theorem, the trajectory must approach either a limit cycle or a fixed point.
Now we consider the different situations that may arise.

4.7.1 One coexistence steady state

In this case, the bacteria-only equilibrium is always unstable (see Section 4.1); if the coexistence steady state is unstable too (this event may occur in cases (a,II), (a,III) and (b,III), as we have seen in Section 4.4), then the only possibility is that trajectories approach a closed stable orbit.

4.7.2 Two coexistence steady states

When two internal steady states E^*_-, E^*_+ are admissible, we have that $(1, 0)$ is stable (Section 4.1) and E^*_- is unstable (Sections 4.5 and 4.6), while the stability of E^*_+ depends

on the specific choice of parameters; if it is unstable (in particular, an unstable node or focus[3]), then Poincaré-Bendixson theorem ensures that the ω-limit set for a trajectory is either an equilibrium or a limit cycle. The trapping region here includes the bacteria-only state which is stable, but it seems difficult here to apply tools such as the Bendixson-Dulac criterion (see Appendix A in [40]); therefore we cannot theoretically exclude the existence of closed orbits.
In fact, by performing numerical simulations we notice that both situations are possible: in some cases all trajectories reach $(1, 0)$; sometimes there exists a limit cycle such that if the starting point lies inside it, then the trajectory approaches it, while if the starting point lies outside, the trajectory approaches $(1, 0)$; or there are two basins of attraction for the points outside the limit cycle, such that trajectories starting from outside the limit cycle can either go to $(1, 0)$ or approach the limit cycle itself.
Figures 4.6 and 4.7 show some examples of these behaviors, by varying μ or γ respectively.

[3]it cannot be a saddle point since the determinant of the Jacobian matrix is always positive.

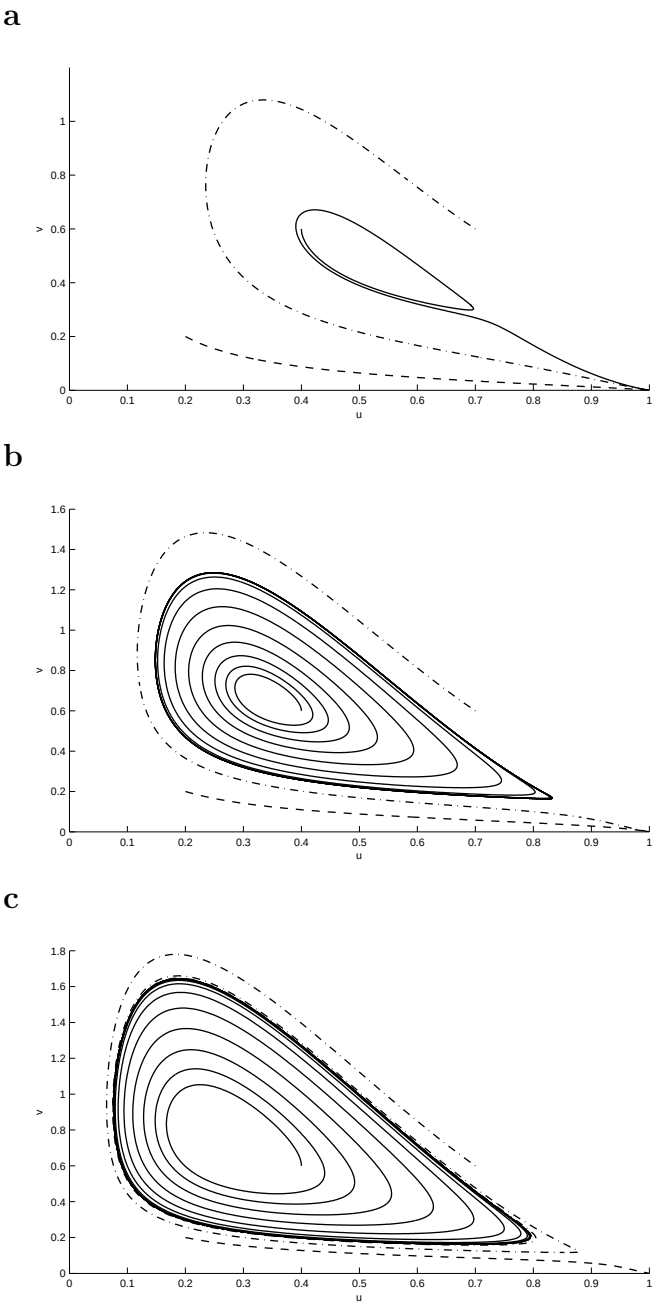

Figure 4.6: Trajectories for system (3.1) in the case of two unstable coexistence steady states when varying μ. Fixed parameters are: $\delta = 5.0$, $\gamma = 4.8$, $\tau = 1.0$. Starting points for trajectories: $(0.4, 0.6)$ (solid line), $(0.2, 0.2)$ (dashed line), $(0.7, 0.6)$ (dashed dotted line). **a** $\mu = 0.9$. **b** $\mu = 0.72$. **c** $\mu = 0.6$.

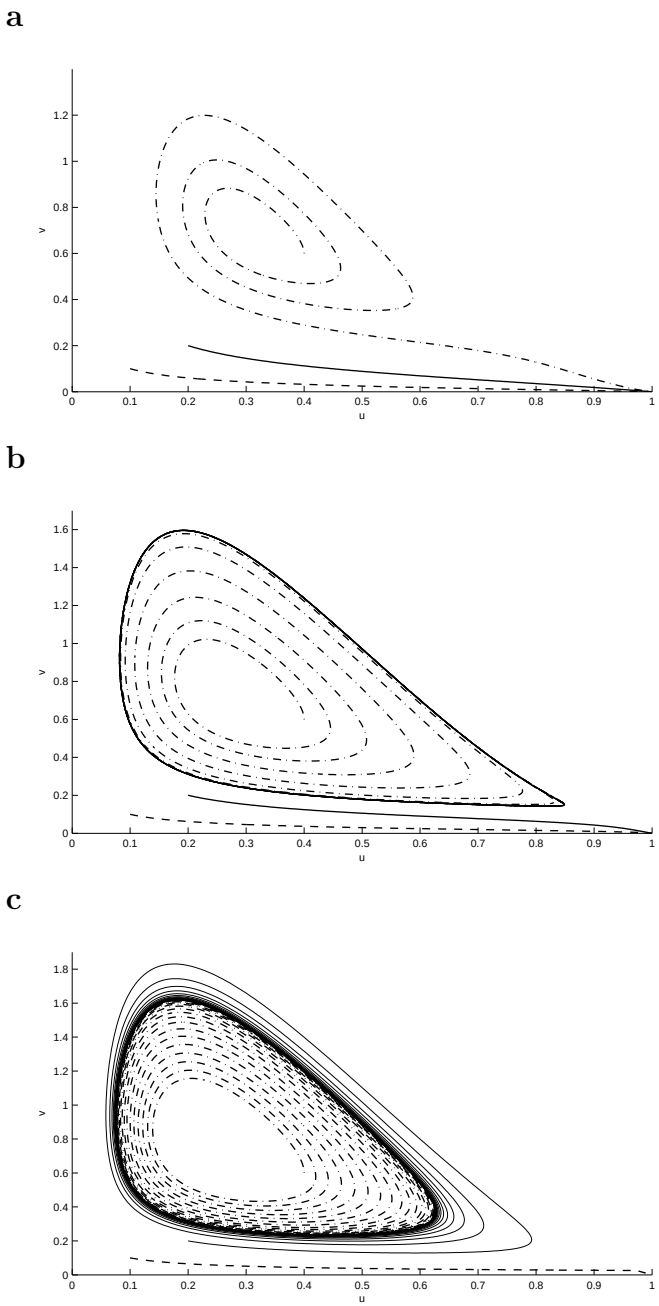

Figure 4.7: Trajectories for system (3.1) in the case of two unstable coexistence steady states when varying γ. Fixed parameters are: $\delta = 5.0$, $\mu = 0.6$, $\tau = 1.0$. Starting points for trajectories: $(0.1, 0.1)$ (dashed line), $(0.2, 0.2)$ (solid line), $(0.4, 0.6)$ (dashed dotted line). **a** $\gamma = 5.2$. **b** $\gamma = 4.88$. **c** $\gamma = 4.5$.

4.8 Examples

The last part of this chapter is devoted to some simulations related to the theoretical results obtained in the previous sections. In particular, we consider three examples corresponding to the three possibilities shown in Figure 4.1; according to the different situations that can arise, we show bifurcation diagrams summarizing the stability of steady states of the model; the bifurcation parameter is γ, i.e., the parameter of the model accounting for virulence of bacteria.
Moreover, we prove whether conditions for stability given in the previous sections are satisfied or not.
Simulations have been performed by using MATCONT, a Matlab package for bifurcation analysis of dynamical systems.

4.8.1 An example from case a)

Firstly, we consider an example corresponding to case **a)** in Figure 4.1, by taking $\delta = 6.0$ and $\tau = 0.2$. The aforementioned graph for this particular choice of parameters is shown in Figure 4.8.

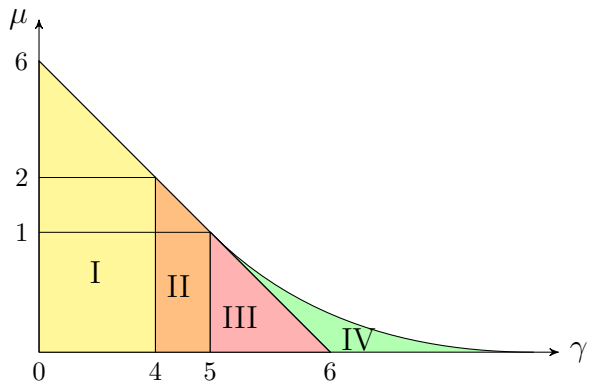

Figure 4.8: An example of the case shown in Figure 4.1 **a**, with $\delta = 6.0$ and $\tau = 0.2$.

First of all we consider the zone with $2.0 < \mu < 6.0$: let us take, for instance, $\mu = 4.0$. By varying γ we see that there is a unique internal steady state for $0 < \gamma < 2.0$, which is a stable focus because the eigenvalues evaluated along the branch in Figure 4.9 **a** are complex conjugate with negative real part. This is confirmed also by Proposition 4.1, because here we are considering region I.
For γ larger than 2.0 there is no coexistence state.

The second case we see is $\mu = 1.5$: since $1.0 < \mu < 2.0$, from Figure 4.8 we have that, by increasing γ, we cross regions I and II where a unique internal state exists. This is confirmed from the simulation (bifurcation diagram in Figure 4.9 **b**): in fact, there is only one positive branch, corresponding to a stable focus (this fact being ensured both by eigenvalues and by Propositions 4.1 and 4.3); for $\gamma > 4.5$, instead, we only have states $(0, 0)$ and $(1, 0)$.

The remaining case, where all the four regions in Figure 4.8 are crossed, is $0 < \mu < 1.0$: we take $\mu = 0.5$. The bifurcation diagram can be seen in Figure 4.9. For $\gamma < 5.5 = \delta - \mu$ there is a unique internal state, which is again a stable focus (in agreement with Propositions 4.1, 4.3); at the branching point BP ($\gamma = 5.5$) state E^*_- appears: evaluation of the eigenvalues lets us conclude that it is a saddle point, while E^*_+ is still stable. In fact, with some calculations it is possible to show that the first set of conditions for stability given by Proposition 4.5 holds.
Finally, at $\gamma = 5.602944$ we have a limit point LP and internal states do not exist anymore.

4.8.2 An example from case b)

Let us consider now an example of case **b)**, with $\delta = 4.5$ and $\tau = 1.0$.

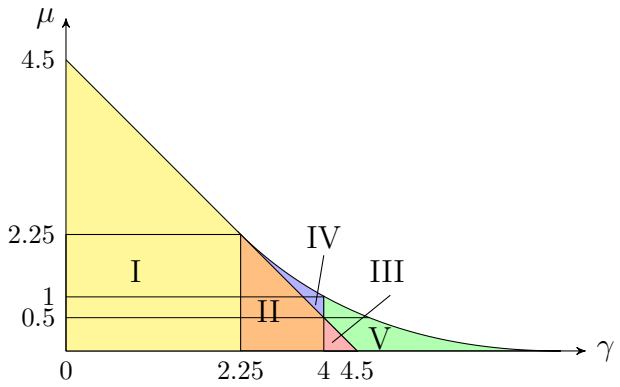

Figure 4.10: Choosing $\delta = 4.5$ and $\tau = 1.0$ our model corresponds to case **b)** of Figure 4.1.

Firstly, let us take $2.25 < \mu < 4.5$, for instance $\mu = 2.6$: this means that we are always in region I in Figure 4.10, The simulation (whose bifurcation diagram is shown in Figure 4.11 **a**) shows that the only internal steady state is a stable focus, since along the positive branch we have complex conjugate eigenvalues with negative real part.
This is expected because we know from Proposition 4.1 that in region (bI) the steady state is always stable.

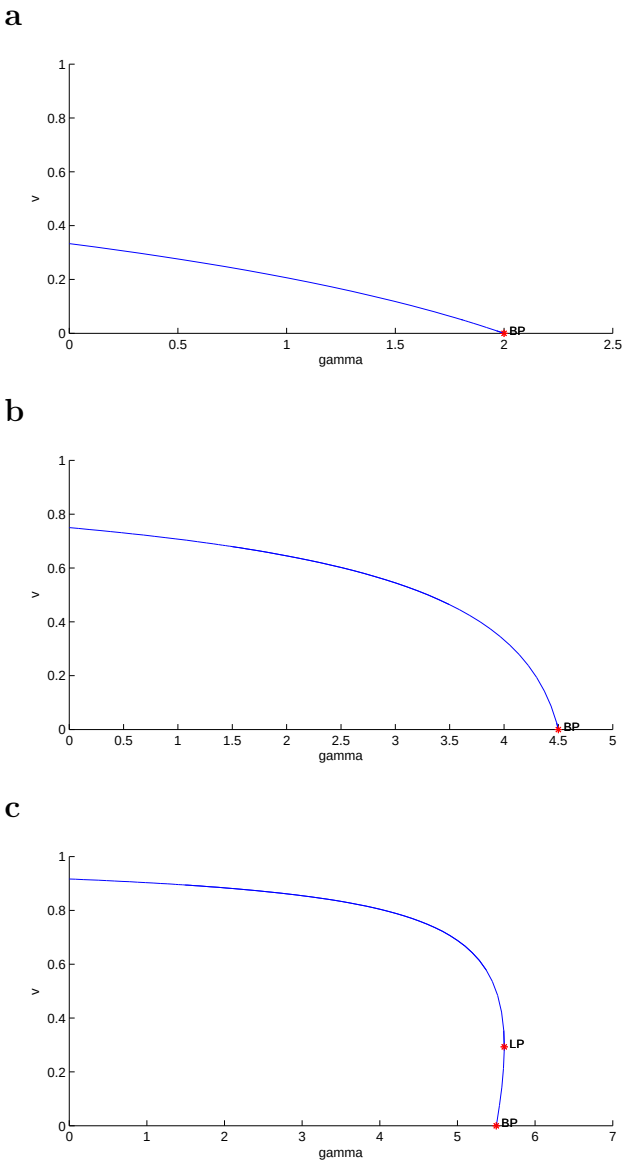

Figure 4.9: Bifurcation diagrams (branch corresponding to $(1, 0)$ not shown) for a choice of parameters corresponding to Figure 4.8: $\delta = 6.0$, $\tau = 0.2$. **a** $\mu = 4.0$. **b** $\mu = 1.5$. **c** $\mu = 0.5$. BP: branching point; LP: limit point.

Then we consider $1.0 < \mu < 2.25$: we take $\mu = 1.5$, so that, when varying γ, we consider situations corresponding to regions I, II and IV. In this case, looking at Figure 4.10, we know that we find only one internal steady state for values smaller than $3.0 = \delta - \mu$, two internal states for $3.0 < \gamma < 3.151531$ and no internal states for larger values of γ. This is confirmed by the bifurcation diagram Figure 4.11 **b**; the branching point BP, where a second state appears, corresponds to $\gamma = 3.0$, while the limit point LP can be

found at $\gamma = 3.151531$. Moreover, from the simulation we can see that E^*_+ (corresponding to the upper branch), since eigenvalues are complex with negative real part, is always a stable focus, while E^*_- (lower branch) is a saddle point (real eigenvalues with opposite sign).
This is confirmed also from the theoretical results of the previous sections: Propositions 4.1, 4.3 and 4.4 tell that in regions (bI), (bII) and (bIV) E^*_+ is always stable.

Now we take into account the case of $0.5 < \mu < 1.0$; for instance, let us take $\mu = 0.7$, so that by varying γ we go through regions I, II, IV and V. The situation here is more complex, as can be seen in Figure 4.11 **c**: there is a unique coexistence state up to $\gamma = 3.8 = \delta - \mu$, where the branching point BP is located, and from the eigenvalues we see that this steady state is a stable focus; this is confirmed also by Propositions 4.1 and 4.2.
Then we enter region IV: the upper branch still corresponds to a stable focus, while the lower branch represents a saddle point. Proposition 4.4 is confirmed again.
In region V, for $\gamma = 4.205955$ and $\gamma = 4.679759$ we have two supercritical Hopf bifurcations (first Lyapunov coefficients $l_1 = -1.798048 \cdot 10^{-1}$ and $l_1 = -1.023855 \cdot 10^{1}$ respectively) and periodic orbits appear. Finally, the limit point corresponds to $\gamma = 4.68004$.
Proposition 4.5 gives four conditions for the stability of E^*_+: after some calculations we find that, for $4 < \gamma < 4.05$ the first condition of the proposition is fulfilled, while for $4.05 < \gamma < 4.205955$ and $4.679759 < \gamma < 4.68004$ the second condition is true, so for these values of γ in region V the state is stable; for the remaining values, i.e. $4.205955 < \gamma < 4.679759$, none of the four conditions is satisfied, so the state is unstable.

Finally, let us deal with a case where $0 < \mu < 0.5$; for instance, $\mu = 0.2$. For values of $\gamma \leq 4$ the set of parameters corresponds to regions I or II and the unique internal state is a stable focus: we can tell it both from the eigenvalues and Propositions 4.1 and 4.2.
At $\gamma = 4.007513$ (that is, in region III) there is a supercritical Hopf bifurcation with first Lyapunov coefficient $l_1 = -1.378195 \cdot 10^{-2}$. The second internal state (a saddle point) appears at $\gamma = 4.3$; for $\gamma = 5.521059$ we have a neutral saddle H (real eigenvalues, coincident in absolute value, one negative and one positive) and for values of γ larger than 6.516718 there are no steady states other than the trivial ones.
Let us see if this is confirmed also theoretically. For $4 < \gamma < 4.3$ we refer to Proposition 4.3: here the second and third conditions can not be satisfied, so the only possibility for E^* to be stable is that the first condition is true; indeed, this happens when $4 < \gamma < 4.007514$. For $4.007514 < \gamma < 4.3$, instead, E^* is unstable.
For greater values we have to consider Proposition 4.5, where four conditions for stability are given. By substitution of the values given for parameters it is possible to see that

none of them is satisfied, so E_+^* is unstable here.

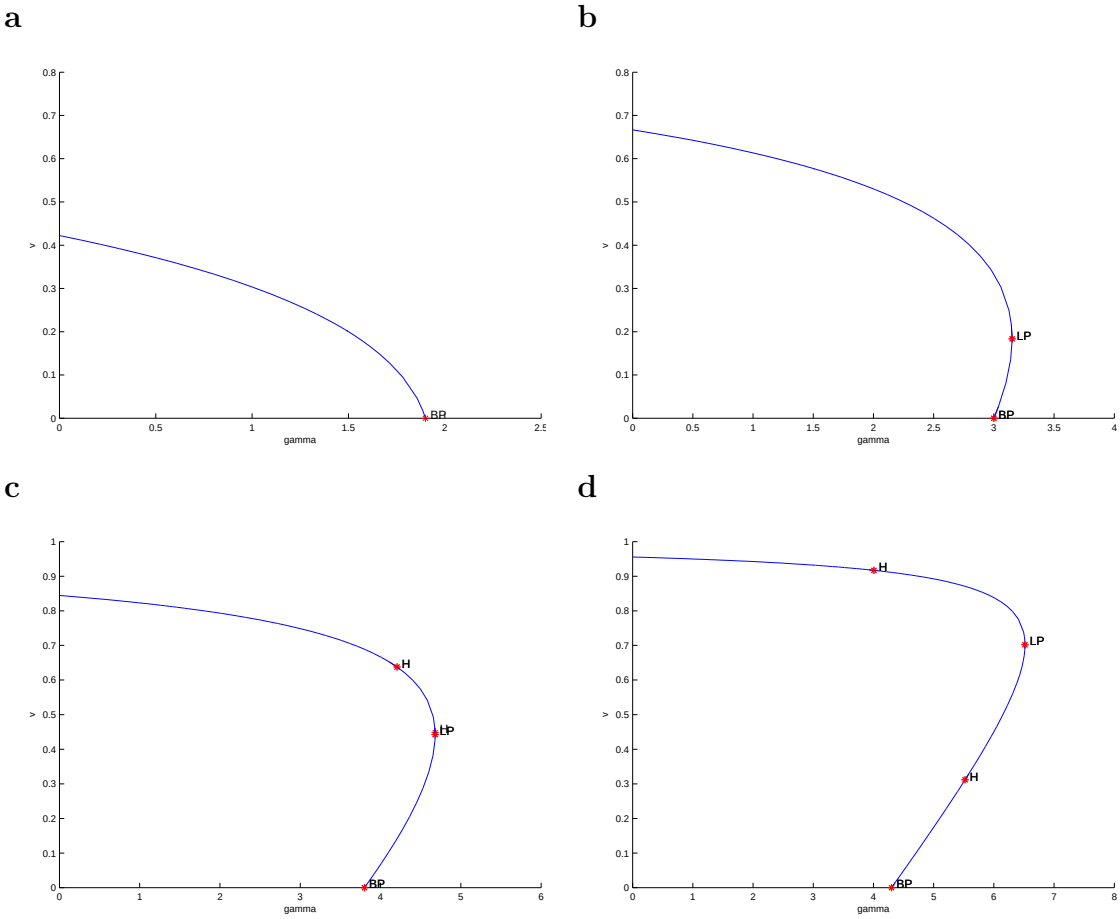

Figure 4.11: Bifurcation diagrams (branch corresponding to $(1, 0)$ not shown) for a choice of parameters corresponding to Figure 4.10: $\delta = 4.5$, $\tau = 1.0$. **a** $\mu = 2.6$. **b** $\mu = 1.5$. **c** $\mu = 0.7$. **d** $\mu = 0.2$. BP: branching point; LP: limit point; H (upper branch): Hopf bifurcation point; H (lower branch): neutral saddle.

4.8.3 An example from case c)

To conclude, we consider a situation corresponding to case **c)** of Figure 4.1, with $\delta = 3.0$ and $\tau = 1.0$: Figure 4.12 represents the setting of the model in this case.

We first consider $1.5 < \mu < 3.0$: let us take $\mu = 2.0$: there is only an internal steady state, which from eigenvalues we can identify as a stable focus. Here we cross only region I, so Proposition 4.1 ensures stability of the unique equilibrium.

Then we take $\mu = 1.0$ to account for the region where $0.202041 < \mu < 1.5$. Here we

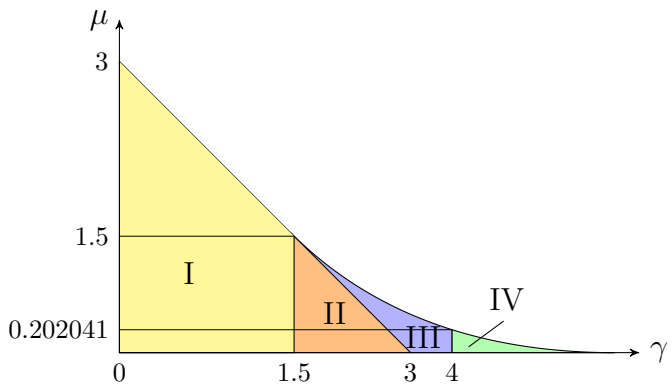

Figure 4.12: When $\delta = 3.0$ and $\tau = 1.0$ we are in a situation corresponding to Figure 4.1 **c**.

have that E_+^* is always a stable focus, while the second internal state, which exists when γ ranges from 2.0 (branching point BP) to 2.101021 (limit point LP), is a saddle point. From the theoretical viewpoint, stability of E_+^* follows from Propositions 4.1, 4.2 and 4.4.

Finally, the third situation $0 < \mu < 0.202041$, where we cross regions I, II, III and IV: let us take $\mu = 0.1$. Here the unique internal state existing for $\gamma < 2.9$ is a stable focus (as already known from Proposition 4.1); at $\gamma = 2.9 = \delta - \mu$ we enter region III and find a branching point BP where the second state appears: E_+^* is still stable and, as we know also from theoretical results, E_-^* is unstable (a saddle point). At $\gamma = 4.014922$ (inside region V) there is a supercritical Hopf bifurcation (first Lyapunov coefficient $l_1 = -2.330104 \cdot 10^{-2}$), and in fact E_+^* becomes unstable too. At $\gamma = 4.335077$ there is a neutral saddle, and then no internal state exists for γ larger than 4.550807.
Theoretical results for assessing stability of E_+^* for $\gamma > 2.9$ are given in Propositions 4.4 and 4.5. The former tells that in region III (that is, $2.9 < \gamma < 4$) the equilibrium is always stable; as regards the latter, calculations reveal that for $4 < \gamma < 4.014922$ the second set of conditions for stability is satisfied, thus E_+^* is stable; for remaining values, namely $4.014922 < \gamma < 4.550807$, none of the four sets of conditions holds, so the equilibrium is unstable.

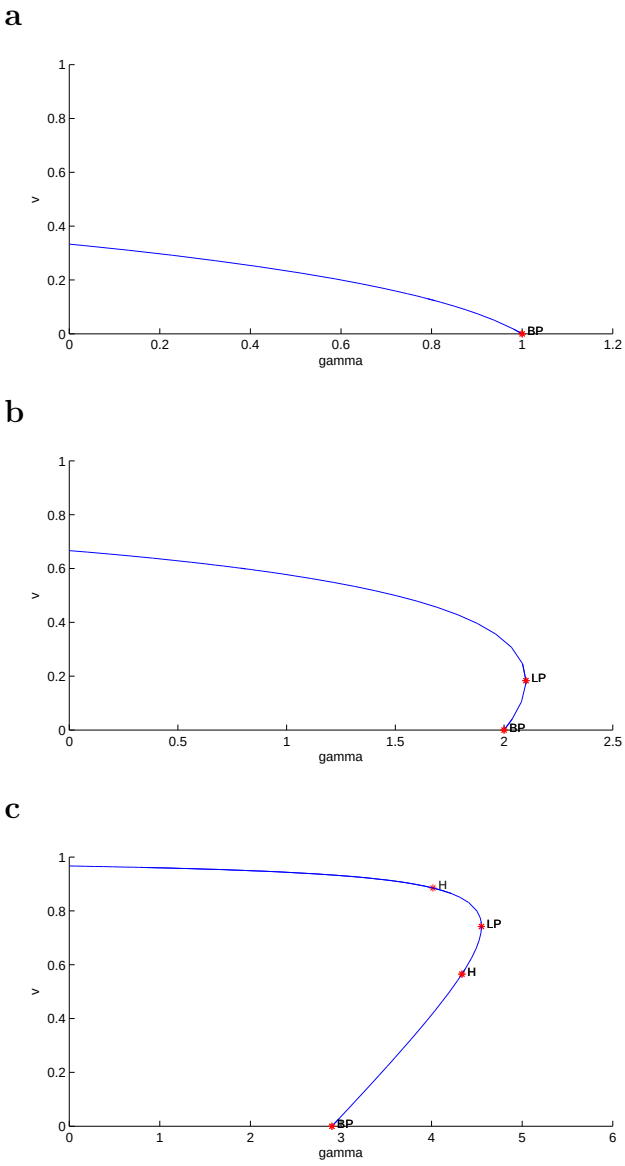

Figure 4.13: Bifurcation diagrams (branch corresponding to $(1, 0)$ not shown) for a choice of parameters corresponding to Figure 4.12: $\delta = 3.0$, $\tau = 1.0$. **a** $\mu = 2.0$. **b** $\mu = 1.0$. **c** $\mu = 0.1$. BP: branching point; LP: limit point; H (upper branch): Hopf bifurcation point; H (lower branch): neutral saddle.

Chapter 5

Spatial pattern formation

Here we consider our model (1.2) for investigating pattern formation and for determining the role of the different mechanisms introduced. First of all, we give a brief overview on Turing pattern formation.

Patterns are a frequently observed phenomenon in chemistry, physics and biology: they occur in chemical reactions, cell growth, animal dispersal into the environment, species interactions, animal coats, just to mention a few examples. So in the last decades there has been a lot of interest in including these mechanisms into a mathematical framework. The mathematical formalization of these phenomena is based on reaction-diffusion and reaction-diffusion-chemotaxis equations.
The first work discussing the relation between reaction-diffusion systems and reacting chemical substances (thus giving an explanation to the process known as morphogenesis) is that from Alan Turing [42], published in 1952. In this paper a novel concept was introduced: diffusion, which had always being regarded as a homogenizing process, indeed can lead to spatial heterogeneity by causing the reacting morphogens to produce patterns when they are slightly perturbed from their homogeneous steady state. Since Turing's work lots of papers and books have focused on the comprehension of these processes ([3],[7], [24], [25] and many others), so that nowadays reaction-diffusion theory and its application to pattern formation is an important research field, also because, though aiming at modeling a great variety of complex phenomena, yet it is analytically tractable and rich.

A general treatment of the theory of Turing pattern formation can be found in [26] and [27].
Many authors have applied this theory to spatially explicit predator-prey systems ([1], [5] among others). Here we are going to show similar results referred to our specific problem.

Basically, we consider our models (1.2) and (1.3) and derive conditions on parameters under which a spatially homogeneously stable steady state of the system can be destabilized by diffusion (and chemotaxis), thus giving rise to the formation of spatial patterns over the domain.

5.1 Theoretical results for the case with chemotaxis and without integral

We consider system (1.2) in one spatial dimension

$$\begin{cases} u_t = D_1 u_{xx} + F(u,v) \\ v_t = D_2 v_{xx} - \chi(v u_x)_x + G(u,v) \end{cases}, \tag{5.1}$$

where we have defined

$$\begin{aligned} F(u,v) &= u(1-u) - uv \\ G(u,v) &= -\mu v + \delta uv - \frac{\gamma uv}{1+\tau v}\,. \end{aligned} \tag{5.2}$$

This first step aims to analyze a basic case where the redistribution mechanism is absent. We linearize around the homogeneously stable[1] coexistence steady state (u^*, v^*).
We call $(\tilde{u}, \tilde{v})$ a small perturbation of the steady state and substitute

$$u = u^* + \tilde{u}\,,\; v = v^* + \tilde{v}$$

into the system:

$$\begin{cases} (\tilde{u}+u^*)_t = D_1(\tilde{u}+u^*)_{xx} + (\tilde{u}+u^*)(1-\tilde{u}-u^*) - (\tilde{u}+u^*)(\tilde{v}+v^*) \\ (\tilde{v}+v^*)_t = D_2(\tilde{v}+v^*)_{xx} - \chi((\tilde{v}+v^*)(\tilde{u}+u^*)_x)_x \\ \qquad\qquad -\mu(\tilde{v}+v^*) + \delta(\tilde{u}+u^*)(\tilde{v}+v^*) - \dfrac{\gamma(\tilde{u}+u^*)(\tilde{v}+v^*)}{1+\tau(\tilde{v}+v^*)} \end{cases},$$

[1] We know that, depending on the choice of parameters, we might have zero, one or two coexistence steady states, and we have already shown that, if the last is the case, the equilibrium with the lowest bacterial component is stable, while the other one is unstable. Since pattern formation theory is based on the assumption that a homogeneously stable situation is destabilized by diffusion, we need only consider the stable steady state. If we are in a situation where there is no such steady state, then of course Turing mechanisms do not apply.

For linearization we drop terms of the type $\tilde{u}^2$, $\tilde{v}^2$ and $\tilde{u}\tilde{v}$ and use a Taylor expansion for the Holling-type term; what is left is

$$\begin{cases} \tilde{u}_t = D_1\tilde{u}_{xx} + \tilde{u}(1-u^*) + u^*(1-u^*) - \tilde{u}v^* - \tilde{v}u^* + u^*v^* \\ \tilde{v}_t = D_2\tilde{v}_{xx} - \chi v^*\tilde{u}_{xx} - \mu\tilde{v} - \mu v^* + \delta\tilde{u}v^* + \delta\tilde{v}u^* + \delta u^*v^* \\ \qquad\qquad - \dfrac{\gamma\tilde{u}v^*}{1+\tau v^*} - \dfrac{\gamma u^*v^*}{1+\tau v^*} - \dfrac{\gamma u^*\tilde{v}}{(1+\tau v^*)^2} \end{cases} ;$$

rearranging terms and having in mind the equations solved by u^* and v^* we get the linearized system

$$\begin{cases} \tilde{u}_t = D_1\tilde{u}_{xx} + F_u^*\tilde{u} + F_v^*\tilde{v} \\ \tilde{v}_t = D_2\tilde{v}_{xx} - \chi v^*\tilde{u}_{xx} + G_u^*\tilde{u} + G_v^*\tilde{v} \end{cases} , \tag{5.3}$$

where F_u^*, F_v^*, G_u^* and G_v^* are the derivatives of $F(u,v)$ and $G(u,v)$ with respect to u and v, evaluated at the steady state; in detail,

$$\begin{aligned} F_u^* &= -u^* \\ F_v^* &= -u^* \\ G_u^* &= \left(\delta - \frac{\gamma}{1+\tau v^*}\right) v^* \\ G_v^* &= \frac{\gamma\tau u^*v^*}{(1+\tau v^*)^2} \end{aligned}$$

This problem is to be solved by means of the separation of variables method.
We look for solutions of the form

$$\mathbf{w}(t,x) = (\tilde{u}(t,x), \tilde{v}(t,x))^T = \mathbf{c}T(t)X(x)\,, \tag{5.4}$$

where $\mathbf{c} = (c_1, c_2)^T$ is a constant vector, whose components can be found by performing a Fourier expansion of the initial conditions.
Substitution into (5.3) yields

$$\begin{cases} c_1T'X = D_1c_1TX'' + F_u^*c_1TX + F_v^*c_2TX \\ c_2T'X = D_2c_2TX'' + G_u^*c_1TX + G_v^*c_2TX \end{cases} ; \tag{5.5}$$

the expression for $T(t)$ consequently is

$$T(t) \propto \exp(\lambda t) \tag{5.6}$$

where λ has to be determined. Next, we determine $X(x)$ as the general solution of the eigenvalue problem

$$-\eta X(x) + X''(x) = 0 \tag{5.7}$$

on $[0,1]$ with zero-flux boundary conditions, finding that a corresponding eigenfunction is

$$X_k(x) \propto \cos(kx), \qquad k = n\pi, \quad n = 0, 1, 2, \ldots, \quad \eta_k = -k^2 \,. \tag{5.8}$$

$X(x)$ will be a combination of $X_k(x)$ for different k, so that the solution to (5.3) will be

$$\mathbf{w}(x,t) = \sum_k \mathbf{c_k} \exp(\lambda t) \cos kx. \tag{5.9}$$

And finally, substituting into system (5.5) we get the following equation for $\mathbf{c}$:

$$X\left[\lambda I + k^2 D - J\right] \mathbf{c} = \mathbf{0}. \tag{5.10}$$

where

$$D = \begin{pmatrix} D_1 & 0 \\ -\chi v^* & D_2 \end{pmatrix}, \quad J = \begin{pmatrix} F_u^* & F_v^* \\ G_u^* & G_v^* \end{pmatrix}.$$

Now, equation (5.10) is satisfied whenever

$$\det\left(\lambda I + k^2 D - J\right) = 0 \,. \tag{5.11}$$

When $k = 0$ (5.11) is equivalent to

$$\lambda^2 - \mathrm{tr} J \lambda + \det J = 0 \,.$$

This is the homogeneous case, that is, no spatial effect is present; since we chose (u^*, v^*) to be the stable steady state, the eigenvalues are negative.

Thus the solution component corresponding to $k = 0$ is

$$\mathbf{w}_0(t) = \mathbf{c_0}\left(A_1 \exp(\lambda_0^- t) + A_2 \exp(\lambda_0^+ t)\right) \,,$$

(where $\lambda_0^{\pm}$ are the negative eigenvalues), which cannot persist at large times.

Considering the case $k \neq 0$, instead, in order to have a nontrivial solution for the eigenvectors, the eigenvalues are found by solving

$$\lambda^2 + \Phi(k^2)\lambda + \Psi(k^2) = 0 \tag{5.12}$$

where $\Phi(x)$ and $\Psi(x)$ are defined, for $x > 0$, as

$$\begin{aligned} \Phi(x) &= (D_1 + D_2)x - (F_u^* + G_v^*) \\ \Psi(x) &= D_1 D_2 x^2 - (D_1 G_v^* + D_2 F_u^* + \chi v^* F_v^*)\, x + \det J \,. \end{aligned}$$

Since we know that (u^*, v^*) is stable, we have that $-(F_u^* + G_v^*) > 0$, therefore $\Phi(x) > 0$ for all x.
The two solutions of (5.12) are given by

$$\lambda_\pm(k^2) = \frac{1}{2}\left[-\Phi(k^2) \pm \sqrt{\Phi^2(k^2) - 4\Psi(k^2)}\right]. \tag{5.13}$$

The values of k^2 for which $\Re(\lambda_+(k^2)) > 0$ are those such that $\Psi(k^2) < 0$.
For this to be satisfied two conditions must necessarily hold: both the coefficient of the first order term and the minimum of Ψ must be negative.
Therefore, first of all we have to impose

$$D_1 G_v^* + D_2 F_u^* + \chi v^* F_v^* > 0 \tag{5.14}$$

(this is possible for proper choices of parameters, since $F_u^*, F_v^* < 0$ and $G_v^* > 0$).
This yields

$$\chi < -\frac{D_1 G_v^* + D_2 F_u^*}{v^* F_v^*} = \tilde{\chi} \tag{5.15}$$

Then we have to find the minimum value for $\Psi(k^2)$:

$$\Psi'(k^2) = 2D_1 D_2 k^2 - (D_1 G_v^* + D_2 F_u^* + \chi v^* F_v^*) = 0$$

is satisfied for

$$k^2 = k^2_{\min} = \frac{D_1 G_v^* + D_2 F_u^* + \chi v^* F_v^*}{2D_1 D_2} > 0 \tag{5.16}$$

(because of (5.14)); therefore $\Psi_{\min} = \Psi(k^2_{\min})$ is given by

$$\Psi_{\min} = -\frac{1}{4D_1 D_2}\left(D_1 G_v^* + D_2 F_u^* + \chi v^* F_v^*\right)^2 + \det J\,, \tag{5.17}$$

and this quantity is negative if and only if

$$\left(D_1 G_v^* + D_2 F_u^* + \chi v^* F_v^*\right)^2 > 4D_1 D_2 \det J\,. \tag{5.18}$$

This is the second condition to be imposed in order to have an instability range for wavenumbers, which is delimited by the two solutions of $\Psi(k^2) = 0$, namely,

$$k^2_\pm = \frac{1}{2D_1 D_2}\left[(D_1 G_v^* + D_2 F_u^* + \chi v^* F_v^*) \pm \sqrt{\left(D_1 G_v^* + D_2 F_u^* + \chi v^* F_v^*\right)^2 - 4D_1 D_2 \det J}\right], \tag{5.19}$$

so that

$$k^2_- < k^2 < k^2_+\,. \tag{5.20}$$

is the instability range.
There is a critical value determining whether the instability range exists or not, that is, when $\Psi_{\min} = 0$: in that case,

$$(D_1 G_v^* + D_2 F_u^* + \chi v^* F_v^*)^2 = 4 D_1 D_2 \det J \,;$$

we can therefore define a critical chemotactic coefficient,

$$\chi_{\text{crit}} = \frac{1}{v^* F_v^*} \left[-(D_1 G_v^* + D_2 F_u^*) + \sqrt{4 D_1 D_2 \det J} \right] , \tag{5.21}$$

such that, when $\chi < \chi_{\text{crit}}$, condition (5.18) is satisfied.

We can compare $\tilde{\chi}$ in (5.15) and χ_{crit} in (5.21) to see if they are compatible; actually, since $F_v^* < 0$, we have that $\chi_{\text{crit}} < \tilde{\chi}$, so the condition for the existence of the range of instability (5.20) is simply

$$\chi < \chi_{\text{crit}} = \frac{1}{v^* F_v^*} \left[-(D_1 G_v^* + D_2 F_u^*) + \sqrt{4 D_1 D_2 \det J} \right] . \tag{5.22}$$

We can summarize these results in the following

Proposition 5.1 *Let* (5.3) *be the system describing the spatio-temporal evolution of the perturbation which is the linearization of the system in one spatial dimension* (5.1)*, where* $F(u, v)$ *and* $G(u, v)$ *are as in* (5.2)*.*
If (5.22) *holds, then the solution to* (5.3) *is, for* t *large,*

$$\mathbf{w}(x, t) \sim \sum_{k=k_-}^{k=k_+} \mathbf{c_k} \exp\left(\lambda(k^2) t\right) \cos(kx) \,, \tag{5.23}$$

where $k_\pm^2$ *are defined in* (5.19)*.*

5.1.1 Special case: $\chi = 0$

A special case is when chemotaxis does not occur, i.e. $\chi = 0$. As a consequence condition (5.22) becomes

$$\frac{1}{v^* F_v^*} \left[-(D_1 G_v^* + D_2 F_u^*) + \sqrt{4 D_1 D_2 \det J} \right] > 0 \,.$$

Therefore we need to impose conditions on the diffusion coefficients in order to have instability and the resulting pattern formation, namely

$$\begin{cases} D_1 G_v^* + D_2 F_u^* > 0 \\ (D_1 G_v^* + D_2 F_u^*)^2 > 4 D_1 D_2 \det J \,. \end{cases} \tag{5.24}$$

The first inequality gives

$$D_2 < -\frac{G_v^*}{F_u^*} D_1. \tag{5.25}$$

The critical situation (dividing cases where pattern formation occurs from cases where perturbations of the steady state are dumped) corresponds to

$$(D_1 G_v^* + D_2 F_u^*)^2 = 4 D_1 D_2 \det J\,;$$

from this we are able to define two critical diffusion coefficients for amoeba, as a function of the diffusion coefficient of bacteria:

$$D_2^{\text{crit}} = \frac{1}{(F_u^*)^2} \left(\det J - F_v^* G_u^* \pm 2\sqrt{-F_v^* G_u^* \det J} \right) D_1 \ , \tag{5.26}$$

such that when either $D_2 < (D_2^{\text{crit}})_-$ or $D_2 > (D_2^{\text{crit}})_+$ the interval (5.20) exists.

We check if the two conditions in (5.24) are compatible. (5.25) may be rewritten as

$$D_2 < \frac{\gamma \tau v^*}{(1+\tau v^*)^2} D_1\,;$$

the quantity on the right-hand side is smaller than D_1: in fact, this is true if and only if $\tau^2 v^{*2} + \tau(2-\gamma)v^* + 1 > 0$ holds; but this expression is equivalent to $\mathrm{tr} J < 0$ (see Equation (4.4) in Chapter 4), which is certainly true since (u^*, v^*) is homogeneously stable.
The two conditions (5.25) and $D_2 > (D_2^{\text{crit}})_+$ are thus compatible if

$$\frac{\det J - F_v^* G_u^* + 2\sqrt{-F_v^* G_u^* \det J}}{{F_u^*}^2} < -\frac{G_v^*}{F_u^*}\,; \tag{5.27}$$

but the left-hand side term is equal to

$$\frac{G_v^*}{F_u^*} - \frac{2G_u^*}{F_u^*} + \frac{2\sqrt{(F_u^*)^2 G_u^* (G_u^* - G_v^*)}}{{F_u^*}^2} = \frac{G_v^*}{F_u^*} - \frac{2G_u^*}{F_u^*} + \frac{2\sqrt{G_u^* (G_u^* - G_v^*)}}{F_u^*}$$

which is less than $-\dfrac{G_v^*}{F_u^*}$ if and only if

$$2\frac{G_v^*}{F_u^*} - \frac{2G_u^*}{F_u^*} + \frac{2\sqrt{G_u^* (G_u^* - G_v^*)}}{F_u^*} < 0\,,$$

that is, if and only if

$$G_v^* - G_u^* - \sqrt{G_u^* (G_u^* - G_v^*)} > 0\,. \tag{5.28}$$

After some calculations, this is satisfied if and only if

$$\delta T^2 (v^*)^2 + 2\delta T v^* + \delta - \gamma - \gamma T < 0 \tag{5.29}$$

which is false: in fact, this implies that $\det J(E^*) < 0$, which is not the case since E^* is homogeneously stable.
Therefore $(D_2^{\text{crit}})_+ > -\dfrac{G_v^*}{F_u^*}$.
Now we look for the compatibility of (5.25) and $D_2 < (D_2^{\text{crit}})_-$. This time $(D_2^{\text{crit}})_- < -\frac{G_v^*}{F_u^*}$ if and only if

$$G_v^* - G_u^* + \sqrt{G_u^*(G_u^* - G_v^*)} > 0 \tag{5.30}$$

that is, if and only if

$$G_v^*(G_v^* - G_u^*) < 0 \tag{5.31}$$

and since $G_v^* > 0$, this means that

$$\delta T^2 (v^*)^2 + 2\delta T v^* + \delta - \gamma - \gamma T > 0 \tag{5.32}$$

which is true ($\det J(E^*) > 0$). Thus we are able to conclude that the two conditions in (5.24) can be summarized as

$$D_2 < (D_2^{\text{crit}})_- \tag{5.33}$$

and we can state the following

Proposition 5.2 *Let $\chi = 0$ in* (5.3)*. Then conditions* (5.14) *and* (5.18) *ensuring* (5.23) *are replaced by*

$$D_2 < (D_2^{crit})_- \tag{5.34}$$

where $(D_2^{crit})_-$ is defined in (5.26)*.*

Notice that condition (5.34) is less restrictive than (5.22).
This means in a sense that chemotaxis has a stabilizing effect on the dynamics of the two populations, possibly because aggregation prevents the perturbation of the steady state from expanding.

5.2 Theoretical results for the case with both integral and chemotaxis

Now we introduce the diffusion and chemotaxis terms in the system with the integral term, in order to study the possibility of having spatial patterns.

We consider the full system with the integral term

$$\begin{cases} u_t = D_1 u_{xx} + u(1-u) - uv \\ v_t = D_2 v_{xx} - \chi(v u_x)_x + \delta v \dfrac{\int_0^1 uv\,dx}{\int_0^1 v\,dx} - \mu v - \dfrac{\gamma uv}{1+\tau v} \end{cases}, \tag{5.35}$$

and linearize about the homogeneously stable coexistence steady state (u^*, v^*): the difference with the system we have seen in the previous section lies in the linearization of the integral part; in fact, if we call $(\tilde{u}, \tilde{v})$ the deviation from the steady state, set

$$u = \tilde{u} + u^* \, , \; v = \tilde{v} + v^*$$

and substitute into the term

$$\delta v \frac{\int_0^1 uv \, dx}{\int_0^1 v \, dx} \, ,$$

we get

$$\begin{aligned}
&\frac{1}{\int_0^1 \tilde{v} \, dx + v^*} \delta(\tilde{v} + v^*) \left(v^* \int_0^1 \tilde{u} \, dx + u^* \int_0^1 \tilde{v} \, dx + u^* v^* \right) = \\
&\quad = \frac{1}{v^* \left(1 + \frac{\int_0^1 \tilde{v} \, dx}{v^*} \right)} \left(\delta u^* \tilde{v} + \delta v^* \int_0^1 \tilde{u} \, dx + \delta u^* \int_0^1 \tilde{v} \, dx + \delta u^* v^* \right) \\
&\quad = \left(1 - \frac{\int_0^1 \tilde{v} \, dx}{v^*} \right) \left(\delta u^* \tilde{v} + \delta v^* \int_0^1 \tilde{u} \, dx + \delta u^* \int_0^1 \tilde{v} \, dx + \delta u^* v^* \right) \\
&\quad = \delta u^* \tilde{v} + \delta v^* \int_0^1 \tilde{u} \, dx + \delta u^* \int_0^1 \tilde{v} \, dx + \delta u^* v^* - \delta u^* \int_0^1 \tilde{v} \, dx \\
&\quad = \delta u^* \tilde{v} + \delta u^* v^* + \delta v^* \int_0^1 \tilde{u} \, dx.
\end{aligned}$$

Therefore, when we add this expression to the other linearized components, this is what we get:

$$\begin{cases}
\tilde{u}_t = D_1 \tilde{u}_{xx} - u^* \tilde{u} - u^* \tilde{v} \\
\tilde{v}_t = -\chi v^* \tilde{u}_{xx} + D_2 \tilde{v}_{xx} - \dfrac{\gamma v^*}{1 + \tau v^*} \tilde{u} + \left(\delta u^* - \mu - \dfrac{\gamma u^*}{(1 + \tau v^*)^2} \right) \tilde{v} \\
\qquad\qquad + \delta v^* \displaystyle\int_0^1 \tilde{u} \, dx + \delta u^* v^* - \mu v^* - \dfrac{\gamma u^* v^*}{1 + \tau v^*}
\end{cases} .$$

By rearranging terms, this can be rewritten as

$$\begin{cases}
\tilde{u}_t = D_1 \tilde{u}_{xx} + F_u^* \tilde{u} + F_v^* \tilde{v} \\
\tilde{v}_t = -\chi v^* \tilde{u}_{xx} + D_2 \tilde{v}_{xx} + (G_u^* - \delta v^*) \tilde{u} + G_v^* \tilde{v} + \delta v^* \displaystyle\int_0^1 \tilde{u} \, dx
\end{cases} , \tag{5.36}$$

where F_u^*, F_v^*, G_u^* and G_v^* are the partial derivatives of the reactions $F(u, v)$ and $G(u, v)$ as defined in Section 5.1, evaluated at the steady state.

Again, we look for a solution

$$\mathbf{w}(t, x) = \mathbf{c} T(t) X(x) \, ;$$

as before $X_k(x) \propto \cos(kx)$, with $k = n\pi$, $n = 0, 1, 2, \ldots$ and $\eta = -k^2$ is a solution to (5.7), and $X(x)$ is a linear combination of $X_k(x)$.
Substitution into (5.36) and some algebra yield

$$\left[\lambda I X + k^2 D X - A X - M \int_0^1 X dx\right] \mathbf{c} = \mathbf{0}. \tag{5.37}$$

where

$$D = \begin{pmatrix} D_1 & 0 \\ -\chi v^* & D_2 \end{pmatrix}, \quad A = \begin{pmatrix} F_u^* & F_v^* \\ G_u^* - \delta v^* & G_v^* \end{pmatrix}, \quad M = \begin{pmatrix} 0 & 0 \\ \delta v^* & 0 \end{pmatrix}.$$

Now, for mode number $k = 0$, system (5.37) reduces to

$$[\lambda I - A - M]\, \mathbf{c} = \mathbf{0}\ ,$$

which is satisfied when

$$\det(\lambda I - A - M) = \lambda^2 - (F_u^* + G_v^*)\lambda + F_u^* G_v^* - F_v^* G_u^* = 0\ : \tag{5.38}$$

but since we know that the steady state (u^*, v^*) is homogeneously stable, we get that the two solutions of (5.38) have negative real part.

When $k \neq 0$, instead, (5.37) becomes

$$\left[\lambda I + k^2 D - A\right] X_k(x) \mathbf{c} = \mathbf{0}\,;$$

so, in order to find the eigenvalues, the equation to be solved is

$$\begin{aligned} \det(\lambda I + k^2 D - A) &= \lambda^2 + \left[k^2(D_1 + D_2) - (F_u^* + G_v^*)\right] \lambda \\ &+ \left[D_1 D_2 k^4 - (D_1 G_v^* + D_2 F_u^* + \chi v^* F_v^*) k^2 + F_u^* G_v^* - F_v^* G_u^* + \delta v^* F_v^*\right] = 0. \end{aligned} \tag{5.39}$$

If we define

$$\begin{aligned} \Phi(x) &= (D_1 + D_2)x - (F_u^* + G_v^*) \\ \Psi(x) &= D_1 D_2 x^2 - (D_1 G_v^* + D_2 F_u^* + \chi v^* F_v^*)\, x + (\det J + \delta v^* F_v^*) \end{aligned}$$

then (5.39) is equivalent to

$$\lambda^2 + \Phi(k^2)\lambda + \Psi(k^2) = 0.$$

As before, since $\Phi(k^2) > 0$, the instability range (that is, the interval of k^2 such that $\Re\lambda(k^2) > 0$) is found by imposing $\Psi(k^2) < 0$.

If we analyze more in detail the y-intercept of the parabola given by $y = \Psi(k^2)$, we get that

$$\begin{aligned}\det J + \delta v^* F_v^* &= F_u^* G_v^* - F_v^* \left(\delta v^* - \frac{\gamma v^*}{1+\tau v^*} - \delta v^* \right) \\ &= -\frac{\gamma \tau u^{*2} v^*}{(1+\tau v^*)^2} - \frac{\gamma u^* v^*}{(1+\tau v^*)} \\ &= -\frac{\gamma u^* v^*}{(1+\tau v^*)^2} \left(1 + \tau(u^* + v^*)\right)\end{aligned}$$

which of course is always negative: therefore there is always some $k \neq 0$ such that $\Psi(k^2)$ is negative, so, differently from the case without integral, there is always an instability range, whatever the sign of $D_1 G_v^* + D_2 F_u^* + \chi v^* F_v^*$, as we can see in Figure 5.1. The width

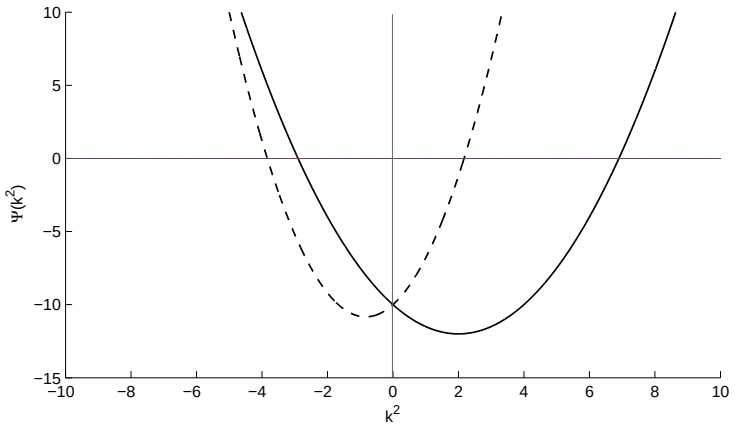

Figure 5.1: Two examples of $\Psi(k^2)$. Since $\det J + \delta v^* F_v^* < 0$, there is always a range of unstable wavenumbers $0 < k^2 < \bar{k}^2$.

of this interval depends on the specific choice of parameters; in particular, it is given by

$$0 < k^2 < \bar{k}^2 \ , \tag{5.40}$$

where

$$\bar{k}^2 = \frac{(D_1 G_v^* + D_2 F_u^* + \chi v^* F_v^*) + \sqrt{(D_1 G_v^* + D_2 F_u^* + \chi v^* F_v^*)^2 - 4 D_1 D_2 \left(\det J + \delta v^* F_v^*\right)}}{2 D_1 D_2} . \tag{5.41}$$

We are able to conclude that the full solution to the linearized system with the integral term is, for t large, given by

$$\mathbf{w}(x,t) \sim \sum_{k=0}^{k=\bar{k}} \mathbf{c_k} \exp\left(\lambda(k^2) t\right) \cos\left(kx\right).$$

Proposition 5.3 *For the problem with redistribution mechanism* (5.35)*, there is always an interval of wavenumbers* $0 < k^2 < \bar{k}^2$*, where* $\bar{k}^2$ *is defined as in* (5.41)*, such that perturbation of the homogeneous steady state persists for* t *large; in other words,*

$$\mathbf{w}(x,t) \sim \sum_{k=0}^{k=\bar{k}} \mathbf{c_k} \exp\left(\lambda(k^2)t\right) \cos\left(kx\right) \quad \textit{for } t \textit{ large.} \tag{5.42}$$

5.3 Destabilizing the bacteria-only state $(1,0)$

Since the bacteria-only homogeneous equilibrium $(1,0)$ is stable when $\mu > \delta - \gamma$, one may wonder if it is possible to destabilize it with diffusion and/or chemotaxis.
The linearization of the full system (1.2) around $(1,0)$ yields

$$\begin{cases} \tilde{u}_t = D_1 \tilde{u}_{xx} - \tilde{u} - \tilde{v} \\ \tilde{v}_t = D_2 \tilde{v}_{xx} + (\delta - \gamma - \mu)\tilde{v} \end{cases},$$

so in this case the matrix appearing in (5.37) become

$$D = \begin{pmatrix} D_1 & 0 \\ 0 & D_2 \end{pmatrix}, \quad A = \begin{pmatrix} -1 & -1 \\ 0 & \delta - \gamma - \mu \end{pmatrix}$$

while M is the 2×2 zero matrix.

Following the usual procedure, the mode corresponding to $k = 0$ is stable, because the corresponding eigenvalues are $\lambda = -1$ and $\lambda = \delta - \gamma - \mu$, which are both negative.
For all the other modes, instead, the dispersion relation is given by $\det \lambda I + k^2 D - A = 0$, i.e.

$$\lambda^2 + \Phi(k^2)\lambda + \Psi(k^2) = 0$$

with

$$\begin{aligned} \Phi(x) &= (D_1 + D_2)x + 1 + \mu + \gamma - \delta \\ \Psi(x) &= D_1 D_2 x^2 + (D_2 + D_1(\mu + \gamma - \delta))x + \mu + \gamma - \delta\,. \end{aligned}$$

We notice that $\Psi(k^2)$ is always strictly positive; this means that the two eigenvalues surely have negative real parts, so there is no instability range in this case.
This lets us deduce that

Proposition 5.4 *When the homogeneous steady state* $(1,0)$ *is stable, it can never be destabilized by means of Turing mechanisms.*

5.4 The two-dimensional case

Now we are going to analyze Turing pattern formation in the case of a two-dimensional domain Ω. We remind that the problem we are taking into account is

$$\begin{cases} u_t = D_1\Delta u + u(1-u) - uv \\ v_t = D_2\Delta v - \chi\nabla\cdot(v\nabla u) - \mu v + \delta v\dfrac{\iint_\Omega uvd\mathbf{x}}{\iint_\Omega vd\mathbf{x}} - \dfrac{\gamma uv}{1+\tau v} \\ u(0,\mathbf{x}) = u_0(\mathbf{x}) \ \ \forall\,\mathbf{x}\in\Omega \\ v(0,\mathbf{x}) = v_0(\mathbf{x}) \ \ \forall\,\mathbf{x}\in\Omega \\ \dfrac{\partial u}{\partial\nu}(t,\mathbf{x}) = \dfrac{\partial v}{\partial\nu}(t,\mathbf{x}) = 0 \ \ \forall\mathbf{x}\in\partial\Omega, \ \ \forall t\geq 0 \end{cases} . \tag{5.43}$$

The corresponding linearized system accounting for the behavior of the perturbation $(\tilde{u},\tilde{v})$ of the homogeneous steady state (u^*,v^*) is then

$$\begin{cases} \tilde{u}_t = D_1\Delta\tilde{u} + F_u^*\tilde{u} + F_v^*\tilde{v} \\ \tilde{v}_t = -\chi v^*\Delta\tilde{u} + D_2\Delta\tilde{v} + G_u^*\tilde{u} + G_v^*\tilde{v} \end{cases}$$

when we do not consider non-local interaction between the two populations, or

$$\begin{cases} \tilde{u}_t = D_1\Delta\tilde{u} + F_u^*\tilde{u} + F_v^*\tilde{v} \\ \tilde{v}_t = -\chi v^*\Delta\tilde{u} + D_2\Delta\tilde{v} + (G_u^* - \delta v^*)\tilde{u} + G_v^*\tilde{v} + \delta v^*\iint\tilde{u}dxdy \end{cases}$$

when this mechanism is involved.

This implies that the solution to the linearized problem is the analogous of (5.4) for the two-dimensional case (be it with or without integral term):

$$\mathbf{w}(t,x) = \mathbf{c}T(t)X(x)Y(y); \tag{5.44}$$

this time the problem $\Delta Z + k^2 Z = 0$ is solved by $Z = X(x)Y(y)$; thus, by separating variables, we have

$$\frac{X''(x)}{X(x)} + \frac{Y''(y)}{Y(y)} = -k^2 = -(k_1^2 + k_2^2) \tag{5.45}$$

where

$$\frac{X''(x)}{X(x)} = -k_1^2 \quad \text{and} \quad \frac{Y''(y)}{Y(y)} = -k_2^2.$$

The solutions are

$$X(x) \propto \cos(k_1 x) \quad \text{and} \quad Y(y) \propto \cos(k_2 y), \tag{5.46}$$

where, by applying Neumann boundary conditions, $k_1 = n\pi$ and $k_2 = p\pi$ for $n,p = 0,1,2\ldots$.

Therefore conditions on wavenumbers ensuring diffusion-driven instability that we found in the previous sections are still valid, provided

$$k^2 = n^2\pi^2 + p^2\pi^2\,, \quad n, p = 0, 1, 2, \dots\,. \tag{5.47}$$

In detail:

Proposition 5.5 *Let us consider the two-dimensional problem* (5.43)*. Then pattern formation of Turing type due to destabilization of the homogeneously stable equilibrium* (u^*, v^*) *always applies for the case with non-local term, while it is feasible under conditions* (5.14) *and* (5.18) *when the interaction is only local.*
In particular the two intervals of instability for wavenumbers are, respectively,

$$k_-^2 < k^2 = k_1^2 + k_2^2 < k_+^2\,,$$

$$k_\pm^2 = \frac{1}{2D_1D_2}\left[(D_1G_v^* + D_2F_u^* + \chi v^*F_v^*) \pm \sqrt{(D_1G_v^* + D_2F_u^* + \chi v^*F_v^*)^2 - 4D_1D_2\det J}\right] \tag{5.48}$$

and

$$0 < k^2 = k_1^2 + k_2^2 < \bar{k}^2\,,$$

$$\bar{k}^2 = \frac{(D_1G_v^* + D_2F_u^* + \chi v^*F_v^*) + \sqrt{(D_1G_v^* + D_2F_u^* + \chi v^*F_v^*)^2 - 4D_1D_2\,(\det J + \delta v^*F_v^*)}}{2D_1D_2}\,. \tag{5.49}$$

Therefore

$$\mathbf{w}(t, x, y) \sim \sum_{k_1,k_2} \mathbf{c_{12}} \cos(k_1x)\cos(k_2y)\,, \tag{5.50}$$

where $k_1 = n\pi$*,* $k_2 = p\pi$ *are taken as above.*

Chapter 6

Numerical approximation of the problem

Our system has been solved with a forward in time, centered in space, explicit finite difference scheme. For reference on numerical approximation of partial differential equations, see for instance [23] or [43].
For standard diffusion equations it is well known that, in order to ensure stability and convergence of this method, the time step Δt and the space step Δx must satisfy

$$\Delta t \leq \frac{(\Delta x)^2}{2}.$$

In the case of a nonlinear reaction-diffusion-chemotaxis equation the situation is much more complicated, and it is quite difficult to derive an analogous bound for Δt. Therefore, space and time steps used for performing numerical simulations have been carefully chosen in order to avoid instability and divergence of the method.

We performed numerical simulations for both one-dimensional and two-dimensional domains: the results of the former are more easily interpreted because we can plot solution profiles, while the latter, though computationally more demanding, has been chosen because density plots in this case are more adequate to be compared with the results of the biological experiments (which basically are performed on disks).

We are going to explain both approaches in the following sections.

6.1 Numerical method for one-dimensional domain

We consider system (1.2), which is in non-dimensionalized form, thus the spatial domain is $\Omega = [0, 1]$. We are interested in computing the solution of the problem from the initial

time $t_0 = 0$ up to a given time T, so we consider $t \in [0, T]$.

First of all, we need to specify a mesh for discretization: suppose that we want to divide Ω and $[0, T]$ in N and M intervals respectively; then we can define the *space step* and *time step* as

$$\begin{aligned} \Delta x &= \frac{1}{N} \\ \Delta t &= \frac{T}{M} \end{aligned} \tag{6.1}$$

respectively; the points on the grid will be (x_i, t_j), where

$$\begin{aligned} x_i &= i\Delta x \quad \text{for} \quad i = 0 \dots N \\ t_j &= j\Delta t \quad \text{for} \quad j = 0 \dots M. \end{aligned}$$

The mesh over which we will perform our simulations is shown in Figure 6.1.

We introduce the following notation:

$$W_i^j = w(x_i, t_j)$$

and approximate the temporal derivatives with a forward difference:

$$\frac{\partial w}{\partial t}(x_i, t_j) \sim \frac{W_i^{j+1} - W_i^j}{\Delta t}, \quad i = 0 \dots N, \, j = 0 \dots M - 1; \tag{6.2}$$

the second order spatial derivatives with a centered difference scheme:

$$\frac{\partial^2 w}{\partial x^2}(x_i, t_j) \sim \frac{W_{i+1}^j - 2W_i^j + W_{i-1}^j}{(\Delta x)^2}, \quad i = 0 \dots (N-1), \, j = 0 \dots M; \tag{6.3}$$

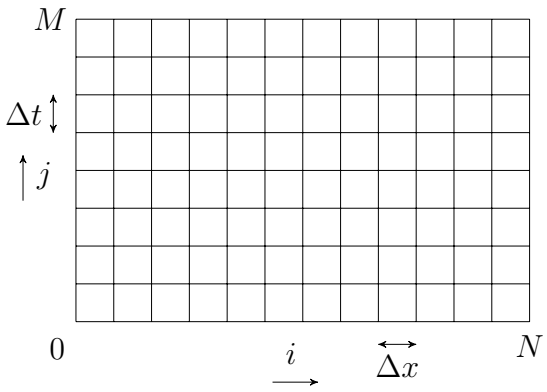

Figure 6.1: The mesh for the discretization of $\Omega \times [0, T]$.

and finally, the first order spatial derivatives appearing in the chemotactic term with a centered difference:

$$\frac{\partial w}{\partial x}(x_i, t_j) \sim \frac{W_{i+1}^j - W_{i-1}^j}{2\Delta x}\,, \quad i = 0 \dots (N-1)\,,\, j = 0 \dots M \tag{6.4}$$

Clearly, depending on the specific derivative considered, we will have either $w = u$ or $w = v$.

These are the discretizations chosen for the derivatives. We need to approximate also the integrals appearing in the equation for v in system (1.2).
To this end we use Simpson's method (see for instance [11]): using the space step defined above, the integral of function w (where this time $w = uv$ or $w = v$) over the spatial domain Ω is discretized as follows:

$$\int_\Omega w(t,x)dx \sim \frac{\Delta x}{3} \sum_{\substack{i=1\dots(N-1)\\ i\,\text{odd}}} \left[W_{i-1}^j + 4W_i^j + W_{i+1}^j\right]. \tag{6.5}$$

We may also use other methods; this issue is briefly addressed in Section 6.1.1.

Therefore the discretization of model (1.2) is, for $i = 1 \dots (N-1)$ and $j = 1 \dots (M-1)$, given by

$$\begin{aligned}
\frac{U_i^{j+1} - U_i^j}{\Delta t} &= D_1 \frac{U_{i+1}^j - 2U_i^j + U_{i-1}^j}{(\Delta x)^2} + U_i^j(1 - U_i^j) - U_i^j V_i^j \\
\frac{V_i^{j+1} - V_i^j}{\Delta t} &= D_2 \frac{V_{i+1}^j - 2V_i^j + V_{i-1}^j}{(\Delta x)^2} - \chi \frac{U_{i+1}^j - 2U_i^j + U_{i-1}^j}{(\Delta x)^2} V_i^j \\
&\quad -\chi \frac{(U_{i+1}^j - U_{i-1}^j)}{2\Delta x} \frac{(V_{i+1}^j - V_{i-1}^j)}{2\Delta x} - \mu V_i^j - \frac{\gamma U_i^j V_i^j}{1 + \tau V_i^j} \\
&\quad +\delta \frac{\sum_{\substack{i=1\dots(N-1)\\ i\,\text{odd}}} \left[U_{i-1}^j V_{i-1}^j + 4U_i^j V_i^j + U_{i+1}^j V_{i+1}^j\right]}{\sum_{\substack{i=1\dots(N-1)\\ i\,\text{odd}}} \left[V_{i-1}^j + 4V_i^j + V_{i+1}^j\right]} V_i^j.
\end{aligned} \tag{6.6}$$

Finally, we have to deal with initial and Neumann boundary conditions. The former are included in the initialization: for all i, U_i^0 and V_i^0 are assigned according to the initial value given as an input.
The latter are taken into account in the following way: at every time step we assume, without loss of generality, that there exist two additional points, one on the left of $x = 0$ (that we are going to name $-\Delta x$) and one on the right of $x = 1 = N\Delta x$ (named

$(N+1)\Delta x$); Neumann boundary conditions hence become

$$\frac{\partial w}{\partial \nu}(0,t_j) \sim \frac{W_1^j - W_{-1}^j}{2\Delta x} = 0$$

$$\frac{\partial w}{\partial \nu}(1,t_j) \sim \frac{W_{N+1}^j - W_{N-1}^j}{2\Delta x} = 0$$

which imply

$$W_1^j = W_{-1}^j \quad \text{and} \quad W_{N+1}^j = W_{N-1}^j$$

for $W = U, V$ and $j = 0 \dots M$.
Consequently, for $i = 0$ and $i = N$ the first-order spatial derivatives in the equation for v are zero, while the second-order spatial derivatives become

$$\begin{aligned} \frac{\partial^2 w}{\partial x^2}(0,t_j) &\sim \frac{W_1^j - 2W_0^j + W_{-1}^j}{(\Delta x)^2} = \frac{2(W_1^j - W_0^j)}{(\Delta x)^2} \\ \frac{\partial^2 w}{\partial x^2}(1,t_j) &\sim \frac{W_{N+1}^j - 2W_N^j + W_{N-1}^j}{(\Delta x)^2} = \frac{2(W_{N+1}^j - W_N^j)}{(\Delta x)^2}\,. \end{aligned} \tag{6.7}$$

6.1.1 On the discretization of integrals

In order to approximate the integrals appearing in model (1.2) we use Simpson's method; clearly, this is not the only admissible choice: other methods may be used, such as, for instance, Romberg's method (see [11]) which is proven to be more accurate. Another possibility is to use the approximation given by Riemann sums: this is a more naive approach, but still accurate if the step is taken small enough.
In our numerical simulations we tested these three types of discretization: the results did not differ significantly, provided the space step was small enough for convergence; moreover, Romberg's method is computationally more demanding than the other two.
Therefore we chose to use Simpson method as a good compromise between accuracy and computational cost.

6.2 Numerical method for a square domain

The aforementioned numerical method can be extended to the case of a two-dimensional spatial domain Ω; that is, when we consider system (1.3).
Firstly, we consider a square domain, i.e. $\Omega = [0,1] \times [0,1]$ (we may also use a rectangular domain: the procedure would be exactly the same). In this case we have to construct a

three-dimensional mesh: assuming that Ω lies on the $x-y$ plane, we divide the side of the square along the x-axis into N intervals, and the side along the y-axis into P intervals; the time interval $[0, T]$ is divided, as before, into M intervals.
Therefore we get the two space steps and the time step as in (6.1):

$$\Delta x = \frac{1}{N}$$

$$\Delta y = \frac{1}{P} \tag{6.8}$$

$$\Delta t = \frac{T}{M}$$

and a generic point on the grid, (a representation of which is shown in Figure 6.2) is (x_i, y_k, t_j) where

$$\begin{aligned} x_i &= i\Delta x \quad \text{for} \quad i = 0 \dots N \\ y_k &= k\Delta y \quad \text{for} \quad k = 0 \dots P \\ t_j &= j\Delta t \quad \text{for} \quad j = 0 \dots M. \end{aligned}$$

Notice that, for simmetry reasons, in our simulations we will always take $N = P$, i.e. $\Delta x = \Delta y$.
Therefore this time the discretized model will be function of $U^j_{i,k} = u(x_i, y_k, t_j)$ and $V^j_{i,k} = v(x_i, y_k, t_j)$.

The second-order derivatives are replaced here by the Laplacian, so we have

$$\begin{aligned} \Delta w(x_i, y_k, t_j) \quad \sim \quad & \frac{W^j_{i+1,k} - 2W^j_{i,k} + W^j_{i-1,k}}{(\Delta x)^2} + \frac{W^j_{i,k+1} - 2W^j_{i,k} + W^j_{i,k-1}}{(\Delta y)^2}\,, \\ & i = 0 \dots (N-1)\,, k = 0 \dots (P-1)\,,\ j = 0 \dots M\,; \end{aligned} \tag{6.9}$$

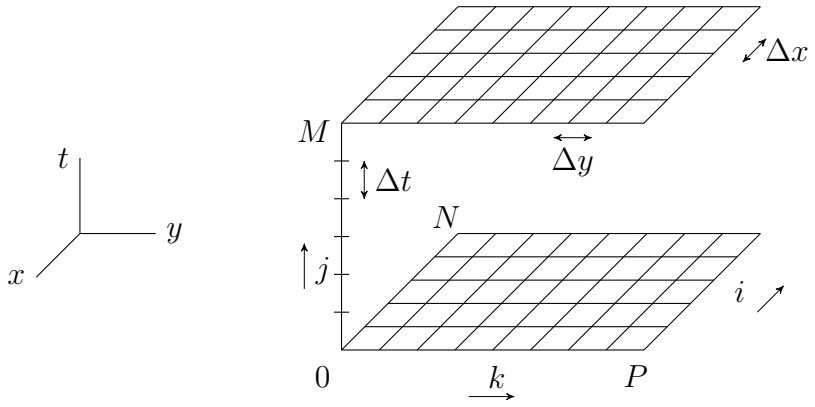

Figure 6.2: The spatial domain Ω is discretized into small rectangles; the system is evaluated over this spatial mesh at times $0 \le t_j \le T$.

the first-order derivative with respect to y is

$$\frac{\partial w}{\partial y}(x_i, y_k, t_j) \sim \frac{W^j_{i,k+1} - W^j_{i,k-1}}{2\Delta y}\,, \quad i = 0 \dots (N-1)\,,\ k = 0 \dots (P-1)\,,\ j = 0 \dots M\,. \tag{6.10}$$

Clearly, the integral term now contains double integrals. We may use Simpson's method as we did in Section 6.1, extended to two dimensions; however, this is more complex to implement and computationally heavier, so we decide to approximate the integral by means of Riemann sums: at every time step j,

$$\iint_\Omega w\, dxdy \sim \sum_{i=0}^{N}\sum_{k=0}^{P} W^j_{i,k}\Delta x\Delta y\,; \tag{6.11}$$

if Δx and Δy are sufficiently small, this simple approximation will be accurate enough to avoid us appealing to more refined methods.

We can therefore write our numerical approximation of system (1.3):

$$\begin{aligned}
\frac{U^{j+1}_{i,k} - U^j_{i,k}}{\Delta t} &= D_1 \left(\frac{U^j_{i+1,k} - 2U^j_{i,k} + U^j_{i-1,k}}{(\Delta x)^2} + \frac{U^j_{i,k+1} - 2U^j_{i,k} + U^j_{i,k-1}}{(\Delta y)^2} \right) \\
&\quad + U^j_{i,k}(1 - U^j_{i,k}) - U^j_{i,k}V^j_{i,k} \\
\\
\frac{V^{j+1}_{i,k} - V^j_{i,k}}{\Delta t} &= D_2 \left(\frac{V^j_{i+1,k} - 2V^j_{i,k} + V^j_{i-1,k}}{(\Delta x)^2} + \frac{V^j_{i,k+1} - 2V^j_{i,k} + V^j_{i,k-1}}{(\Delta y)^2} \right) \\
&\quad - \chi \left(\frac{U^j_{i+1,k} - 2U^j_{i,k} + U^j_{i-1,k}}{(\Delta x)^2} + \frac{U^j_{i,k+1} - 2U^j_{i,k} + U^j_{i,k-1}}{(\Delta y)^2} \right) V^j_{i,k} \\
&\quad - \chi \frac{(U^j_{i+1,k} - U^j_{i-1,k})}{2\Delta x} \frac{(V^j_{i+1,k} - V^j_{i-1,k})}{2\Delta x} \\
&\quad - \chi \frac{(U^j_{i,k+1} - U^j_{i,k-1})}{2\Delta y} \frac{(V^j_{i,k+1} - V^j_{i,k-1})}{2\Delta y} \\
&\quad - \mu V^j_{i,k} - \frac{\gamma U^j_{i,k}V^j_{i,k}}{1 + \tau V^j_{i,k}} + \delta \frac{\sum_{i=0}^{N}\sum_{k=0}^{P} U^j_{i,k}V^j_{i,k}\Delta x\Delta y}{\sum_{i=0}^{N}\sum_{k=0}^{P} V^j_{i,k}\Delta x\Delta y} V^j_i\,,
\end{aligned} \tag{6.12}$$

for $i = 1 \dots (N-1)$, $k = 1 \dots (P-1)$ and $j = 1 \dots M$.

Finally, we come to initial and boundary conditions. For initial conditions, U^0_{ik} and V^0_{ik} are assigned for every point of the spatial mesh (x_i, y_k), $i = 0 \dots N$, $j = 0 \dots P$.

As regards Neumann boundary conditions, we need to divide the points of the sides of the square into three categories:

a) points of the kind $(0, y_k)$ and $(1, y_k)$, $k = 1 \dots (P-1)$;

b) points of the kind $(x_i, 0)$ and $(x_i, 1)$, $i = 1 \dots (N-1)$;

c) vertices $(0,0)$, $(0,1)$, $(1,0)$ and $(1,1)$.

For points of type a) the normal derivative is parallel to the x-axis: so, as in Section 6.1, we can think, without loss of generality, of having two additional points $(x_{-\Delta x}, y_k)$ and $(x_{(N+1)\Delta x}, y_k)$ so that first-order derivatives are zero while the Laplacians become

$$\begin{aligned} \Delta w(0, y_k, t_j) &\sim \frac{2(W^j_{1,k} - W^j_{0,k})}{(\Delta x)^2} + \frac{W^j_{0,k+1} - 2W^j_{0,k} + W^j_{0,k-1}}{(\Delta y)^2} \\ \Delta w(1, y_k, t_j) &\sim \frac{2(W^j_{N+1,k} - W^j_{N,k})}{(\Delta x)^2} + \frac{W^j_{N,k+1} - 2W^j_{N,k} + W^j_{N,k-1}}{(\Delta y)^2} \,. \end{aligned} \tag{6.13}$$

For the points of type b), instead, the normal derivative is parallel to the y-axis, so the additional points are $(x_i, y_{-\Delta y})$ and $(x_i, y_{(P+1)\Delta y})$, and the Laplacians are

$$\begin{aligned} \Delta w(x_i, 0, t_j) &\sim \frac{W^j_{i+1,0} - 2W^j_{i,0} + W^j_{i-1,0}}{(\Delta x)^2} + \frac{2(W^j_{i,1} - W^j_{i,0})}{(\Delta y)^2} \\ \Delta w(x_i, 1, t_j) &\sim \frac{W^j_{i+1,P} - 2W^j_{i,P} + W^j_{i-1,P}}{(\Delta x)^2} + \frac{2(W^j_{i,P+1} - W^j_{i,P})}{(\Delta y)^2} \,. \end{aligned} \tag{6.14}$$

Finally, for the four vertices (points of type c)) the Laplacians are taken to be

$$\begin{aligned} \Delta w(0,0,t_j) &\sim \frac{2(W^j_{1,0} - W^j_{0,0})}{(\Delta x)^2} + \frac{2(W^j_{0,1} - W^j_{0,0})}{(\Delta y)^2} \\ \Delta w(1,0,t_j) &\sim \frac{2(W^j_{N,0} - W^j_{N-1,0})}{(\Delta x)^2} + \frac{2(W^j_{N,1} - W^j_{N,0})}{(\Delta y)^2} \\ \Delta w(0,1,t_j) &\sim \frac{2(W^j_{1,P} - W^j_{0,P})}{(\Delta x)^2} + \frac{2(W^j_{0,P} - W^j_{0,P-1})}{(\Delta y)^2} \\ \Delta w(1,1,t_j) &\sim \frac{2(W^j_{N,P} - W^j_{N-1,P})}{(\Delta x)^2} + \frac{2(W^j_{N,P} - W^j_{N,P-1})}{(\Delta y)^2} \,. \end{aligned} \tag{6.15}$$

6.3 Numerical method for a circular domain

As we said in the introduction of this chapter, in order to compare our model with experiments from biology, we need to use a two-dimensional domain; moreover, since co-cultures of amoebae and bacteria are made on petri dishes, it is more suitable considering a circular domain (rather than a square one). This is the issue we address in this section.

If Ω is a circle, we may use finite elements methods rather than finite differences; or we may write our problem in polar coordinates, build a polar mesh and use finite differences. Actually, we choose an alternative approach. Since we have already implemented the numerical approximation on a square domain, we can maintain the rectangular mesh and build the new circular domain over it: we assign a negative value (say, -2) to the nodes of the mesh lying outside the circle of radius $1/2$ inscribed in the square.
In this way, points where u and v have this value are not considered when evaluating (6.12), because they do not belong to the circle.

One may think that a rectangular mesh on a circular domain is not so appropriate; actually, if space steps are sufficiently small, the rectangular grid is almost the same as the polar one.

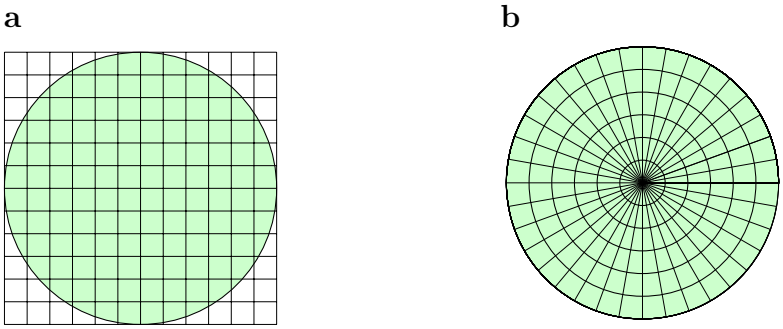

Figure 6.3: On a circular domain we may use either a polar grid or a rectangular one: if steps are sufficiently small, the two options are almost equivalent. **a** Rectangular mesh. **b** Polar mesh.

Therefore, for all rows $i = 0 \dots N$ we define two indices, named left$[i]$ and right$[i]$, which approximate the margins of the circle for that specific row[1], as shown in Figure 6.4; so that at every time step $0 < t_j \leq T$, we evaluate (6.12) for all i between 1 and $N - 1$ and for j between left$[i]$ and right$[i]$ (instead of $j = 1 \dots (M - 1)$). The integrals appearing in the equation for amoebae have obviously been evaluated only on the circle. Consequently, also Neumann boundary conditions have to be imposed on left$[i]$ and right$[i]$

[1] for small space steps this is a good approximation.

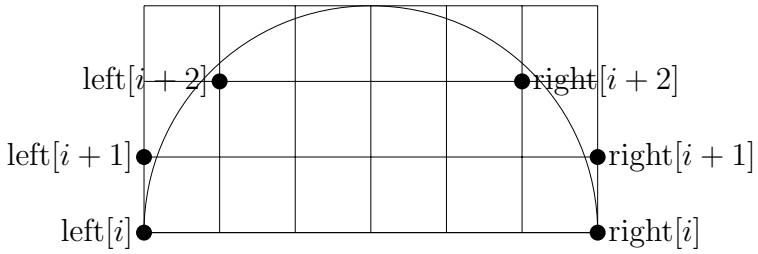

Figure 6.4: Definition of column indices left[i] and right[i].

instead of the sides of the square.
These are the only changes to be done in order to adapt the method presented in the previous section.

6.4 Initial conditions

Simulations were run with initial conditions of two types: either both amoeboid and bacterial populations are distributed all over the domain Ω, or there is a homogeneous layer of bacteria with a spot of amoebae in the center.
The first choice corresponds to a situation where it is interesting to study and verify numerically the formation of Turing patterns. The latter, instead, reproduces the initial conditions of *in vivo* experiments, where bacteria are plated homogeneously on the petri dish and then a small amount of amoebae is inoculated.
Since, of course, in real experiments there are some fluctuations, so that the concentration of cells in a homogeneous layer actually is not exactly homogeneous, we have also performed simulations accounting for a perturbed initial datum. This stochastic variability has been modeled by W_{ik}^0 ($W = U$ or $W = V$), where W_{ik}^0 are independent Gaussian random variables of mean w^0 and variance assigned.

Chapter 7

Simulations

In this part we will show the results of some representative simulations taken from these that we have performed to validate the findings of the previous chapters. In particular we will focus on whether Turing pattern formation occurs or not depending on the conditions presented in Chapter 5.
We will consider firstly a one-dimensional domain, and then a two-dimensional circular domain; on both of them we will start from a perturbation of the spatially uniform steady state.
We will investigate the role of the integral term on determining the type of pattern emerging at large times. Finally, we will perform some simulations with initial data related to biological experiments: a spot of amoeboid population is put over a homogeneous layer of bacteria.
Numerical methods used have been presented in Chapter 6.

7.1 Simulations without integral term

In this Section we show the results of simulations regarding Turing pattern formation when assuming that the uptake of bacteria is only local (i.e., the predation term is not integral). We are going to consider both the case of one-dimensional and two-dimensional domains, and for these two cases we are going to see what is the behavior when the chemotactic coefficient satisfies conditions for pattern formation, when conditions are violated or when chemotaxis is absent. Moreover, we are going to show that there is no qualitative difference if the case under examination gives one or two homogeneous coexistence steady states.

Parameter	value
D_1	0.7
D_2	0.05
χ	0.0, 0.03, 1.0
μ	0.95
δ	5.0
γ	4.0
τ	0.5
u_0	0.5
v_0	0.4

Table 7.1: Parameters for simulations without integral. This combination leads to one coexistence steady state.

7.1.1 One-dimensional domain

We consider the problem without integral over the domain $\Omega = [0, 1]$.
Firstly we give an example where there is only one internal steady state; this equilibrium is homogeneously stable, and we are going to show how it can be destabilized by diffusion and chemotaxis.
The set of parameters for the model is summarized in Table 7.1. The resulting steady state is given by $u^* = 0.545952$, $v^* = 0.454048$; it is stable because $\mathrm{tr}J(E^*) = -0.216661$ and $\det J(E^*) = 0.251569$. Calculations lead to deduce that the critical value for χ (see Equation (5.21)) is equal to $\chi_{\mathrm{crit}} = 0.062679$.
Therefore if we take $\chi = 0.0$, then we have that condition (5.14) is satisfied and $\chi < \chi_{\mathrm{crit}}$, so patterns should arise. This is in fact what happens, as can be seen in Figure 7.1.

If we take $\chi = 0.03$, conditions remain valid, so we still have patterns, as in Figure 7.2.

If instead we consider $\chi = 1.0$, then we cannot have diffusion-driven instability because conditions are not satisfied. This is confirmed from simulations: after some initial oscillations, then solution tends homogeneously to the initially perturbed steady state, as can be seen in Figure 7.3.

a

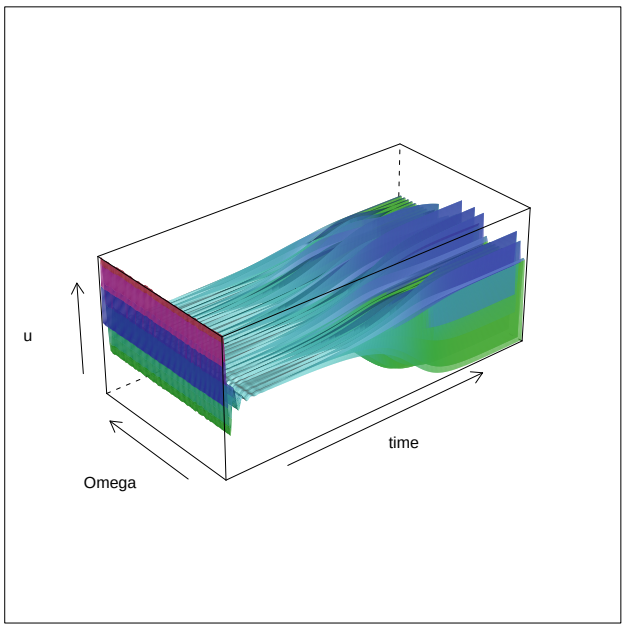

b

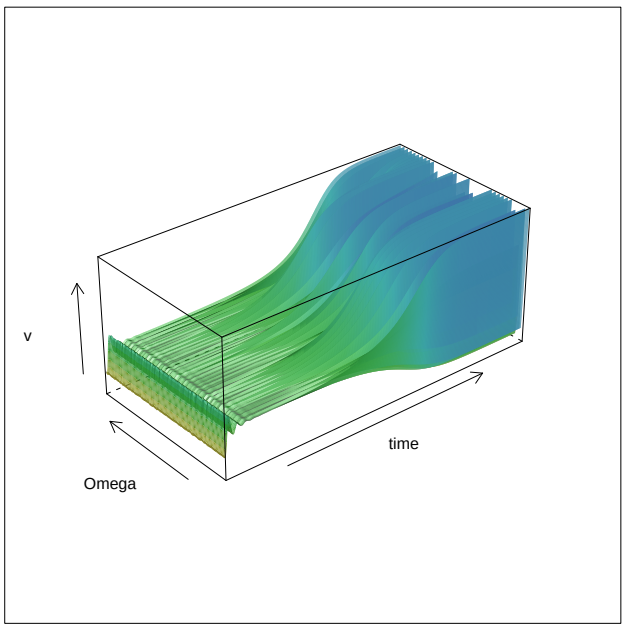

Figure 7.1: Behavior of the solution over time and space with parameters as in Table 7.1 and $\chi = 0.0$. **a** Representation of u (bacteria). **b** Representation of v (amoebae).

a

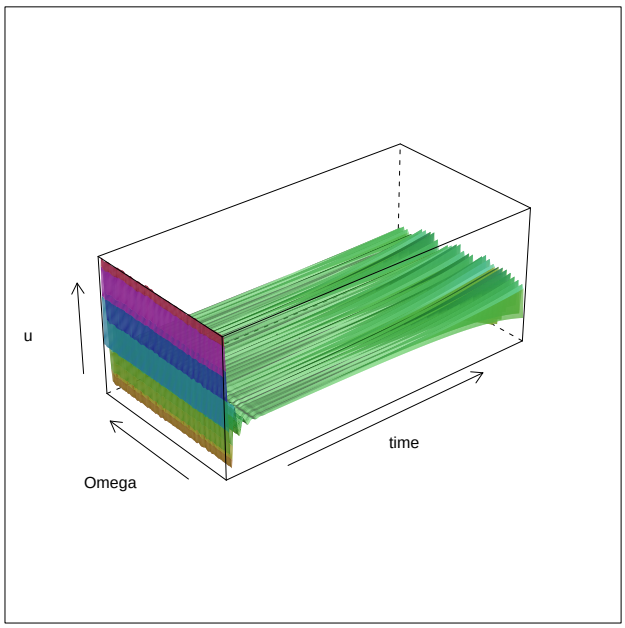

b

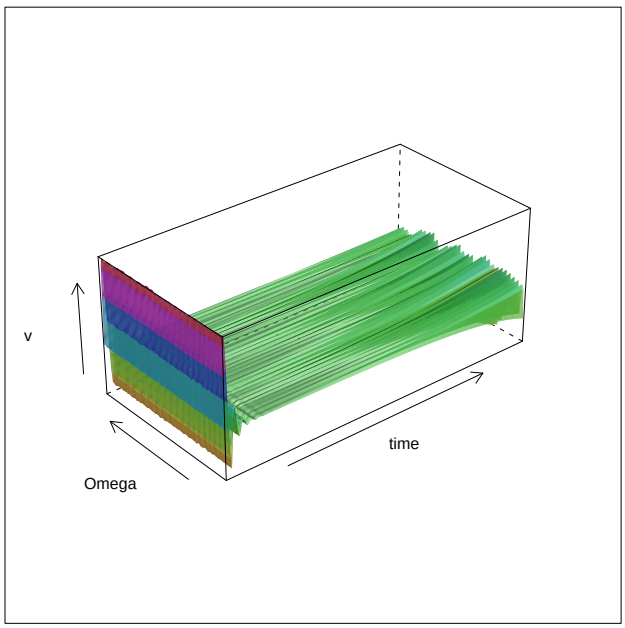

Figure 7.2: Behavior of the solution over time and space with parameters as in Table 7.1 and $\chi = 0.03$. **a** Representation of u (bacteria). **b** Representation of v (amoebae).

a

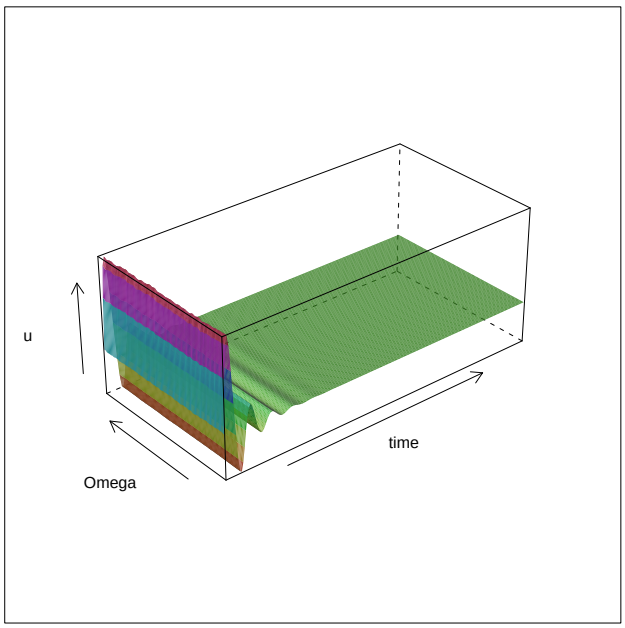

b

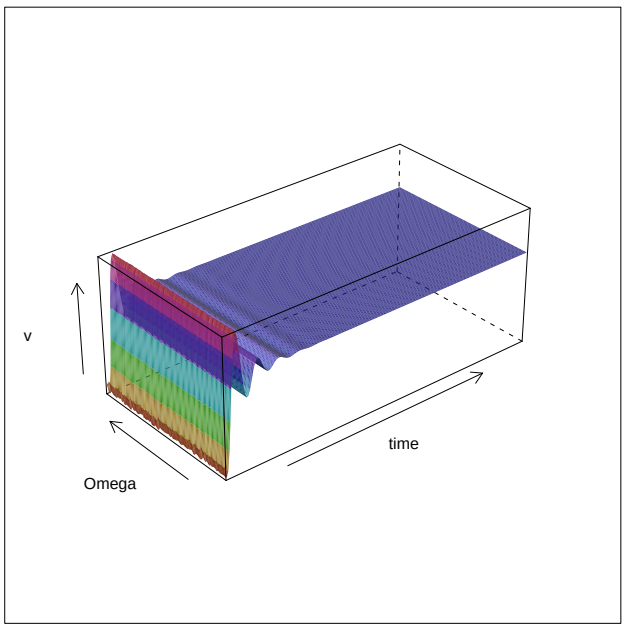

Figure 7.3: Behavior of the solution over time and space with parameters as in Table 7.1 and $\chi = 1.0$. **a** Representation of u (bacteria). **b** Representation of v (amoebae).

Parameter	value
D_1	0.7
D_2	0.05
χ	0.0, 0.03, 0.07
μ	1.05
δ	5.0
γ	4.0
τ	1.0
u_0	0.4
v_0	0.6

Table 7.2: Parameters for simulations without integral. This combination leads to two coexistence steady states.

In the second example we investigate what happens if there are two coexistence states. We may expect the same behavior as in the previous example, since we know that one of the internal states is certainly unstable, so we have to start from the other one, which needs to be stable, and try to destabilize it and form patterns. The parameters are summarized in Table 7.2.

The two coexistence steady state here are $E_+^* = (0.427466, 0.572534)$ and $E_-^* = (0.982534, 0.017466)$; by evaluating the corresponding Jacobian matrices we see that the former is stable, while the latter is unstable. Moreover, the critical value for χ (evaluated from (5.21)) is $\chi_{\text{crit}} = 0.040181$.
As before, we first take $\chi = 0.0$: conditions (5.14) and (5.18) are satisfied so that spatial patterns form, as we can see in Figure 7.4.

The same happens when $\chi = 0.03$; there is pattern formation again, but we can notice from Figure 7.5 that the resulting pattern is different. This means, as it may be expected, that we can observe a variety of patterns by simply varying the value for χ.

For values $\chi > \chi_{\text{crit}}$ patterns cannot form. Figure 7.6 shows the results when taking $\chi = 0.07$.

These two examples show a qualitatively similar behavior so, as it may be expected, the fact that system (3.1) admits one or two internal steady states does not affect the occurrence of patterns.

a

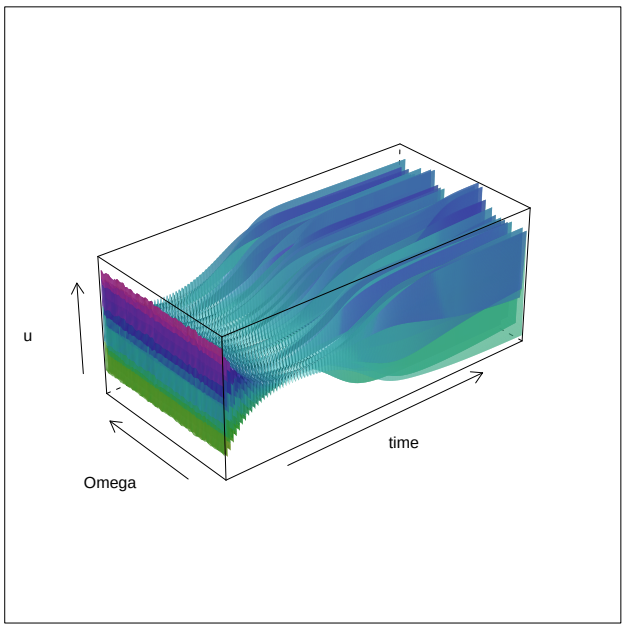

b

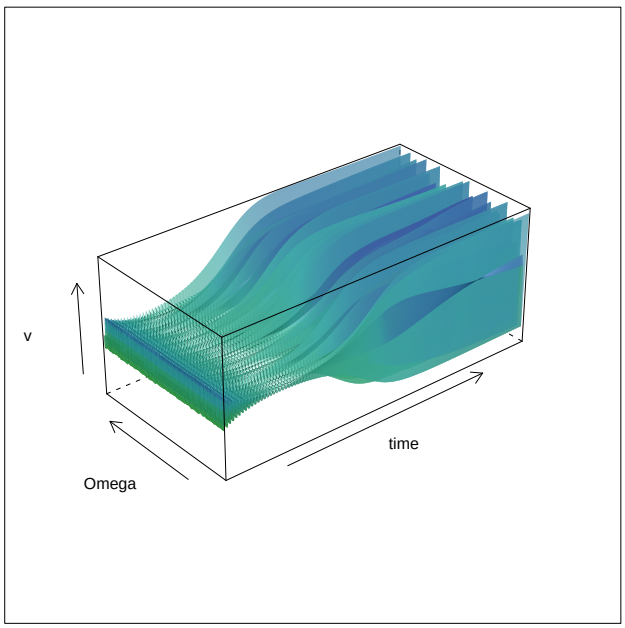

Figure 7.4: Behavior of the solution over time and space with parameters as in Table 7.2 and $\chi = 0.0$. **a** Representation of u (bacteria). **b** Representation of v (amoebae).

a

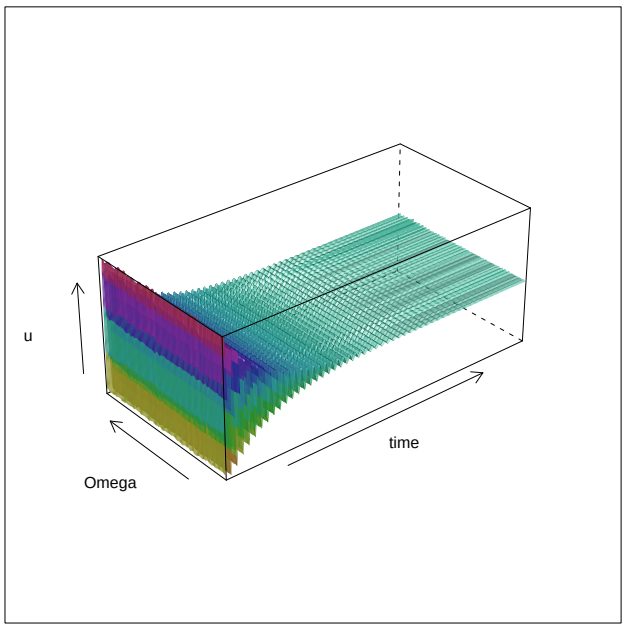

b

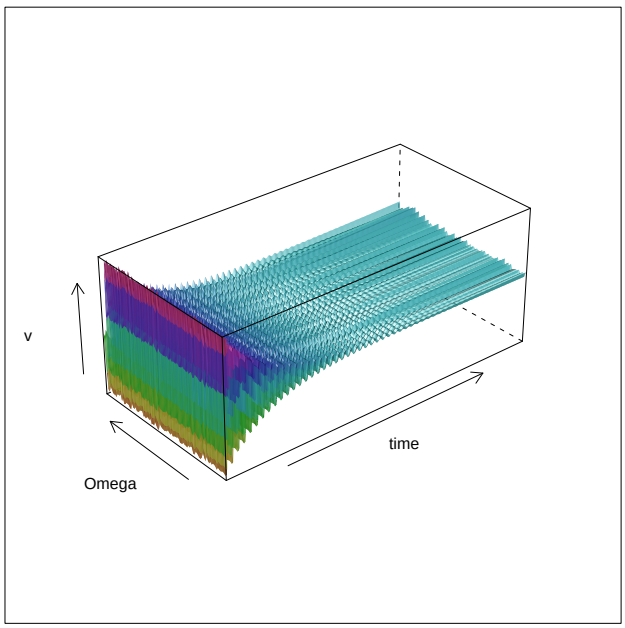

Figure 7.5: Behavior of the solution over time and space with parameters as in Table 7.2 and $\chi = 0.03$. **a** Representation of u (bacteria). **b** Representation of v (amoebae).

a

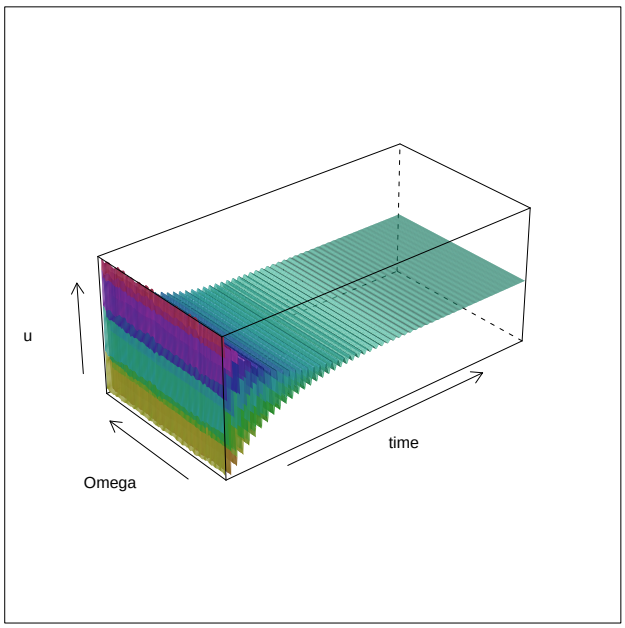

b

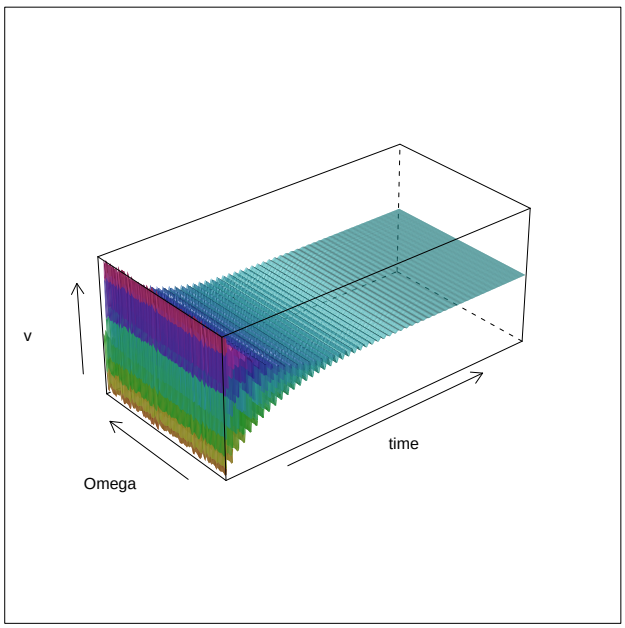

Figure 7.6: Behavior of the solution over time and space with parameters as in Table 7.2 and $\chi = 0.07$. **a** Representation of u (bacteria). **b** Representation of v (amoebae).

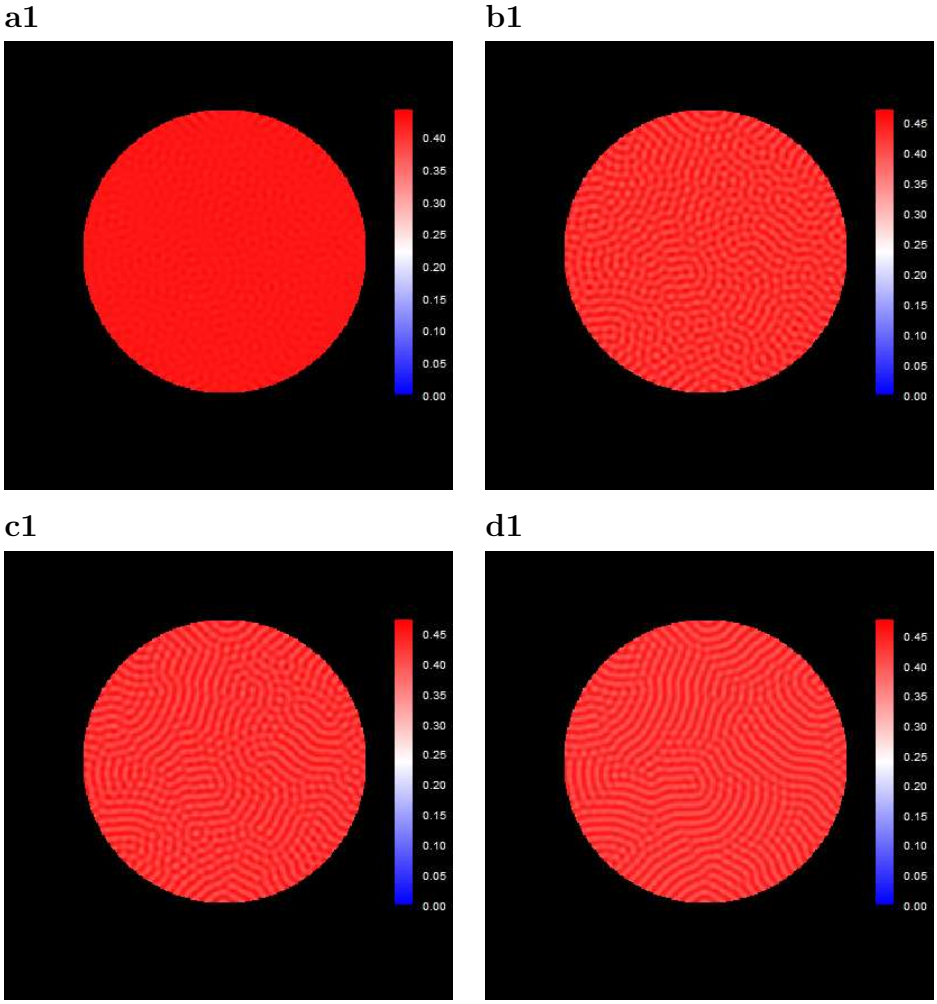

Figure 7.7: Simulation results for bacteria on a circular domain when parameters are as in Table 7.2 and $\chi = 0.0$ (conditions for pattern satisfied). **a1** $t = 200$; **b1** $t = 600$; **c1** $t = 1000$; **d1** $t = 2000$.

7.1.2 Two-dimensional domain

We also show the corresponding simulations for a circular domain. We use the same parameters as in the example with two internal states (see Table 7.2), so conditions for pattern formation are exactly the same.
Taking $\chi = 0.0$ and $\chi = 0.03$ we get two different patterns, shown in Figures 7.7, 7.8 and 7.9, 7.10 respectively.

These figures confirm that resulting patterns can be quite different: the experiment without chemotaxis gives a "striped" pattern, while the other one has a more "spotted" structure. This may depend on the fact that chemotaxis is an aggregation process, so it

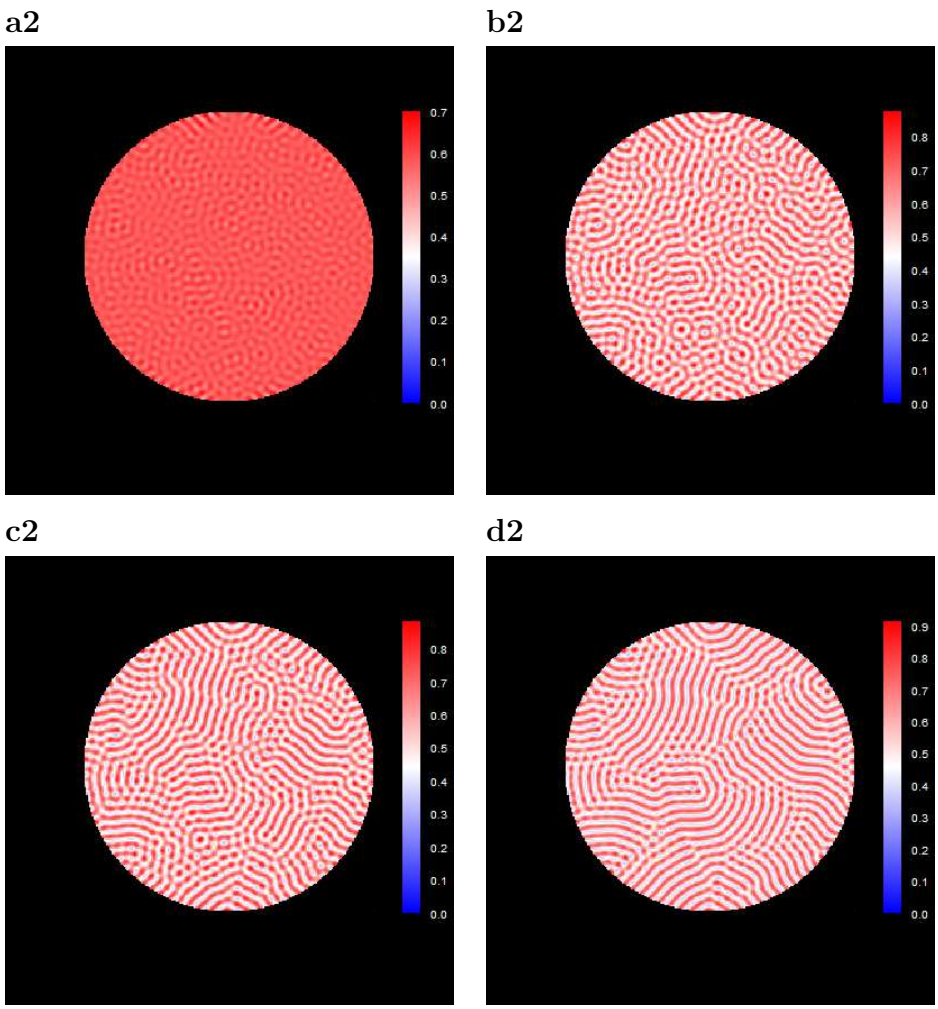

Figure 7.8: Simulation results for amoebae on a circular domain when parameters are as in Table 7.2 and $\chi = 0.0$ (conditions for pattern satisfied). **a2** $t = 200$; **b2** $t = 600$; **c2** $t = 1000$; **d2** $t = 2000$.

may enhance the formation of spots instead of stripes. From the mathematical viewpoint, the instability interval for wavenumbers is different in the two cases ($2.65008 < k^2 < 4.65684$ and $3.04721 < k^2 < 4.04993$ respectively), so the unstable modes of the solution at large times are not the same, and this can explain the variability in the type of pattern emerging.

When χ is such that theoretical conditions for pattern formation are violated, simulations confirm that the homogeneously stable steady state cannot be destabilized by means of chemotaxis (figures not shown).

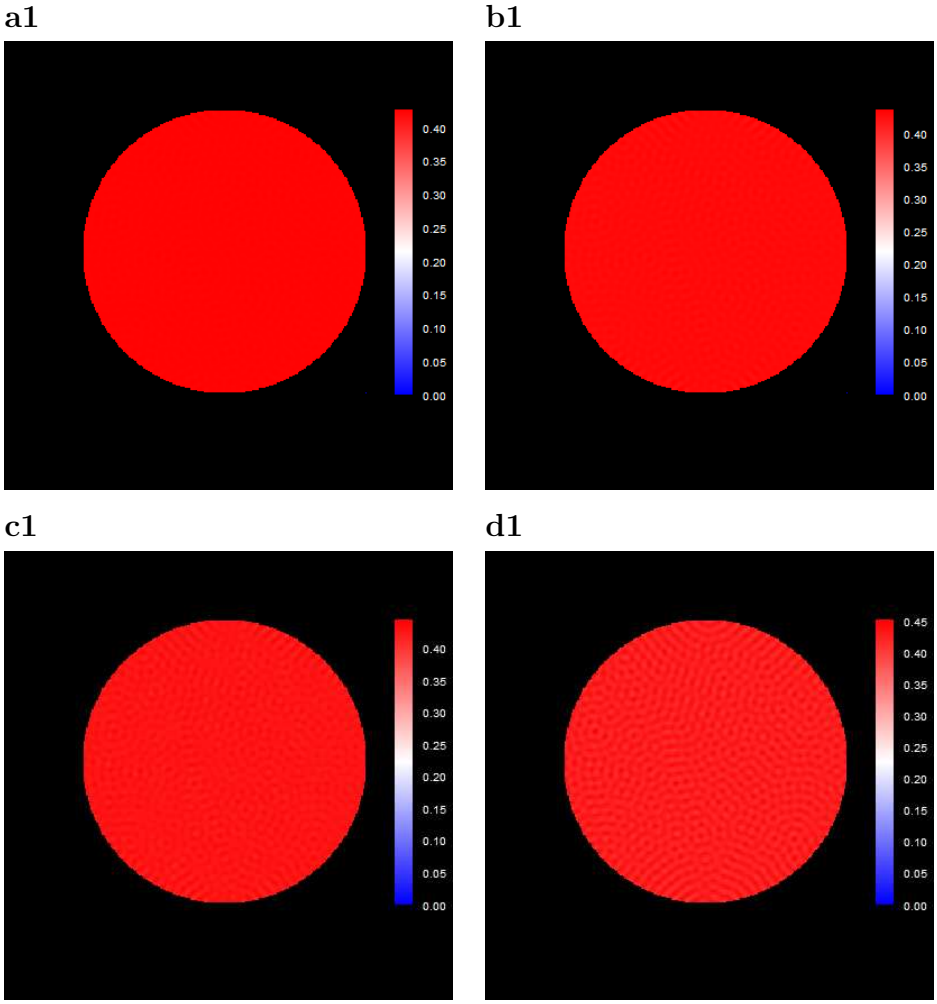

Figure 7.9: Simulation results for bacteria on a circular domain when parameters are as in Table 7.2 and $\chi = 0.03$ (conditions for pattern satisfied). **a1** $t = 200$; **b1** $t = 600$; **c1** $t = 1000$; **d1** $t = 2000$.

7.2 Simulations with integral term

In this Section we consider the same sets of parameters used in Section 7.1, and we are going to perform simulations for the model with integral term. We will see that the behavior of the solution differs from the case of a local interaction.

7.2.1 One-dimensional domain

Over the one-dimensional domain $\Omega = [0, 1]$ we first use parameters as in Table 7.1. We remind that in this case the stable internal state is $E^* = (0.545952, 0.454048)$; this

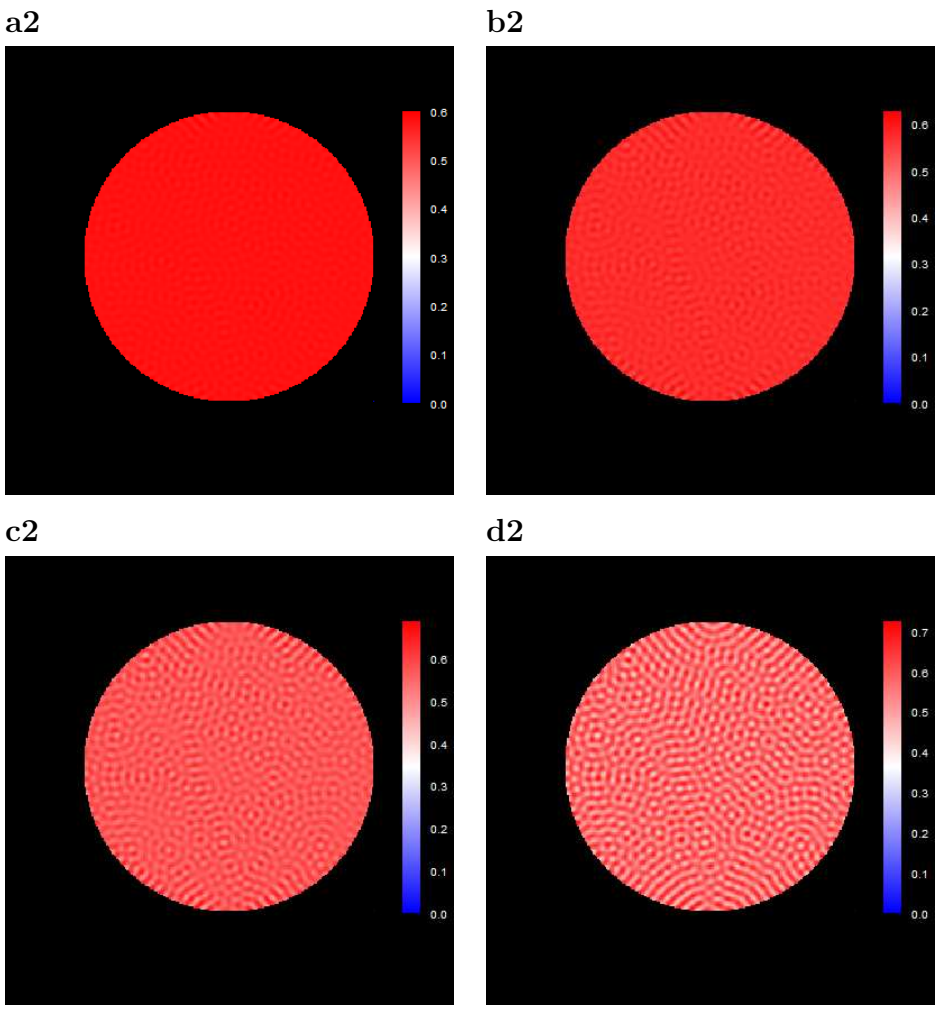

Figure 7.10: Simulation results for amoebae on a circular domain when parameters are as in Table 7.2 and $\chi = 0.03$ (conditions for pattern satisfied). **a2** $t = 200$; **b2** $t = 600$; **c2** $t = 1000$; **d2** $t = 2000$.

time instead, from the results of Section 5.2 we know that there is no critical value for chemotactic sensitivity, because pattern formation always occurs. We are going to use the same chemotactic coefficients as before, so that we can compare the two cases (without and with integral).
Firstly we consider $\chi = 0.0$: the results are shown in Figure 7.11.

The simulation shows a completely different pattern: starting from the perturbation of E^*, the solution has some small oscillations over Ω which after a short time are dumped, except for one small region where a peak appears; in the end, the solution is constant with a peak of constant height and width for concentration of amoebae v and a corresponding

a

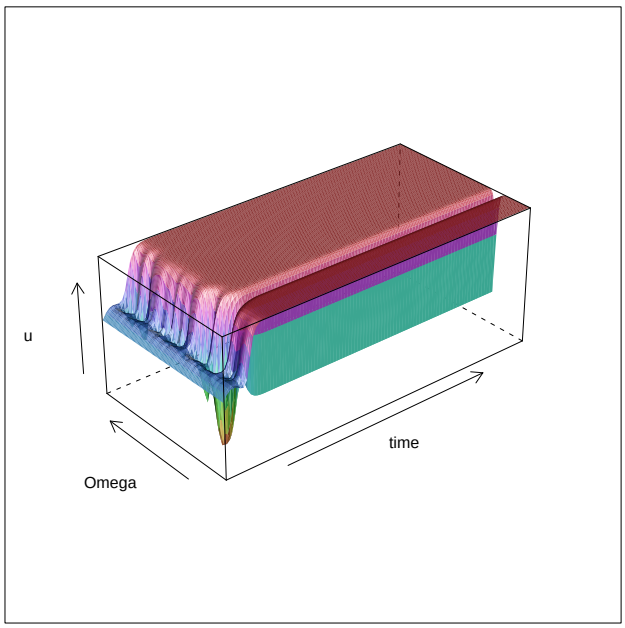

b

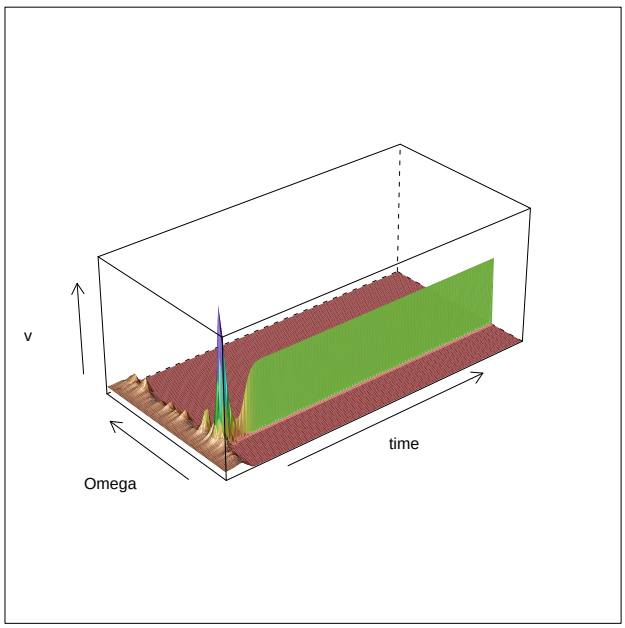

Figure 7.11: Behavior of the solution over time and space with parameters as in Table 7.1 and $\chi = 0.0$. **a** Representation of u (bacteria). **b** Representation of v (amoebae).

sink for concentration of bacteria u. The same qualitative behavior appears if we take $\chi = 0.03$ and $\chi = 1.0$ (results in Figures 7.12 and 7.13 respectively) as well as other values (results not shown), which differ from one another in the transient phase and for the values reached at large times.

The output does not change qualitatively when we take the parameters of the model as in Table 7.2, so that we have the stable state $E_+^* = (0.427466, 0.572534)$ and the unstable state $E_-^* = (0.982534, 0.017466)$. Also here we compute the solution for $\chi = 0.0$ (Figure 7.14), $\chi = 0.03$ (Figure 7.15) and $\chi = 0.07$ (Figure 7.16), to find, again, that at large times amoebae form a single peak while in bacterial population correspondingly there is a sink. Different chemotactic sensitivities result only in different values reached.
The location of the peak and sink in Ω depends on the perturbation of the initial datum: if another simulation is run with a different noise for perturbing (u_0, v_0), then the behavior is the same, except that the peak (and sink) may change its position (figures not shown).

a

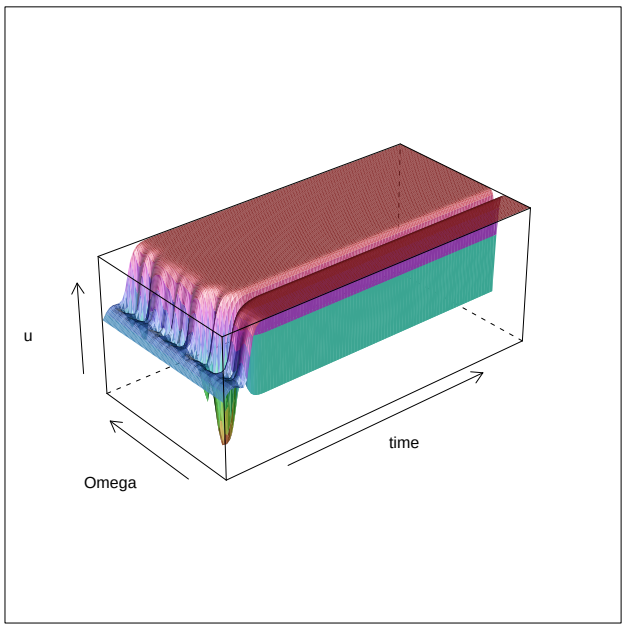

b

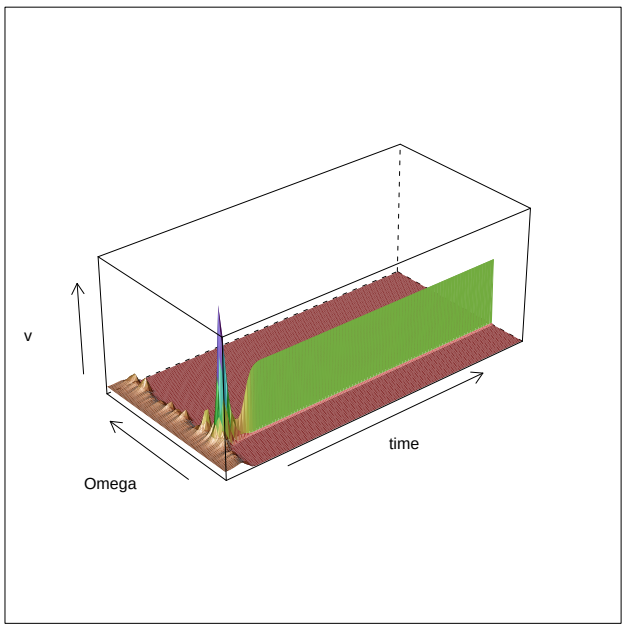

Figure 7.12: Behavior of the solution over time and space with parameters as in Table 7.1 and $\chi = 0.03$. **a** Representation of u (bacteria). **b** Representation of v (amoebae).

a

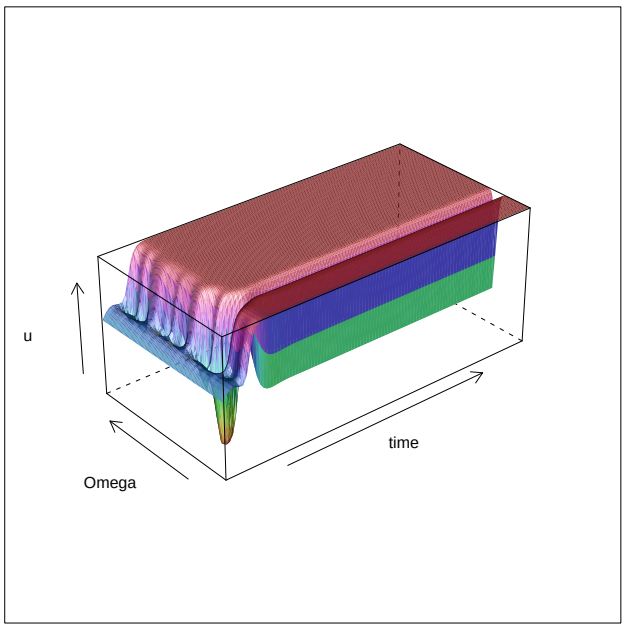

b

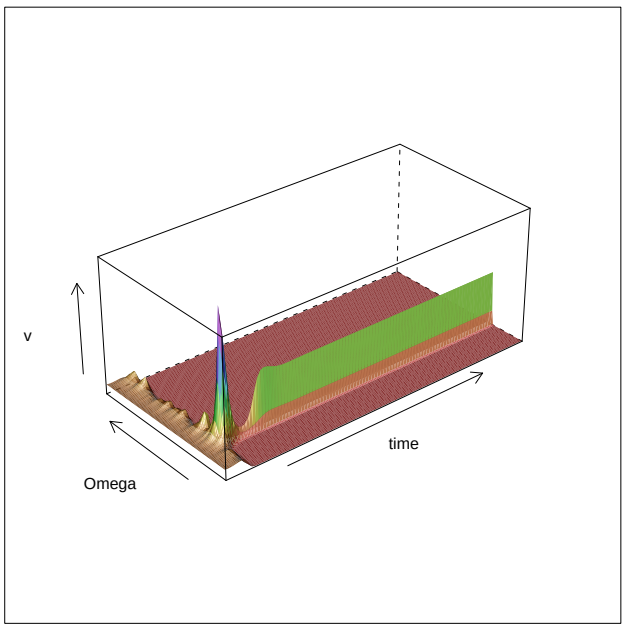

Figure 7.13: Behavior of the solution over time and space with parameters as in Table 7.1 and $\chi = 1.0$. **a** Representation of u (bacteria). **b** Representation of v (amoebae).

a

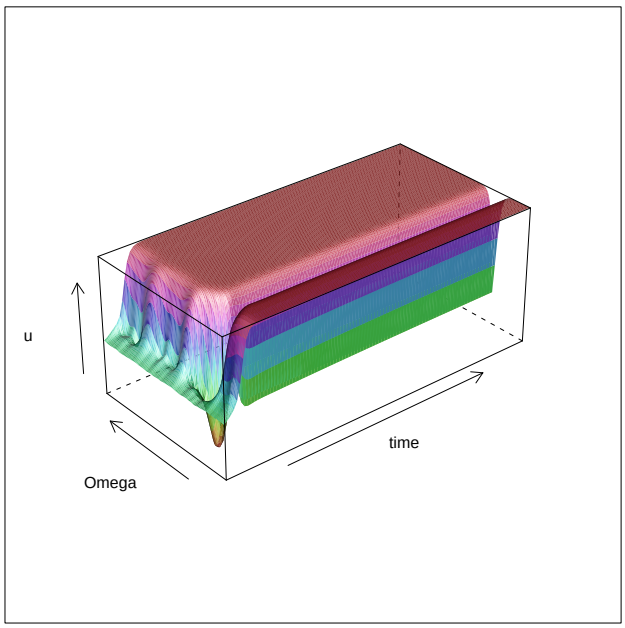

b

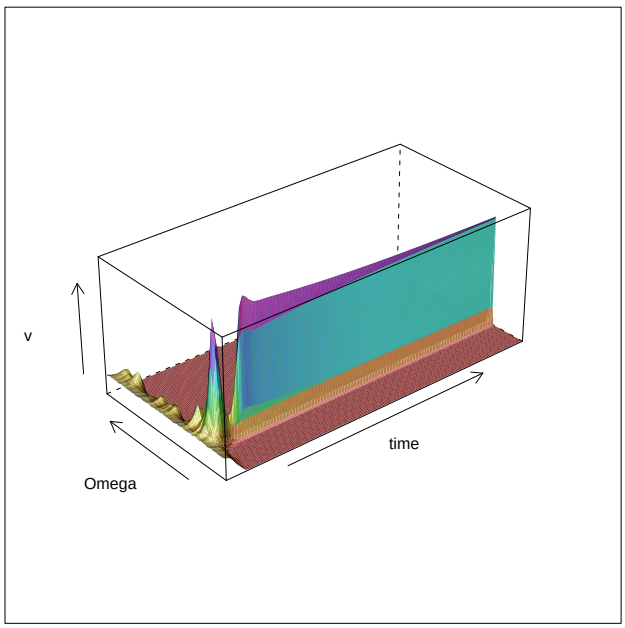

Figure 7.14: Behavior of the solution over time and space with parameters as in Table 7.2 and $\chi = 0.0$. **a** Representation of u (bacteria). **b** Representation of v (amoebae).

a

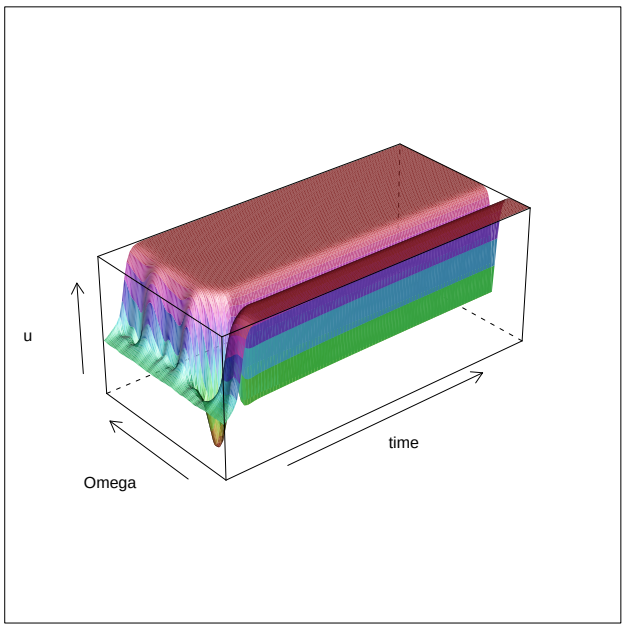

b

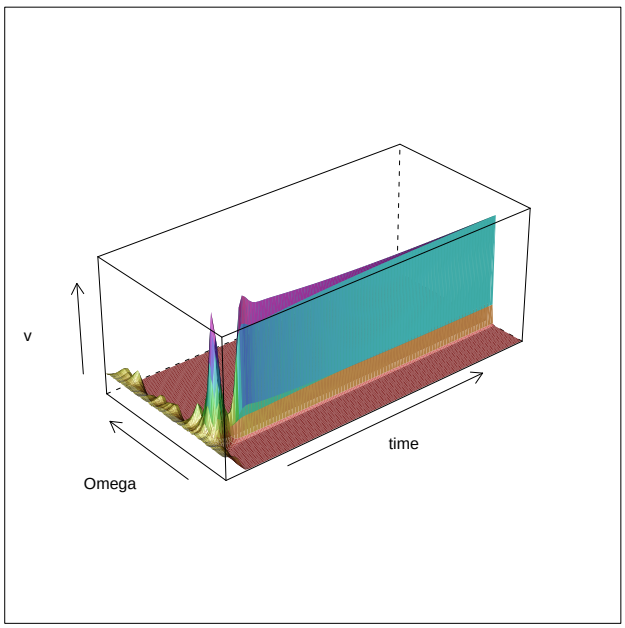

Figure 7.15: Behavior of the solution over time and space with parameters as in Table 7.2 and $\chi = 0.03$. **a** Representation of u (bacteria). **b** Representation of v (amoebae).

a

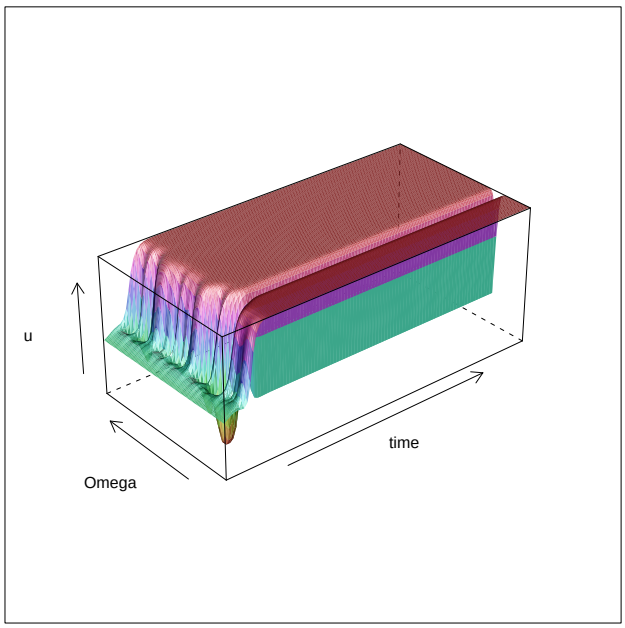

b

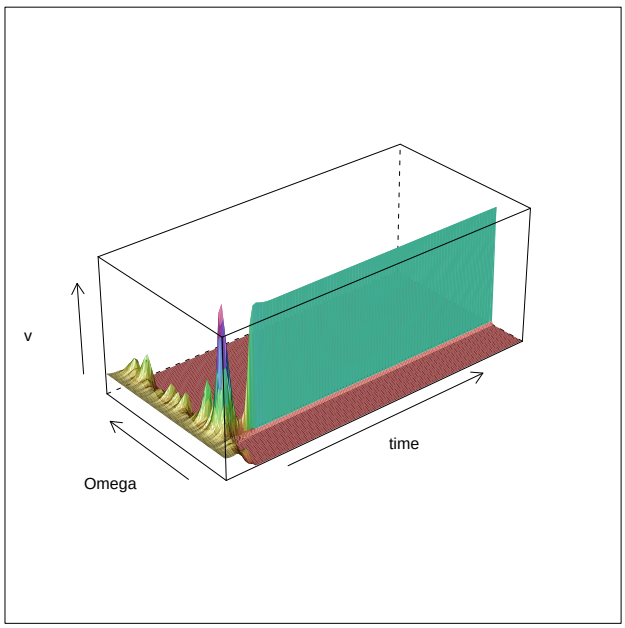

Figure 7.16: Behavior of the solution over time and space with parameters as in Table 7.2 and $\chi = 0.07$. **a** Representation of u (bacteria). **b** Representation of v (amoebae).

7.2.2 Two-dimensional domain

The results of Section 5.2 clearly hold also for a circular domain, so our expectation is to have patterns for every value of χ. In particular, the pattern will likely be the analogous of the one-dimensional case, that is, a homogeneous layer of bacteria with a spot of amoebae. As a matter of fact, this is what happens: Figures 7.17 (bacteria) and 7.18 (amoebae) show the results without chemotaxis, while Figures 7.19 (bacteria) and 7.20 (amoebae) have been obtained with $\chi = 0.03$. As for the one-dimensional situation, a change in the noise used for perturbing the initial datum influences the position of the final spot, but not the qualitative behavior of the solution.

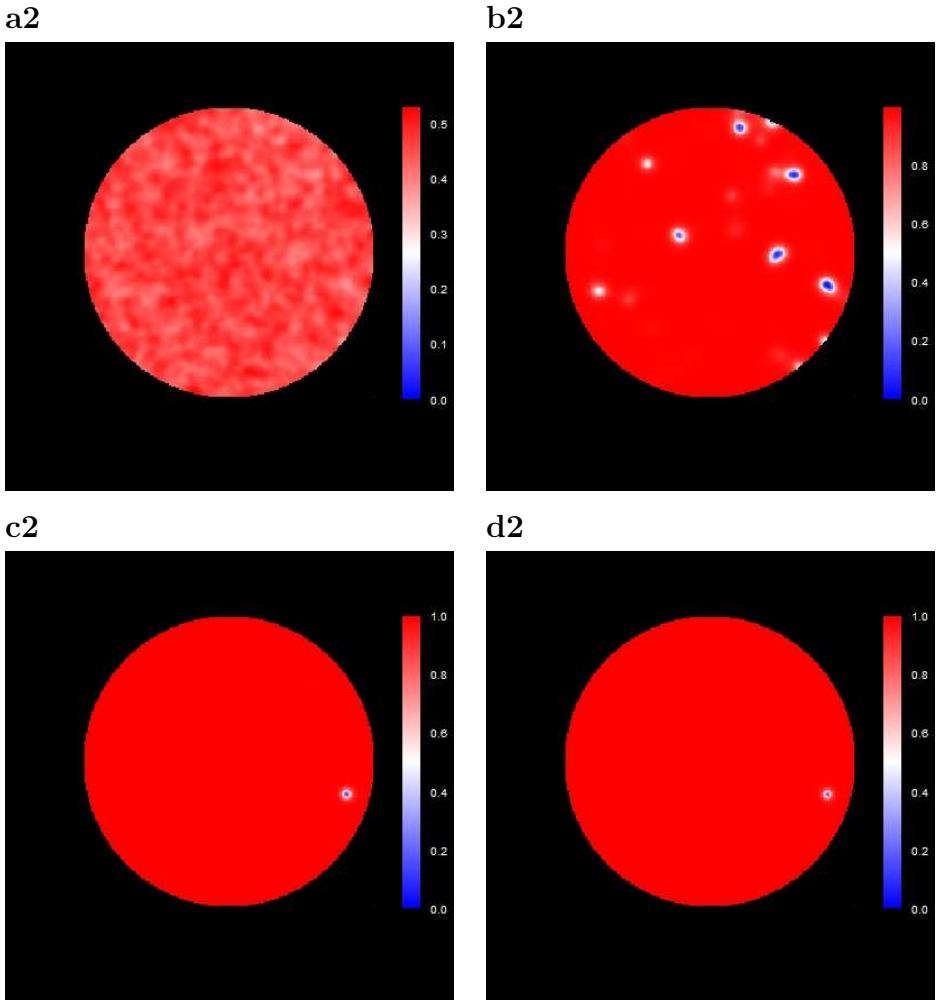

Figure 7.17: Levelplot for concentration of bacteria as resulting from simulations for the model with integral term on a circular domain, when parameters are as in Table 7.2 and $\chi = 0.0$. **a2** $t = 5$; **b2** $t = 15$; **c2** $t = 25$; **d2** $t = 100$.

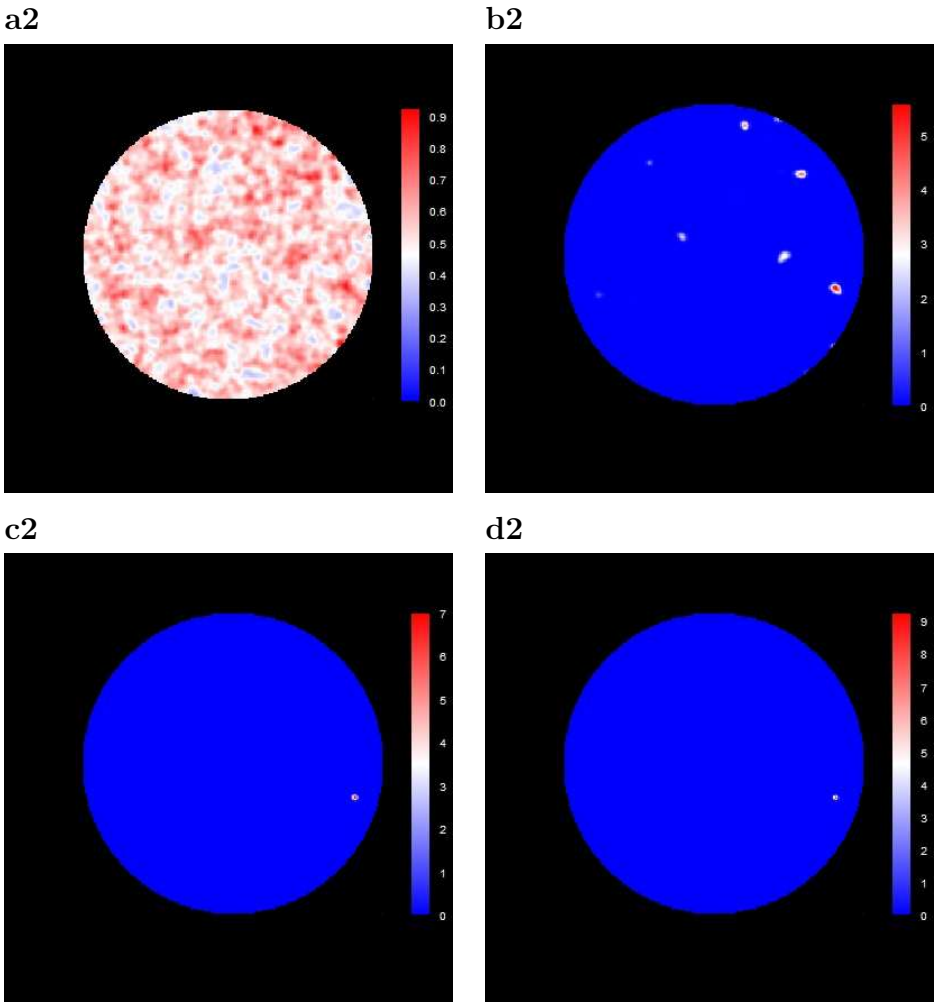

Figure 7.18: Levelplot for concentration of amoebae as resulting from simulations for the model with integral term on a circular domain, when parameters are as in Table 7.2 and $\chi = 0.0$. **a2** $t = 5$; **b2** $t = 15$; **c2** $t = 25$; **d2** $t = 100$.

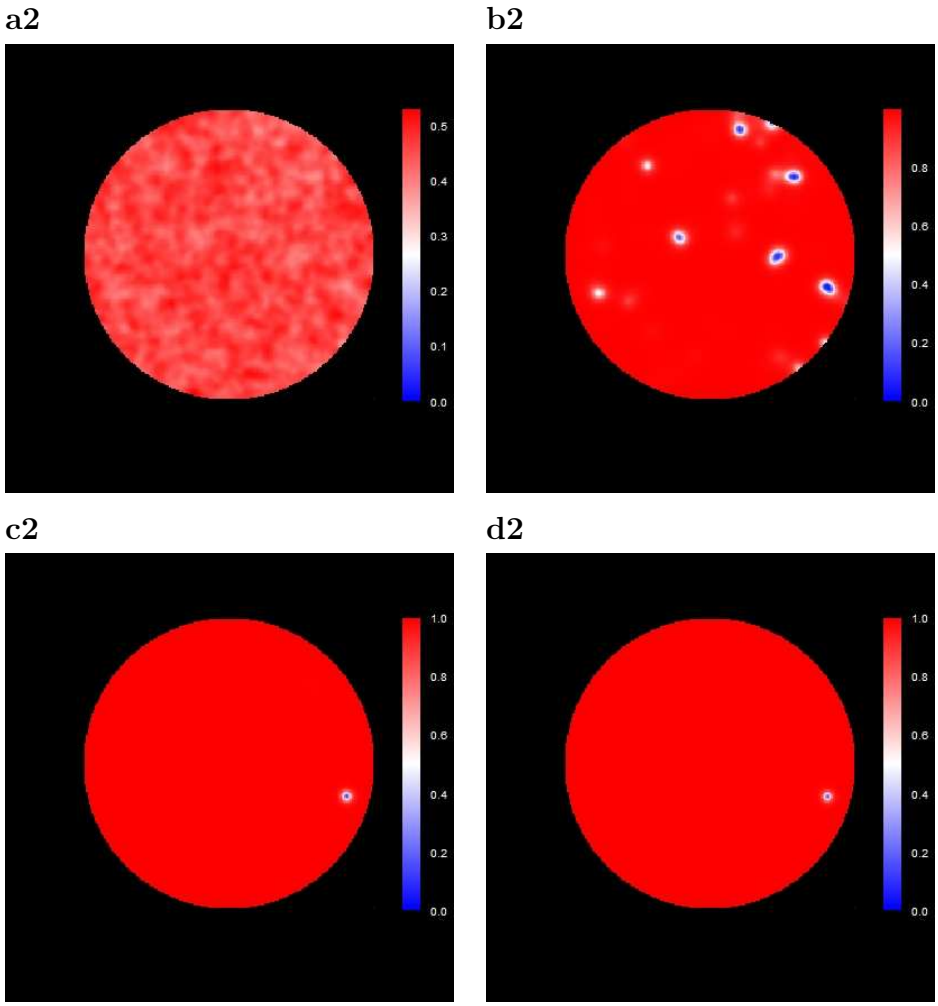

Figure 7.19: Levelplot for concentration of bacteria as resulting from simulations for the model with integral term on a circular domain, when parameters are as in Table 7.2 and $\chi = 0.03$. **a2** $t = 5$; **b2** $t = 15$; **c2** $t = 25$; **d2** $t = 100$.

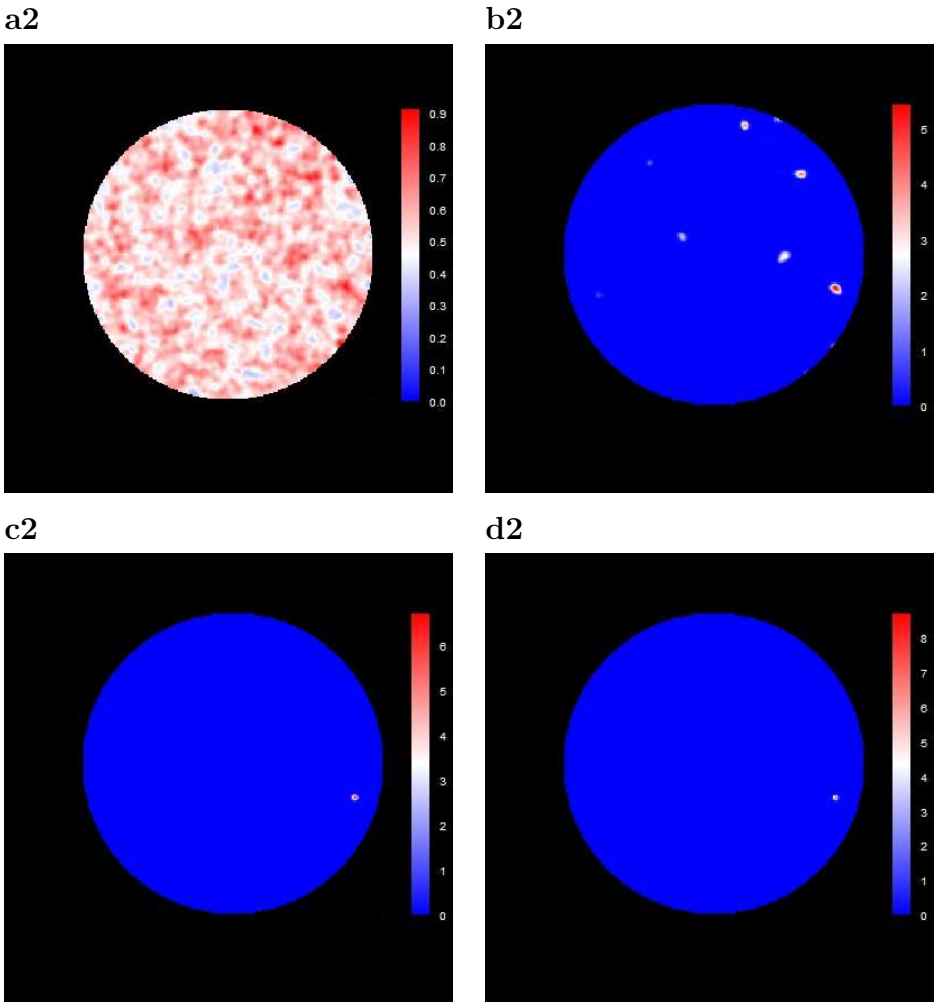

Figure 7.20: Levelplot for concentration of amoebae as resulting from simulations for the model with integral term on a circular domain, when parameters are as in Table 7.2 and $\chi = 0.03$. **a2** $t = 5$; **b2** $t = 15$; **c2** $t = 25$; **d2** $t = 100$.

7.3 Simulations related to biological experiments

The experimental setting for biological studies under consideration consists in a spot with some amoeboid cells on a homogeneous layer of bacteria; different strains of *Pseudomonas aeruginosa*, from weakly to highly virulent, are employed. The plates are observed for a short period (about 4-7 days), during which the two populations grow and interact; at the end of experiments amoeboid cells can be counted, and it is possible to see how the initial spot has expanded.

The results are basically the following: if bacteria belong to a permissive strain, then amoebae are able to expand and form a small disk; in some cases it is possible to see a sort of intermediate region between the populations, called *clear zone*, which is a ring surrounding the disk, with a lower concentration of amoebae.
When the bacterial strain is more aggressive, instead, amoebae can still expand, but they are limited in their growth, and the clear zone never occurs; highly virulent isolates do not allow amoeboid population to grow at all.

In this Section we show the results of some of the simulations related to these phenomena. The numerical method for discretization of system (1.3) is the same used in the previous Section; here we consider only a circular domain, which represents the plate used for experiments.
Clearly, the initial conditions are different from the simulations performed so far: in fact, here we need to consider a homogeneous layer of bacteria u_0 and a spot of amoebae v_0 in the center.

Parameters used are summarized in Table 7.3 below.

Parameter	value
D_1	0.7
D_2	0.05
χ	0.01
μ	1.05
δ	5.0
γ	0.0, 1.0, 7.0
τ	1.0
u_0	0.4
v_0	0.6

Table 7.3: Parameters used for simulations in Figures 7.21, 7.22, 7.23, 7.24, 7.25.

Firstly, we consider the case of a completely permissive (i.e. non virulent) isolate; this

means that we take $\gamma = 0.0$. Actually, the system becomes a predator-prey model where predation is non-local, so the expectation is to see that amoebae can grow indefinitely because they are not killed by bacteria; this is in fact what happens: in Figures 7.21 and 7.22 we can see that the disk of amoebae expands while bacteria are eaten correspondingly. The expanding white ring is a zone with few of both populations, so it may correspond to the clear zone observed in experiments.

Next we consider an intermediate situation, with $\gamma = 1.0$. The results of the corresponding simulations are visible in Figures 7.23 and 7.24: amoebae initially expand, but after a while the disk does not increase neither in size nor in number of cells; the clear zone is much less evident.

If we increase γ the spot of amoebae gets smaller, and for $\gamma > \delta$ after a short time it disappears, so that the final configuration is a homogeneous layer of bacteria and no amoeboid cells. This fact is not unexpected, because this means that bacteria are so virulent that the killing of amoeboid cells cannot be compensated by feeding, so in the end amoebae disappear.
An example of a simulation for a very virulent strain ($\gamma = 7.0$) is represented in Figure 7.25.

These simulations seem to be consistent with the behavior observed in the experiments with a spot of *Dictyostelium discoideum* on a homogeneous layer of *Pseudomonas aeruginosa*, so we can conclude that model (1.3) is able to describe the interaction between these two populations properly.

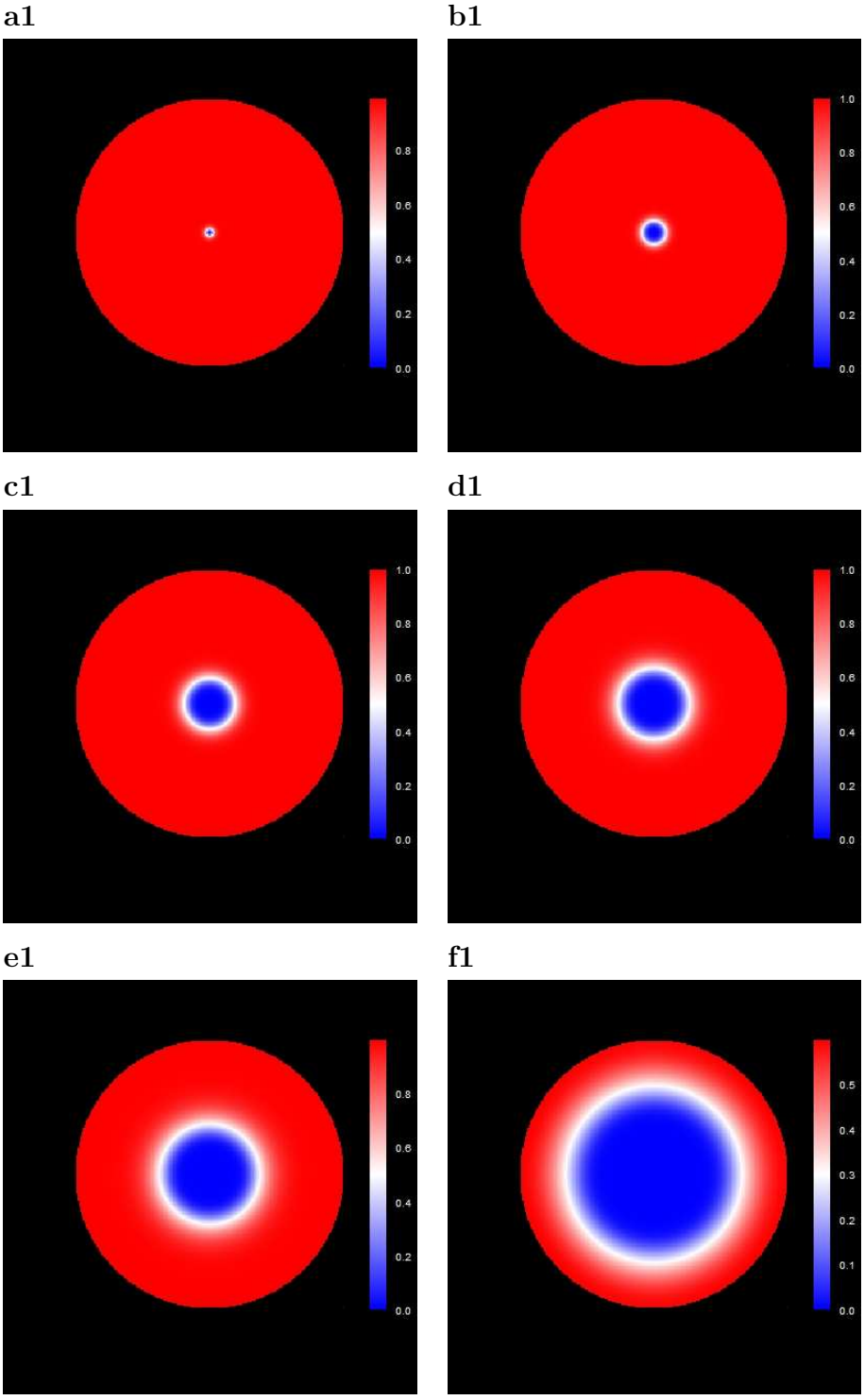

Figure 7.21: Levelplot for concentration of bacteria. Initial conditions: spot of amoebae on a homogeneous layer of bacteria. Parameters as in Table 7.3 and $\gamma = 0.0$. **a1** $t = 5$; **b1** $t = 50$; **c1** $t = 250$; **d1** $t = 500$; **e1** $t = 1000$; **f1** $t = 5000$.

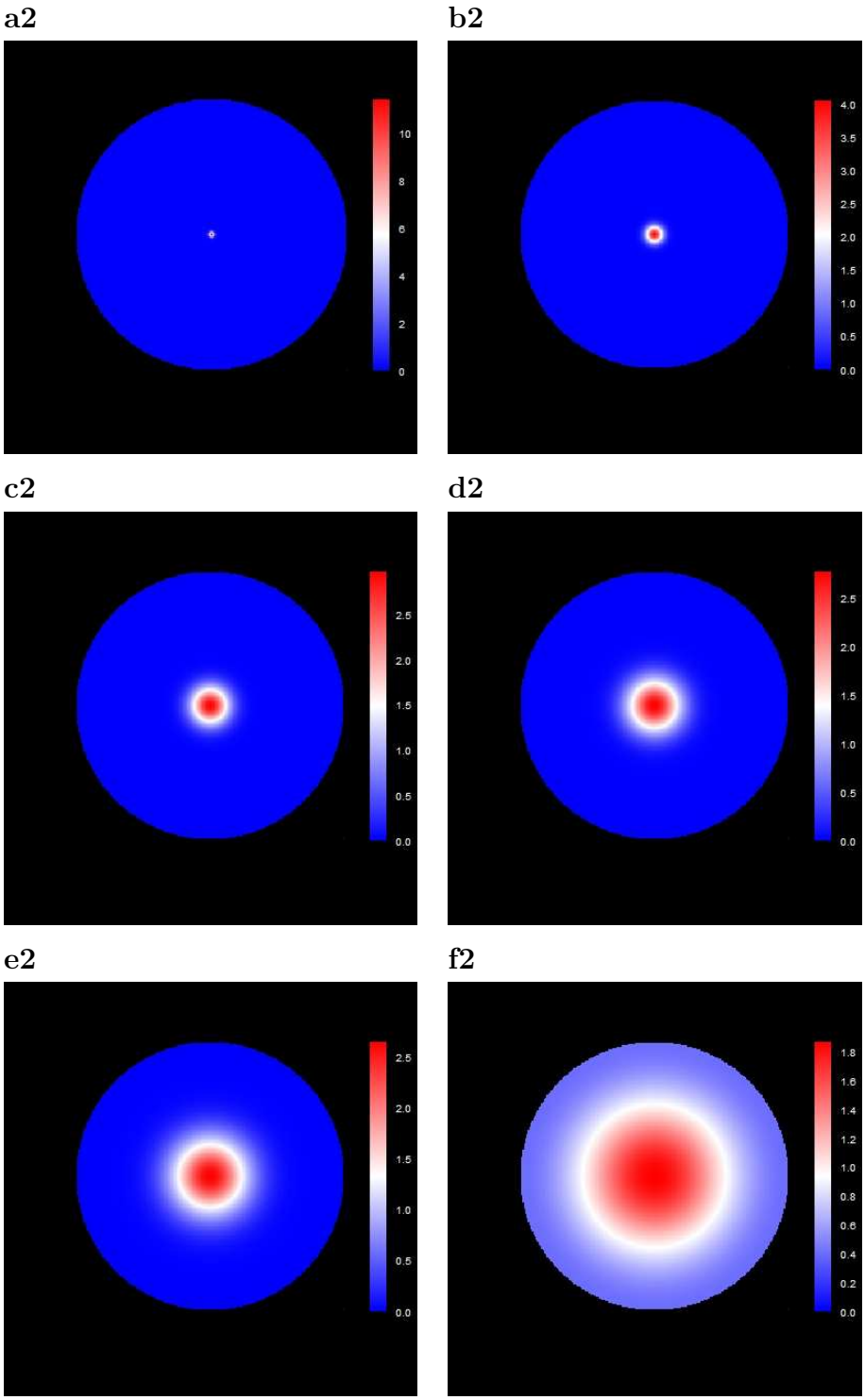

Figure 7.22: Levelplot for concentration of amoebae. Initial conditions: spot of amoebae on a homogeneous layer of bacteria. Parameters as in Table 7.3 and $\gamma = 0.0$. **a2** $t = 5$; **b2** $t = 50$; **c2** $t = 250$; **d2** $t = 500$; **e2** $t = 1000$; **f2** $t = 5000$.

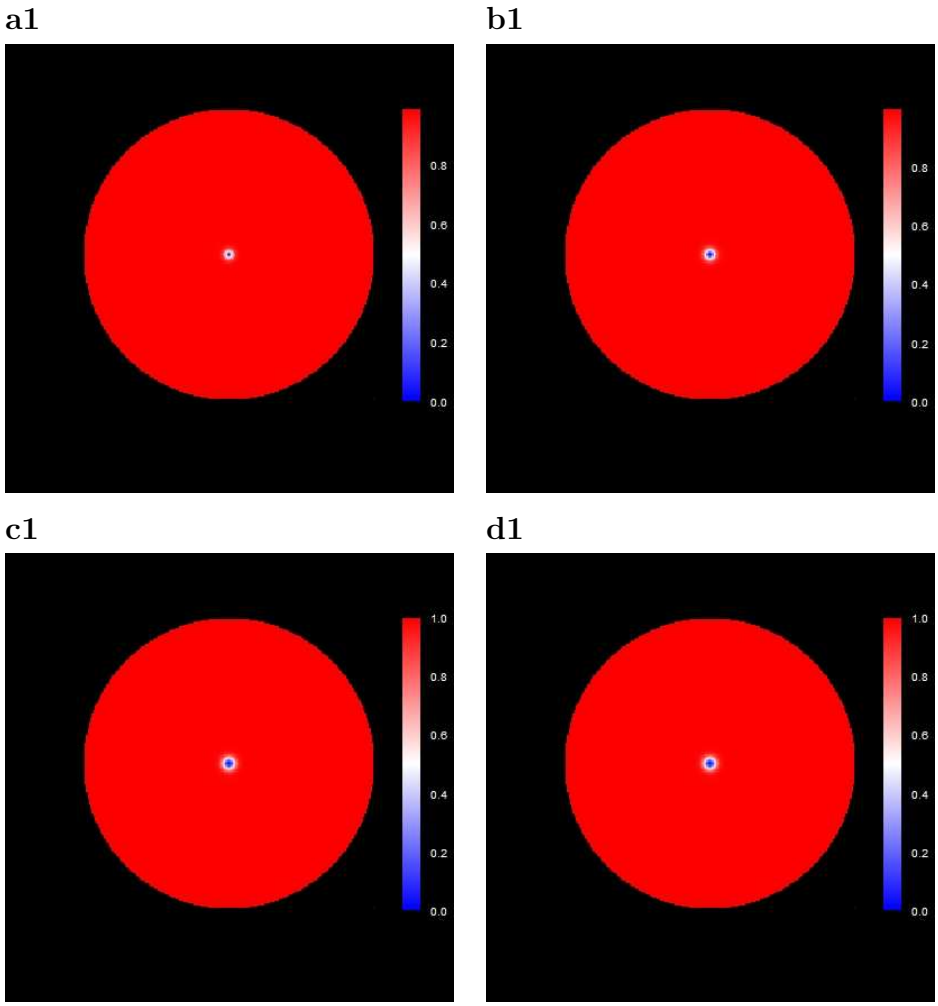

Figure 7.23: Levelplot for concentration of bacteria. Initial conditions: spot of amoebae on a homogeneous layer of bacteria. Parameters as in Table 7.3 and $\gamma = 1.0$. **a1** $t = 5$; **b1** $t = 50$; **c1** $t = 250$; **d1** $t = 500$.

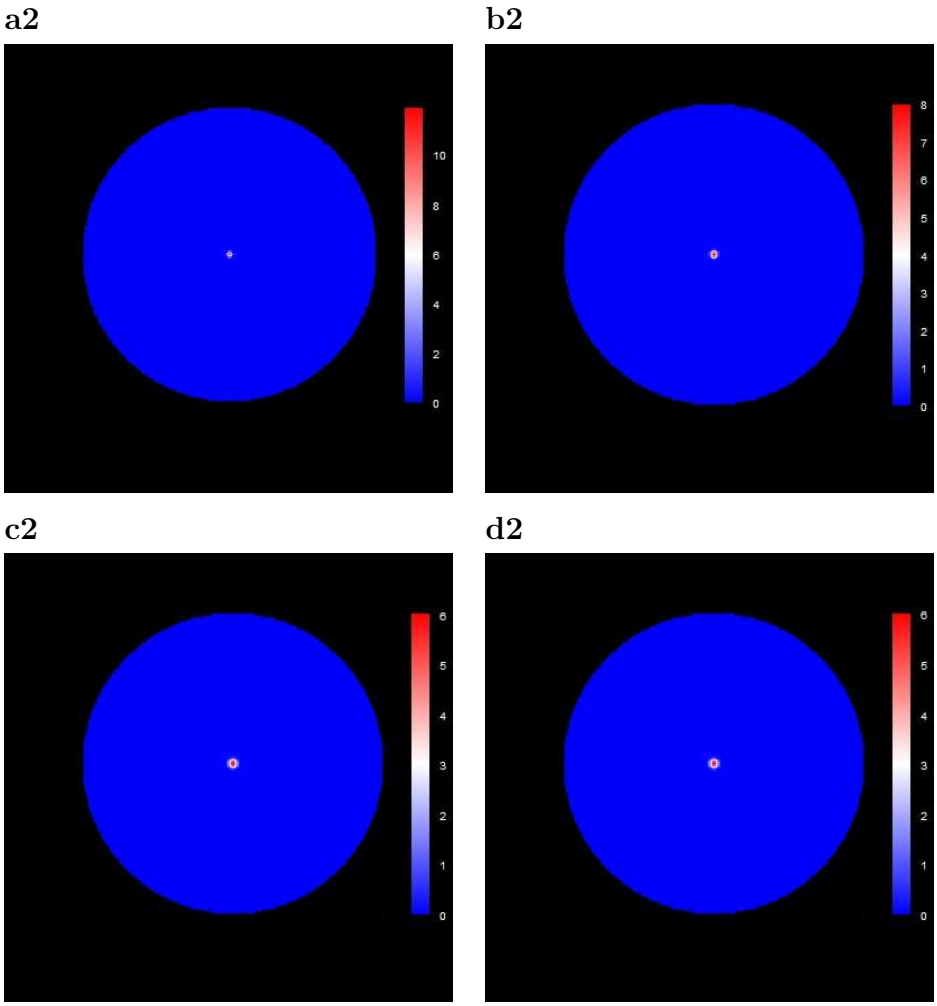

Figure 7.24: Levelplot for concentration of amoebae. Initial conditions: spot of amoebae on a homogeneous layer of bacteria. Parameters as in Table 7.3 and $\gamma = 1.0$. **a2** $t = 5$; **b2** $t = 50$; **c2** $t = 250$; **d2** $t = 500$.

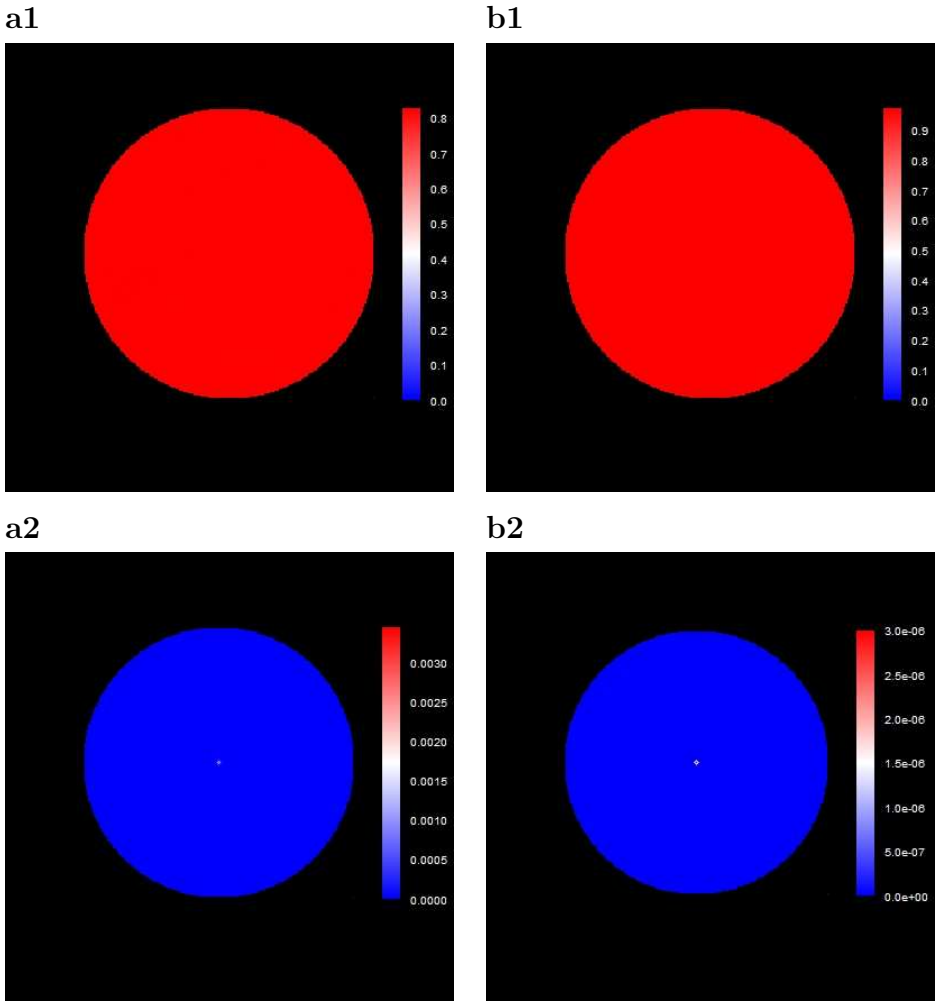

Figure 7.25: Levelplot for concentration of amoeba (**a1**, **b1**) and bacteria (**a2**, **b2**). Initial conditions: spot of amoebae on a homogeneous layer of bacteria. Parameters as in Table 7.3 and $\gamma = 7.0$. **a** $t = 2$; **b** $t = 4$.

Chapter 8

Conclusions and future directions

In this thesis we have designed and analyzed a mathematical model describing the population dynamics of interacting bacterial and amoeboid populations. This model belongs to the class of parabolic semilinear systems: specifically, it is a reaction-diffusion-chemotaxis predator-prey system with non-local effect of predation, where the prey acts also as a pathogen.

First of all we have proved with fixed point techniques that, in the absence of chemotaxis, the system admits a unique continuous solution. Then we have been concerned with the analysis of homogeneous steady states: we have considered different cases depending on the value of the parameter accounting for bacterial virulence, and we have proved the existence of one or two coexistence equilibria and their stability, providing conditions on the natural mortality rate of amoebae. Moreover, we have shown that, upon certain parameters choices, it is also possible to have periodic solutions.

The issue following the study of the stability of internal equilibria has been to assess the possibility of having patterns of Turing type: we have considered a slight perturbation of the spatially homogeneous stable steady state, solved the resulting system by separation of variables and derived conditions for pattern formation, or diffusion-driven instability, on parameters related to chemotaxis and diffusion. We have considered both the cases with and without the integral (corresponding to non-local and local predation effect respectively), and the interesting feature that we have found is that, for the system with the integral term, pattern formation is always possible, which is not the case of the simpler model.

We have also dealt with the numerical aspects of the problem. We have discretized our system with finite differences, and we have solved it numerically with two types of initial conditions: homogeneous initial datum for both populations (both on a line segment and

on a circle), or homogeneous datum for bacteria and a delta function (single spot) for amoebae (only on a circular domain). The former kind of simulations were aimed at validating the analytical results on pattern formation, while the purpose of the latter type has been to show the behavior of the solutions when varying the virulence parameter, which corresponds to using different strains for experiments.
These numerical studies have shown on the one hand that theoretical results are confirmed and that a variety of patterns can appear depending on the choice of parameters; on the other hand that the model is able to reproduce the behaviors observed during *in vivo* experiments.

Some topics have not been covered in this thesis, but are the subjects of future work: firstly, the proof of the existence of a unique solution to the full problem with chemotaxis, which would complete what has been done in Chapter 2.
Another issue to be addressed is the study of stationary solutions of the system: this part is actually quite complex due to the integral term; preliminary results show that multiple solutions can be found, thus possibly explaining the complex dynamics arising from simulations.

Bibliography

[1] M. Baurmann, T. Gross, and U. Feudel. Instabilities in spatially extended predator–prey systems: Spatio-temporal patterns in the neighborhood of Turing–Hopf bifurcations. *Journal of Theoretical Biology*, 245(2):220–229, 2007.

[2] C. J. Briggs and M. F. Hoopes. Stabilizing effects in spatial parasitoid–host and predator–prey models: a review. *Theoretical Population Biology*, 65(3):299–315, 2004.

[3] N. F. Britton. *Reaction-Diffusion Equations and their Applications to Biology*. Academic Press, New York, 1986.

[4] P. Cosson, L. Zulianello, O. Join-Lambert, F. Faurisson, L. Gebbie, M. Benghezal, C. van Delden, L.K. Curty, and T. Kohler. Pseudomonas aeruginosa Virulence Analyzed in a Dictyostelium Discoideum Host System. *Journal of Bacteriology*, 184(11):3027–3033, 2002.

[5] A. M. de Roos, E. McCauley, and W. G. Wilson. Pattern formation and the spatial scale of interaction between predators and their prey. *Theoretical Population Biology*, 53(2):108–130, 1998.

[6] R. Erban and H. G. Othmer. Taxis equations for amoeboid cells. *Journal of Mathematical Biology*, 54:847–885, 2007.

[7] P. C. Fife. Mathematical aspects of reacting and diffusing systems. *Lecture Notes in Biomathematics*, 28, 1979.

[8] R. A. Fisher. The wave of advance of advantageous genes. *Annals of Eugenics*, 7(353):355–369.

[9] R. Froquet, N. Cherix, S. Burr, J. Frey, S. Vilches, J.M. Tomas, and P. Cosson. Alternative Host Model To Evaluate Aeromonas Virulence. *Applied and Environmental Microbiology*, 73(17):5657–5659, 2007.

[10] J. Furter and M. Grinfeld. Local vs. non-local interactions in population dynamics. *Journal of Mathematical Biology*, 27(1):65–80, 1989.

[11] D. Greenspan and V. Casulli. *Numerical Analysis for Applied Mathematics, Science, and Engineering*. Westview Press, 1994.

[12] T. Hillen and K. Painter. Global Existence for a Parabolic Chemotaxis Model with Prevention of Overcrowding. *Advances in Applied Mathematics*, 26:280–301, 2001.

[13] C. S. Holling. The components of predation as revealed by a study of small mammal predation of the European Pine Sawfly. *Canadian Entomologist*, 91:293–320, 1959.

[14] E. E. Holmes, M. A. Lewis, J. E. Banks, and R. R. Veit. Partial differential equations in ecology: spatial interactions and population dynamics. *Ecology*, 75(1):17–29, 1994.

[15] M. Iannelli. A Note on Some Non-Linear Non-Contraction Semigroups. *Bollettino dell'Unione Matematica Italiana*, 6:1015–1025, 1970.

[16] M. Iannelli. On a Certain Class of Semilinear Evolution Systems. *Journal of Mathematical Analysis and Applications*, 56(2):351–367, 1976.

[17] R. H. Kessin. *Dictyostelium: Evolution, Cell Biology, and the Development of Multicellularity*. Cambridge University Press, 2001.

[18] D. A. Kessler and H. Levine. Pattern formation in Dictyostelium via the dynamics of cooperative biological entities. *Physical Review E*, 48(6):4801–4804, 1993.

[19] E. Kipnis, T. Sawa, and J. Wiener-Kronish. Targeting mechanisms of Pseudomonas aeruginosa pathogenesis. *Médecine et maladies infectieuses*, 36:78–91, 2006.

[20] W. Ko and K. Ryu. Qualitative analysis of a predatorprey model with Holling type II functional response incorporating a prey refuge. *Journal of Differential Equations*, 231:534–550, 2006.

[21] C. L. Kurz and J. J. Ewbank. Infection in a dish: high-throughput analyses of bacterial pathogenesis. *Current Opinion in Microbiology*, 10:10–16, 2007.

[22] A. F. M. Marée and P. Hogeweg. How amoeboids self-organize into a fruiting body: Multicellular coordination in Dictyostelium discoideum. *Proceedings of the National Academy of Sciences*, 98(7):3879–3883, 2001.

[23] R. M. M. Mattheij, S. W. Rienstra, and J. H. M. ten Thije Boonkkamp. *Partial Differential Equations: Modeling, Analysis, Computation*. Siam, 2005.

[24] M. Mimura, H. Sakaguchi, and M. Matsushita. Reaction-diffusion modelling of bacterial colony patterns. *Physica A*, (282):283–303, 2000.

[25] A. Morozov, S. Petrovskii, and B.-L. Li. Spatiotemporal complexity of patchy invasion in a predator-prey system with the Allee effect. *Journal of Theoretical Biology*, 282:18–35, 2006.

[26] J. D. Murray. *Mathematical Biology Vol. I : An Introduction*. Springer London, 2003.

[27] J. D. Murray. *Mathematical Biology Vol. II : Spatial Models and Biomedical Applications*. Springer London, 2003.

[28] A. Okubo. *Diffusion and Ecological Problems: Mathematical Models*. Springer Heildelberg, 1980.

[29] A. Okubo and S. A. Levin. *Diffusion and Ecological Problems: Modern Perspectives*. Springer New York, 2001.

[30] H. G. Othmer, B. Lilly, and J. C. Dallon. Pattern formation in a cellular slime mold. *IMA volumes in Mathematics and its applications*, 119:359–384, 2000.

[31] C. Ou and J. Wu. Persistence of wavefronts in delayed nonlocal reaction-diffusion equations. *Journal of Differential Equations*, 235:219–261, 2007.

[32] A. Pazy. *Semigroups of linear operators and applications to partial differential equations*. Springer-Verlag New York, 1983.

[33] I. G. Pearce, M. A. J. Chaplain, P. G. Schofield, A. R. A. Anderson, and S. F. Hubbard. Modelling the spatio-temporal dynamics of multi-species host–parasitoid interactions: Heterogeneous patterns and ecological implications. *Journal of Theoretical Biology*, 241(4):876–886, 2006.

[34] I. G. Pearce, M. A. J. Chaplain, P. G. Schofield, A. R. A. Anderson, and S. F. Hubbard. Chemotaxis-induced spatio-temporal heterogeneity in multi-species host-parasitoid systems. *Journal of Mathematical Biology*, 55(3):365–388, 2007.

[35] S. Pukatzki, R. H. Kessin, and J. J. Mekalanos. The human pathogen Pseudomonas aeruginosa utilizes conserved virulence pathways to infect the social amoeba Dictyostelium discoideum. *Proceedings of the National Academy of Sciences*, 99(5):3159–3164, 2002.

[36] J. B. Raquepas and J. D. Dockery. Dynamics of a reaction-diffusion equation with nonlocal inhibition. *Physica D: Nonlinear Phenomena*, 134(1):94–110, 1999.

[37] J. G. Skellam. Random Dispersal in Theoretical Populations. *Biometrika*, 38(1/2):196–218, 1951.

[38] M. Steinert and K. Heuner. Dictyostelium as host model for pathogenesis. *Cellular Microbiology*, 7(3):307–314, 2005.

[39] S. H. Strogatz. *Nonlinear Dynamics And Chaos: With Applications To Physics, Biology, Chemistry, And Engineering*. Addison-Wesley, 1996.

[40] H. R. Thieme. *Mathematics in Population Biology*. Princeton University Press, 2003.

[41] H. M. Tsuchiya, J. F. Drake, J. L. Lost, and A. G. Fredrickson. Predator-Prey Interactions of Dictyostelium discoideum and Escherichia coli in Continuous Culture. *Journal of Bacteriology*, 110(3):1147–1153, 1972.

[42] A. M. Turing. The Chemical Basis of Morphogenesis. *Philosophical Transactions of the Royal Society of London B*, 237:37–72, 1952.

[43] A. Tveito and R. Winther. *Introduction to Partial Differential Equations: A Computational Approach*. Springer, 1998.

[44] B. N. Vasiev, P. Hogeweg, and A. V. Panfilov. Simulation of dictyostelium discoideum aggregation via reaction-diffusion model. *Physical review letters*, 73(23):3173–3176, 1994.

[45] P. F. Verhulst. Notice sur la loi que la population suit dans son accroissement. *Correspondence Mathématique et Physique*, 10:113–121, 1838.

[46] P. F. Verhulst. Recherche mathémathiques sur le loi d'accroissement de la population. *Nouveau Mémoires de l'Académie Royale des Sciences et Belles Lettres de Bruxelles*, 18:3–38, 1845.

[47] N. S. Wingreen and S. A. Levin. Cooperation among Microorganisms. *PLoS Biology*, 2006.